Performance Analysis of Enhancement Techniques for 3-D Cellular Networks

Soumaya Bachtobji

▶ **To cite this version:**

Soumaya Bachtobji. Performance Analysis of Enhancement Techniques for 3-D Cellular Networks. Signal and Image Processing. UNIVERSITÉ DU MANS; UNIVERSITÉ TUNIS ELMANAR, 2019. English. NNT : . tel-02445442

HAL Id: tel-02445442

https://theses.hal.science/tel-02445442v1

Submitted on 20 Jan 2020

HAL is a multi-disciplinary open access archive for the deposit and dissemination of scientific research documents, whether they are published or not. The documents may come from teaching and research institutions in France or abroad, or from public or private research centers.

L'archive ouverte pluridisciplinaire **HAL**, est destinée au dépôt et à la diffusion de documents scientifiques de niveau recherche, publiés ou non, émanant des établissements d'enseignement et de recherche français ou étrangers, des laboratoires publics ou privés.

THESE DE DOCTORAT EN COTUTELLE DE L'UNIVERSITE TUNIS EL MANAR ET LE MANS UNIVERSITE

ECOLE DOCTORALE N° 602
Spécialité : *Sciences pour l'Ingénieur*

Par
Soumaya BACHTOBJI

Performance Analysis of Enhancement Techniques for 3-D Cellular Networks

Thèse présentée et soutenue à Le Mans Université, le « 08 Novembre 2019 »
Unité de recherche : LAUM UMR CNRS 6613 France et INNOV'COM, SUP'COM, Tunisie.
Thèse N° : 2019LEMA1028

Rapporteurs avant soutenance :

Ros Laurent Maitre de conférences (HDR) Grenoble-INP (Gipsa-Lab)
Eric Simon Maitre de conférences (HDR) Université de Lille

Composition du Jury :

Examinateurs :	Rodolphe Vauzelle	Professeur Université de Poitiers (Xlim)
	Jean-Hugh Thomas	Professeur Le Mans Université *(LAUM)*
	Marie Zwingelstein	Maitre de conférences Université Polytechnique Haut- de France
Dir. de thèse :	Kosai Raoof	Professeur Le Mans Université *(LAUM)*
Co-dir. de thèse :	Ridha Bouallegue	Professeur INNOV'COM SUPCOM (Tunis)
Co-encadrant :	Kais Hassan	Maitre de conférences Le Mans Université *(LAUM)*

To my dear parents, husband, and daughter.

Acknowledgment

I would like to gratefully and sincerely thank my supervisors, Professor Ridha BOUALLEGUE and Professor Kosai RAOOF whose support and guidance made my thesis work possible. They have been actively interested in my work and have always been available to advise me. I am very grateful for their patience, motivation, enthusiasm, and immense knowledge that, taken together, make them great mentors. I would like to thank my committee members for their interest in my work.

I would like to show my gratitude to my thesis reviewers: Dr. Eric Simon and Dr. Ros Laurent, and to the jury members: Prof. Rodolphe Vauzelle, Prof Jean-Hugh Thomas, and Dr. Marie Zwingelstein for evaluating my Ph.D. work.

This work was possible because of the unconditional support provided by Dr. Aymen OMRI. A person with an amicable and positive disposition, he has always made himself available to clarify my doubts despite his busy schedules. Thank you, for all your help and support.

I would like to thank Dr. Kais HASSAN for his directions, technical support, his time and insightful comments that helped me improve my works.

A special thanks to my family. Words can not express how grateful I am to my parents, Nabil and Elhem, for their faith in me and allowing me to be as ambitious as I wanted. It was under their watchful eye that I gained so much drive and an ability to tackle challenges head on. I would like to express my thanks to my dear sisters Sarah and Soukayna for their help and encouragement to finish my education.

Finally, and most importantly, I would like to thank my husband Mahdi MAHMOUD, my love and my life partner by my side. You are the most amazing person in my life, you take care of me beyond my dreams and expectations. Thank you for always being there for me through thick and thin. Thank you my cute little daughter, Lyne, for being a good girl and making it possible for me to complete what I started. Also, I thank my dears Yassine and Samy.

Soumaya BACHTOBJI

Résumé

Le réseau mobile de cinquième génération (5G) est défini pour prendre en charge un trafic de données considérable, réduire la consommation d'énergie et améliorer la qualité de service (QoS). Pour atteindre ces objectifs, des contributions importantes aux réseaux de radio mobile doivent être réalisées. Dans ce contexte, des technologies clés telles que les réseaux hétérogènes (HetNets), les communications massives à entrées multiples et à sorties multiples (MIMO), les communications à ondes millimétriques (mmWave) et la récupération d'énergie (EH) ont été identifiées pour mener à bien la 5G . La densification cellulaire constitue une solution simple et efficace pour augmenter la capacité du réseau. Elle repose sur une réutilisation intensive du spectre sur une zone géographique donnée et rapproche ainsi les stations de base des utilisateurs.

Les réseaux 5G présentent de nombreux défis et opportunités pour la conception des réseaux sans fil denses. Par conséquent, des efforts de recherche substantiels sont consacrés aux problèmes de la modélisation 3-D dans les réseaux HetNets basés sur les mmWave et la récupération d'énergie respectivement. Ainsi, la modélisation et l'amélioration des performances des réseaux cellulaires hétérogènes 3-D pour la prochaine génération méritent une étude approfondie, qui est l'objectif principal de cette thèse.

Les réseaux cellulaires sont généralement modélisés par la théorie des processus de points et la géométrie stochastique, qui sont généralement utilisés pour modéliser des réseaux cellulaires dans un espace bidimensionnel (2-D). Cependant, les modèles bidimensionnels bien connus conviennent aux zones rurales ou périurbaines mais ne conviennent pas aux environnements urbains denses. Dans ces mileux urbains, un grand nombre de petites cellules hétérogènes sont déployées dans les réseaux de nouvelle génération afin de satisfaire l'augmentation rapide du nombre d'abonnés mobiles ainsi que la demande de services de communication.

Les travaux de recherche ont proposé divers modèles de propagation pour se con-

centrer sur les effets de blocage tels que les arbres, les bâtiments, pouvant entraîner une diminution des performances des réseaux sans fil. Considérant des blocages à grande échelle, ces travaux de recherche ont utilisé une fonction de probabilité Line of Sight (LOS) dépendante de la distance, dans laquelle les stations de base (BS) ont été déployées sous forme des processus de point homogènes indépendants, LOS et NLOS. Le concept de théorie des formes aléatoires a été utilisé pour modéliser les réseaux cellulaires avec des bâtiments distribués de manière aléatoire. En fait, ces blocages ont été modélisés comme un schéma booléen de rectangles, ce qui permet une caractérisation complète du caractère aléatoire du blocage, tels que les tailles, les emplacements, les orientations, et des hauteurs. Cependant, la modélisation dans la plupart des recherches se limite à l'étude des réseaux cellulaires bidimensionnels homogènes. Ainsi, ils ont étudié les environnements NLOS (LOS) sous l'hypothèse d'une atténuation du canal de Rayleigh ou Rice, respectivement. D'autre part, certains papiers ont utilisé Nakagami et ont estimé que Rayleigh n'était pas adéquat pour les réseaux mmWave en raison de leur faible propriété de diffusion. Ils ont étudié les performances des réseaux cellulaires dans les zones urbaines où l'atténuation de Nakagami-m a été considérée pour modéliser l'atténuation du LOS et NLOS.

Récemment, le relais de D2D (Device to Device) est en train de devenir une solution pour dépasser les limites de la couverture mmWave, car il maintient la topologie du réseau et les exigences de l'infrastructure. Dans la littérature, les auteurs ont introduit les relais D2D dans les réseaux cellulaires mmWave et ont évalué la probabilité de couverture et l'efficacité spectrale. Cependant, ces travaux de recherche présentent des limites, en négligeant les faible propriété de diffusion dans le modèle de canal mmWave et en considérant un processus de points de Poisson (PPP) homogène en 2D pour modéliser les BS, les utilisateurs et les obstacles. Par conséquent, des schémas de mode de sélection ont été proposé pour sélectionner le mode de communication D2D ou le mode de communication cellulaire. Les schémas proposés, en général, se résument en deux méthodes, la sélection en se basant sur la distance en Down-Link ou bien en se basant sur la distance en Up-Link.

Ce travail de thèse porte sur la modélisation et l'amélioration des performances des réseaux cellulaires hétérogènes 3-D pour la prochaine génération 5G. Ce travail présente

aussi des propositions des schémas, ainsi que des études sur les améliorations apportées tout en utilisant ces solutions .

Les principaux apports de la thèse se résument comme suit:

- **Proposition de nouveaux modéles 3-D pour les réseaux cellulaire:**

  Dans cette thèse, la première partie introduit un modèle général 3-D pour les réseaux cellulaires multi-niveaux basés sur mmWaves et UHF. Le modèle proposé est basé sur un processus de points Matèrn Hard Core Process (MHCP II) qui respecte une distance minimale entre les stations de bases dans les réseau cellulaires. La deuxième partie présente un modèle de 3-D pour les systèmes de communication sans fils afin d'évaluer leurs performances sous l'hypothèse d'un canal hybride pour les environnements LOS et NLOS. Ce modèle est basé sur les concepts de la géométrie stochastique, qui décrivent les positions des différentes cellules dans le réseau avec des contraintes réalistes, et la théorie de la forme aléatoire qui caractérise les blocages aléatoires dans des réseaux cellulaires urbains. Cette thèse propose aussi des expressions exactes de la fonction de densité de probabilité, la probabilité moyenne de couverture, le taux d'erreur par bit moyen (BER), ainsi que la capacité ergodique moyenne pour chaque étude et proposition. Ces critères sont utilisés pour évaluer les modèles 3-D et les impacts des schémas proposés sur les performances du système de communications. Une étude comparative est en outre menée.

- **Développement de nouvelles techniques efficaces améliorant les performances du système de communication:**

  Cette thèse propose deux nouvelles techniques efficaces améliorant les performances du système de communication. En effet, la première partie introduit un système basé sur la récupération d'énergie pour les réseaux cellulaires 3-D afin d'améliorer les performances des systèmes de communication. Nous proposons d'utiliser la récupération d'énergie pour réduire le délai de transmission et améliorer la capacité ergodique. La géométrie stochastique est utilisée pour décrire les positions des différentes cellules dans le réseau avec des contraintes réalistes. Sur cette base, le délai de transmission moyen et les expressions de capacité ergodique sont détaillés et dérivés. En utilisant des résultats numériques, les expressions dérivées analy-

tiques sont évaluées et les avantages du schéma proposé sont examinés. Dans la seconde partie, en considérant une hypothèse de canal nakagami-m pour les communications MmWaves, nous proposons un nouveau schéma min / max pour améliorer la réussite de la transmission. Ce schéma est basé sur la sélection d'un relais disponible pouvant assister à la transmission.

Les grandes lignes du mémoire sont les suivantes:

Le premier Chapitre présente l'introduction générale de la thèse. Il décrit l'énoncé du problème et la motivation. Ensuite, les travaux liés à modelisation en 3-D dans la littérature sont détaillés et étudiés. Les contributions de cette thèse sont ensuite présentées et détaillées et qui peuvent principalement être groupées sur trois axes; proposer de nouveaux modéles 3-D pour les réseaux cellulaire, dériver des expressions exactes des différents paramètres d'évaluation des performances, et finalement développer de nouvelles techniques efficaces améliorant les performances du système. Par la suite, la liste des publications au cours de la période de thèse est introduite. Enfin, l'organisation de la thèse est présentée.

Le chapitre 2 donne un aperçu des outils mathématiques et présente les deux modèles spatiaux tridimensionnels des réseaux de communication sans fil proposés au cours de cette thèse. Ces modèles décrivent le système lorsque l'effet de blocage est pris en compte et quand il est négligé. Ce chapitre présente également la dérivation des expressions de la densité de probabilité des distances utilisateur-station de base, du rapport SINR et du path loss pour chaque modèle.

Le chapitre 3 propose une analyse des performances des réseaux de communication sans fil 3-D basés sur UHF et mmWave. Il présente également la dérivation des expressions approchées de la probabilité de transmission réussie, du débit moyen, et du BER moyen. Les résultats analytiques sont validés par des résultats de simulation et une analyse comparative est menée.

Le chapitre 4 présente l'analyse des performances des effets de blocage dans les réseaux de communication sans fil 3-D. En prenant en compte le modèle introduit dans le chapitre 2, ce chapitre déduit également les expressions de la probabilité de LOS et de la probabilité de couverture pour les systèmes UHF et mmWaves.En utilisant des résultats numériques, les expressions dérivées sont évaluées pour mettre en valeur les contributions

présentées.

Un nouveau schéma pour les réseaux cellulaires 3-D a été proposé dans le chapitre 5 afin d'améliorer les performances du système de communication. Le schéma proposé est basé sur la récupération d'énergie afin de réduire le délai de transmission et, par conséquent, d'améliorer la capacité ergodique. Dans cette partie, nous dérivons les expressions du délai de transmission moyen et de la capacité ergodique. Enfin, les résultats de la simulation servent à valider les expressions analytiques et à confirmer l'avantage des schémas proposés dans l'amélioration des performances du réseau cellulaire.

Dans le chapitre 6, afin de limiter les blocages et d'améliorer la probabilité de couverture, le relais D2D est utilisé pour améliorer la fiabilité de la liaison directe. Ainsi, nous proposons un nouveau schéma de communication pour sélectionner un relais. Sur la base de la géométrie stochastique et de la théorie de la forme aléatoire, nous dérivons les expressions de la densité de probabilté des distances au relais le plus proche et la probabilité de transmission réussie du schéma proposé. En utilisant des résultats numériques, les expressions dérivées sont évaluées et les avantages du schéma proposé sont examinés.

Enfin, la conclusion génrale et les perspectives sont présentées.

Mots clés: Analyse des Performances, Cinquième Cénération (5G), Géométrie Stochastique, Modélisation 3-D, Onde Millimétrique (mmWave), Réseaux Cellulaires Hétérogènes, Ultra Haute Fréquence (UHF).

Abstract

With the explosive growth of mobile data demand, cellular networks have experienced several major evolutions, from the first generation to the present fifth generation new radio cellular networks. These networks can cover a larger geographical area, with high network capacity, and low power consumption. For the next generation, the cellular networks consist of deploying a big number of small cells, such as femto-cells and picocells, which offer a lager zone of radio coverage. In fact, cell concentration presents a simple and efficient solution to increase the network capacity, which relies on reusing densely the spectrum across a geographical area and hence brings base stations closer to users. Thus, the 3-D modeling and the performance enhancement of the increasingly heterogeneous cellular networks become important issues.

The current thesis focuses on the study and the enhancement of 3-D cellular networks. The research work introduced in this thesis has two main axes. First, we focus on three-dimensional modeling of wireless communication networks. These models, not only describe the system when the blockages effect are neglected, but also capable of modeling the obstacles (such as buildings) in order to study their effect and propose solution to overcome them. The performance analysis expressions for each proposed model are derived, and the simulation results are used to validate the analytical expressions, and to confirm the advantages of the proposed 3-D model on dense urban wireless communication system performances and based on which comparative studies are conducted.
Second, new transmission schemes are proposed to enhance the performances of the urban wireless communication systems. Thus, we introduce an energy harvesting (EH) based scheme for ultra high frequency that employs the EH to reduce the transmission delay and to enhance the ergodic capacity. Based on that, the average transmission delay and the ergodic capacity expressions are detailed and derived. Finally, under the assumption of Nakagami-m fading channel for mmWaves communications, we propose a new min/max

scheme to enhance the successful transmission. This scheme proposes how to select an available relay that can assist the transmission. Using numerical results, the analytical derived expressions of each proposed scheme are evaluated, and the advantages of each one are investigated.

Keywords: 3-D Modeling, Fifth Generation (5G), Heterogeneous Cellular Networks, Millimeter Wave (mmWave), Performance analysis, Stochastic Geometry, Ultra High Frequency (UHF).

Abbreviations

In this thesis, we have adopted the following Abbreviations:

A	
AWGN	Additive White Gaussian Noise
B	
BER	Bit Error Rate
BS	Base Station
BDL	Best Down-Link based Scheme
BUL	Best Up-Link based Scheme
C	
CCDF	Complementary Cumulative Distribution Function
CSMA	Carrier Sense Multiple Access
C-RANs	Cloud Radio Access Networks
D	
D2D	Device-to-Deviced
DL	Down-Link
E	
EH	Energy Harvesting
F	
FSPL	Free Space Path-Loss
1G	First Generation
4G	Fourth Generation
5G	Fifth Generation
FAF	Floor Attenuation Factor

H

HetNets	Heterogeneous Networks
HPPP	Homogeneous Poisson Point Process

I

IC	Interference Cancellation
IM	Interference Management
INE	Interference plus Noise Environment
ILE	Interference Limited Environment
IoT	Internet of Things

L

LOS	Line-of-Sight
LTE	Long Term Evolution

M

MmWave	Millimeter Wave
MIMO	Multiple-Input and Multiple-Output
MHCP	Matern Hard-Core Point Process
mMTC	massive Machine-Type Communication

N

NLOS	Non-Line-Of-Sight
NBS	Nearest BS
NR	new radio
NOMA	Non-orthogonal multiple access

P

PL	Path Loss
PLE	Path Loss Exponent
PDF	Probability Density Function
PPP	Poisson Point Process

Q

QoS Quality of Service

R

RAT Radio Access Technologies

RRH Radio Remote Heads

S

2G Second Generation

SINR Signal-to-Interference-plus-Noise Ratio

SNR Signal-to-Noise Ratio

STP Successful Transmission Probability

SBS Strongest BS

T

2-D Two-Dimensional Space

3-D Three-Dimensional Space

3G Third Generation

3GPP Third Generation Partnership Project

U

UHF Ultra High Frequency

UE User Equipment

UP Up-Link

Notations

In this thesis, we have adopted the following notations:

$E(.)$	Expectation function
$\mathcal{L}[.]$	Laplace transform
$\exp(.)$	Exponential function
x_n	n^{th} abscissa (root) of the N^{th} order Laguerre Polynomial
w_n	n^{th} weight of the N^{th} order Laguerre Polynomial
R_N	n^{th} remainder of the N^{th} order Laguerre Polynomial
N_0	Noise power
λ_k	Density of k^{th} tier, $k \in \{1, 2, .., K\}$
P_k	Transmit power of tier k
d_{min}	Minimum distance between each two BSs
λ_{BS}	BS's density
α	Path loss exponent
μ	Constant attenuation per unit of path length
τ	Mean slope correction factor
ν	Carrier wavelength in meters
C	Celerity of light
f_c	Carrier frequency
A	Signal attenuation factor
h	Complex channel fading gain
P_{BS}	Transmit power of BS
η	Interference management efficiency

H_{BS}	Height of BS
C_K	Centers of rectangles (buildings)
λ_{BL}	Density of blockages
L_K	Lengths of blockages
W_K	Widths of blockages
H_K	Height of blockages
$f_L(x)$	Probability density functions of L_K
$f_W(x)$	Probability density functions of W_K
$f_H(x)$	Probability density functions of H_K
H_{UE}	Height of user
H_{BDG}	Height of buildings
$H_{\text{BDG}}^{(\text{max})}$	Maximum Height of buildings
$H_{\text{BDG}}^{(\text{min})}$	Minimum Height of buildings
ξ	Parameter equal to one (two) for the LOS (NLOS) case
$S_{\xi[\text{dB}]}$	Random shadowing factor
$F_{\xi[\text{dB}]}$	Random small-scale fading factor
f_ξ	Power in Watts of the small-scale fading
s_ξ	Log-normal shadowing power in Watts
$f^{(\text{NBS})}$	Probability density function of the nearest BS
$f^{(\text{SBS})}$	Probability density function of the strongest BS
γ_{th}	Predefined SINR threshold
P_{pc}	Transmit power of the picocells
P_{fc}	Transmit power of the femtocells
P_{BS}	Transmit power of the base station
λ_{pc}	Picocells' density
λ_{fc}	Femtocells' density
f_I	PDF of I
q	Transmission probability
K_{Rice}	the Rician factor
T_s	Sampling time
f_{max}	Maximum Doppler frequency shift

ν_{EH}	Rate of added power
TS_{max}	Maximal number of time slots
r_{EH}	Rayon of the spherical harvesting zone
λ_{RL}	Relays' density
H_{RL}	Height of relays
N_{RL}	Number of relays

Contents

Chapter 1

Introduction

1.1 Problem Statement and Motivations

The last two decades have seen a rapid growth of radio systems [1]. From the analog system of the first generation (1G) which provided public voice service [2], to the digital system introduced by the second generation (2G) which supported text messaging. In 1998, the third generation (3G) were launched, in order to improve data connectivity by providing data transfer up to 200kbit/s. The evolution of 3G technologies gave birth to the fourth generation (4G) network with the high-speed mobile broadband [3, 4]. Aimed to increase 4G performance, the fifth generation (5G) mobile network presents a new progressive version of the 4G /IMT-Advanced standards [5]. By providing higher capacity, lower suspension and low battery consumption, the 5G would support higher density of mobile users, ultra reliability and massive communications [6, 7].

Actually, the Third Generation Partnership Project (3GPP) is specifying the New Radio (NR), a new 5G radio interface [8–10]. The aim of 5G is wider than driving to higher system capacity, better coverage, and higher data rates [11, 12]. To achieve these targets, important contributions to the radio mobile networks have to be realized [13]. In this context, key enabling technologies, such as heterogeneous networks (HetNets), massive multiple-input and multiple-output (MIMO), millimeter wave (mmWave) communications, energy harvesting (EH), and massive machine-type communication (mMTC) or Internet of Things (IoT) [14–16] have been identified to bring 5G to fruition [17, 18]. 5G NR is defined to support very low device cost and energy consumption, provide extreme coverage, and handle very large numbers of devices. The 3GPP New Radio (NR)

is currently defined the three main categories for 5G communications: enhanced mobile broadband, ultra-reliable low-latency communication, and massive internet of things. Besides, NR presents the future of important 5G vertical applications especially applications dedicated to the automotive and health care industries [19]. Mmwaves, already in the first release, present one of the important NR features[20, 21]. Their high frequencies can support large transmission bandwidths, and offer huge traffic capacity and extreme data throughput [22–24].

Research papers discuss the potential directions to achieve goals of 5G radio access technologies (RATs), such as future releases of 5G and 6G. Future wireless challenges aimed to be addressed by flexible RATs components: service heterogeneity, spectrum scarcity, application variety, massive connectivity, device variety, and asynchrony of users [25]. In this context, to migrate to a new 5G NR, these challenges need more attention in order to improve quality of service (QoS), and network compatibility with current technologies. 5G wireless communication technology is expected to be the cure-all wonder solution to the current wireless networks' deficiencies [1].

To address these challenges, we need accurate realistic modeling, and new enhancement techniques. Hence, substantial research efforts are dedicated to the issues of realistic models and their impacts on the performance analysis, and on the proposed enhancement techniques, respectively. Assumptions usually present limits to describe the real characteristics of the network. Studies of cellular networks were mostly assuming unrealistic hypotheses such as 2-D wireless networks [26, 27]. In fact, 2-D models are tractable and very suitable for macro BSs in rural or suburban environments. But, they are inadequate for a dense urban areas, notably the small cells in high-rise centers. These models can't describe the system characteristics, mainly the real distance between a user and the BS. To improve the system model and to gain the exactitude of analytical expressions, it is important to elaborate models with realistic constraints.

In addition, new efficient techniques that enhance the communication system performances are needed. Otherwise, the key enabling technologies of 5G can have some serious performance implications. For example, mmwaves or high frequencies are associated with higher radio channel attenuation, limiting the network coverage. That's why, proposing techniques, algorithms, and schemes is recently becoming a trend for cellular network

research works.

Thus, accurate system modeling, performance analysis and development of enhancement techniques of cellular networks for current and next generations deserve a comprehensive study, which is the main focus of this thesis. In the next subsection, we present the literature review.

1.2 Related Works

In literature, different cellular networks models have been based on the Wyner model [28],[29], which is overly simple and typically one-dimensional, is inaccurate because of the dramatic variation in the signal-to-interference-plus-noise ratio (SINR) value. Some studies were concerned by the 2-D network model, where the locations of the base stations (BSs) were modeled as a homogeneous Poisson point process (HPPP) [30] with given density instead of assuming they were placed on a regular grid. Besides, others have been focusing their researches on a multi-tier cellular networks, where all network tiers were assumed to follow independent HPPPs and all tiers used the same frequency channel [31]. In [32], the 2-D network model was adopted to analyze the optimal BS density for both homogeneous and heterogeneous cellular networks with service outage probability constraint. These abovementioned works are all based on a 2-D network models. Thus, we need to elaborate a model closer to the reality.

To the best of our knowledge, few papers have addressed the 3-D modeling of cellular networks. In [33], considering a high-rise centers for cellular network, the coverage probability of a target user was studied extending the classical 2-D model to the 3-D one. By assuming that, for any distance between the transmitter and the receiver, the floor attenuation factor (FAF) is constant, the proposed model in [33] presents limits to describe the real characteristics of the network. Actually, the numbers of obstacles and the attenuation varie as a function of this distance. Moreover, the derivation of the coverage probability expression consider only path loss exponent (PLE) coefficient $\alpha \geq 4$. Unlike to realistic scenario, all the cells are assumed to transmit at the same time and with the same transmit power for each cell. However, [33] has supposed that only one type of small cells are deployed, which presents an additional limitations to model different microcells, e.g.,

picocells and femtocells. In the same context, [34] has presented a new 3-D model for 2-tier cellular networks. This 3-D based Poisson point process (PPP) model described the small cells positions in HetNet. However, the nodes did not simultaneously transmit such as a different transmission probability is employed for each type of cells.
The models in [33, 34] did not consider the constraint of minimum inter-BSs distance. Also, the performance of UHF based cellular networks was analyzed without examining other telecommunication technologies such as mmWave for example.
Moreover, researchers have proposed various propagation models to focus on the blockage effects such as trees, buildings,.. that can cause the decrease of the wireless networks performance. In [35], the authors have proposed a stochastic geometry framework in order to analyze the coverage, and the transmission rates of mmWave networks for both outdoor users and infrastructure. Considering large-scale blockages, this research work has used a distance-dependent line-of-sight (LOS) probability function, where BSs were deployed as independent homogeneous LOS and non-line-of-sight (NLOS) point processes. The random shape theory concept has been used in [36], to model the cellular networks with randomly distributed buildings. Actually, these blockages have been modeled as a Boolean scheme of rectangles, which allows a comprehensive characterization of the blockage randomness, such as sizes, locations, orientations, and heights. However, the proposed modeling in [35, 36] is limited to studying the homogeneous 2-D cellular networks, where a more realistic 3-D space modeling is needed. The authors in [35, 36] have studied the NLOS (LOS) environments under the assumption of Rayleigh (Rice) channel fading, respectively.
Furthermore, some research work [37, 38] has employed Nakagami fading and have considered that Rayleigh fading is not accurate for mmWave networks due to their poor scattering property. The authors in [39] have studied heterogeneous down-link mmWave cellular networks by considering different Nakagami fading parameters for LOS and NLOS components. The authors in [40] studied channel modeling in lab environment. They designed a directional antenna and calculated the PLE by modeling the channel with their proper measurement setup. They proposed an active down conversion wireless system at 2.4 GHz, in order to improve the measured path loss of the channel. These papers have

not addressed the problem of blockages for 3-D mmWave based cellular networks. By taking into account small-scale and large-scale fading, the authors in [41] have studied the 3-D cellular networks performance in urban areas. This research work has been focusing on both closest and strongest BS association, where Nakagami-m fading has been considered to only model the LOS fading.

In carried out literature, many related research works, developing techniques for the enhancement of cellular networks, have been published so far. Recently, some researchers have emerging device-to-device (D2D) relaying as a solution to overcome the limits of mmWave coverage, since it maintains the topology of network and requirements of infrastructure. In [42], the authors have introduced D2D relays in mmWave cellular networks, and evaluated the coverage probability and spectral efficiency. However, this research paper presents limits, by neglecting multi-path fading in mmWave channel model and, by considering a 2-D homogeneous Poisson Point Process (PPPs) to model BSs, users, and obstacles. The mmWave transmission is only possible when a LOS path exists, the above criterion indicates that the UE always associates with the nearest LOS BS in cellular mode or the nearest LOS candidate relay UE in mmWave D2D relay mode. In [43], the communication scenario underlying a cellular network for uploading the content toward the eNodeB. The channel is modelled as the Rayleigh fading channel, where the bandwidth is assumed to be 1.4 MHz and 20 MHz. Besides, the contribution of this research paper is considered when direct communication does not provide a better rate, then, the device attempt for Multihop communication. In this scenario, the authors assumed two hop communication. First hop communication is in D2D mode while second hop communication is in cellular mode. Unlike to our proposed scheme where the selection mode is based on the distance, in this research work, the first constraint dictates that the cell edge device pursue Multihop communication if it seconds better channel gain for both hops compared to direct channel gain. The second constraint indicates that the power depleted in a two hop communication should be less than the direct power that is depleted. The third constraint means that the selected relay has sufficient energy. The fourth constraint means that the required number of resource blocks in two hops (D2D and CU) is less than single hop. The fifth constraint means that the required uploading time in two hops (D2D and CU) is less than the uploading time for a single hop. [44] model the cellular/D2D links as

well as the interference links, both the large-scale power law propagation model and the small-scale (e.g., Rayleigh fading) model are taken into account. In the relay cooperative communication, the most secure relay node is selected for data forwarding based on the consideration of security. The stronger the social relationship between users is, the larger the security of data forwarding is. In this paper, a social-aware based secure D2D cooperative communication relaying scheme is proposed. A distance-based scheme is also introduced, so the selection of the most appropriate relay is based on the minimum sum of the distances from the D2D transmitter to the relay and the receiver to the relay respectively. On the other hand, in [45], a mode selection scheme has been proposed to select either the D2D or the cellular communications mode. This proposed scheme is based on a comparison between the D2D and up-link (UL) distances. In the same context, [46] has presented a comprehensive and tractable study for D2D enabled UL cellular networks, where, based on truncated channel inversion power control, a mode selection scheme was introduced. [47] has proposed a D2D mode selection, where the down-link (DL) received signal strengths of cellular and D2D links are considered. This paper has studied the problems of D2D mode selection, with user mobility. In addition, it has proposed an analytical framework for mode selection in moving D2D scenarios. However, [42, 45–47] present limits, by neglecting multi-path fading in mmWave channel model and, by considering a 2-D homogeneous PPPs to model BSs, users, and obstacles.

On the other hand, to enhance the cellular wireless networks, researches have been focusing on studying the energy harvesting for 5G mobile networks. Energy harvesting can increase the transmit power, which leads systematically to reduce the delay of the successful transmission, and by consequence, it contributes to improve the ergodic capacity. Some research studies have supposed that BSs and users harvest energy from environment. For instance, [48] investigated the effects of different orientated photovoltaic cells on the green energy utilization of small BSs. Others have supposed that the energy is harvested from ambient radio signals. The authors in [49] investigated the feasibility of implementing UHF-based ambient energy harvesting in ultradense small cell networks and examined the related tradeoffs for a typical user in the down-link. In [50], D2D communication with UHF energy harvesting in down-link cellular network has been proposed such as the battery free dynamic D2D transmitters scavenge the energy from UHF signal

interference. However, these contributions [49–52] have proposed to employ the energy harvesting to improve the communication in 2-D modeled mobile networks.
In light of the aforementioned related work, our contributions in this thesis can be summarized as presented in the following subsection

1.3 Contributions

This thesis work focuses on a new general 3-D space model for a cellular network based on PPP. The 3-D model can better capture the increasingly opportunistic and dense small cells deployment in future heterogeneous cellular networks. In particular, the key contributions of our work are summarized as follows:

- **Proposing a new 3-D space model for a cellular network :**
  In the first part of this contribution, we propose a general 3-D model for mmWaves and UHF based multi-tier cellular networks. The proposed model is based on a Matrn Hard-Core Point Process (MHCP) which respects a minimum inter-BSs distance between cells positions in the network [53, 54]. The second part introduces a 3-D model for wireless communication systems in order to evaluate their performance under hybrid fading assumption for LOS and NLOS environments [55]. This model is based on the concepts of 3-D stochastic geometry that describes the different cells positions in the network with realistic constraints, and the random shape theory which characterizes the random blockages in urban cellular networks. This thesis includes a detailed derivations of closed form expressions of the probability density function (PDF), the successful transmission probability, the average bit error rate (BER) as well as the average ergodic capacity under the proposed 3-D model. Furthermore, the expressions of the PDF and coverage probability under the proposed 3-D modeling. are derived when blockages effect is taken into consideration. Those metrics are used to investigate the advantages of the proposed 3-D model on dense urban wireless communications systems performances and based on which comparative studies are conducted.

- **Developing new efficient techniques that enhance the communication system performances:**

This thesis develop new efficient techniques in order to enhance communications systems performance. First, we introduce an energy harvesting based scheme for 3-D cellular network which reduces the transmission delay and enhances the ergodic capacity [18]. The stochastic geometry is used to describe the different cells' positions in the network with realistic constraints. Based on that, the average transmission delay and the ergodic capacity expressions are detailed and derived. Then, by considering a nakagami-m fading channel assumption for MmWaves communications, we propose a new min/max scheme to enhance the successful transmission. This scheme is based on the selection of an available relay UE that can assist the transmission [56]. Based on stochastic geometry and random shape theory, we derive the expressions of the probability density function, and the successful transmission probability. Using numerical results, the analytical derived expressions are evaluated, and the advantages of each proposed scheme are investigated.

1.4 Publications

The work presented in this thesis has led to the following publications:

Journal papers

1. **S. Bachtobji**, A. Omri, R. Bouallegue, and K. Raoof, Modeling and Performance Analysis of MmWaves and Radio Frequency based 3-D Heterogeneous Networks, IET Communications, Volume 12, No. 3, pp. 290 - 296, 2018.

2. **S. Bachtobji**, A. Omri, k. Hassan, R. Bouallegue, and K. Raoof, Relay Selection Scheme for Device-to-Device based 3-D Millimeter-Wave Cellular Networks, IET Communications, August 2019.

Conference papers

1. **S. Bachtobji**, A. Omri, and R. Bouallegue, Modelling and performance analysis of 3-D mmWaves based heterogeneous networks, IEEE International Wireless Communications & Mobile Computing Conference (IWCMC), Paphos / Cyprus, 2016.

2. **S. Bachtobji**, A. Omri, K. Hassan, R. Bouallegue, and K. Raoof, Performance Analysis of Energy Harvesting based scheme for 3-D Cellular Networks, IEEE International Wireless Communications & Mobile Computing Conference (IWCMC), Limassol / Cyprus, 2018.

3. **S. Bachtobji**, K. Hassan, A. Omri, K. Raoof, and R. Bouallegue, 3-D Modeling and Analysis of Blockage Effects on the Performance of Urban Wireless Communication Systems, International Conference on ICT Convergence (ICTC), Jeju Island / Korea, 2018.

1.5 Thesis Organization

The outline of the thesis are as follows:

Chapter 2 provides an overview of fading effects in wireless communications and some details of mathematics tools. It presents the two three-dimensional space models of wireless communication networks proposed within this thesis. These models describe the system, when the blockages effect is taken into consideration, and when they are neglected, respectively. This chapter presents also the derivation of the closed form expressions of the PDF, the SINR and the path loss for each model.

Chapter 3 proposes a performance analysis of 3-D wireless communication networks introduced in the chapter 2. It presents comparative studies, and details derivation of the closed form expressions of the successful transmission probability, average throughput, and the average BER.

By taking into account blockage effects, chapter 4 details the performance analysis, and derives, also, the expressions of LOS probability and coverage probability for UHF and mmwaves systems. The Analytical results are validated by simulation results, and comparative analysis of the proposed model is provided.

A new scheme for 3-D cellular networks was proposed in chapter 5 in order to enhance communications system performance. The proposed scheme is based on the energy harvesting in order to reduce the transmission delay and consequently, enhance the ergodic

capacity. In this part, we derive the expressions of the average transmission delay and the ergodic capacity. Finally, simulation results are used to validate the analytical expressions, and to confirm the advantage of the proposed schemes in enhancing cellular network performances.

In Chapter 6, in order to mitigate blockages effect and enhance the coverage probability, D2D relaying is used to improve the direct link (DLK) reliability. Thus, we propose a new communication scheme to select the relay user equipment (UE). Based on stochastic geometry and random shape theory, we derive the expressions of the PDF, and the successful transmission probability of the proposed scheme. Using numerical results, the derived expressions are evaluated, and the advantages of the proposed scheme is investigated.

Finally, general conclusions and perspectives are presented.

Chapter 2

Three-Dimensional Space Modeling of Wireless Communication Networks

2.1 Introduction

Three-dimensional space modeling of cellular networks offers realistic and accurate system models. These 3-D models can be used to efficiently evaluate the performances of the current and next mobile network generations. This chapter proposes two 3-D models of wireless communication networks in two different cases: (i) when the blockages effect is taken into consideration, and (ii) when they are neglected. In this context, we present the employed mathematical tools in the 3-D modeling. Then, we detail first the fading effects in wireless communications. Based on that, we derive closed form expressions of the probability density function (PDF) of the distance from user to the selected BS, and the signal-to-noise ratio (SNR).

2.2 Mathematical Tools

In this research work, stochastic geometry is the main mathematical tool that has been used in communication systems modeling. As a probability theory branch, stochastic geometry can be used to describe the behavior of random configurations, such as random graphs, random networks, random cluster processes, random unions of convex sets, random mosaics, and many other random geometric structures. This theory may be im-

plicated in a large number of applications. This is because its strong connections to the classical field of stereology, to communication theory and spatial statistics.

The stochastic geometry is very useful for studying wireless networks, since the interference, the capacity, and system performances are sensitive to nodes positions [57, 58]. Stochastic geometry offers, in several cases, closed form expressions for the spatial component, which allows to further study the wireless systems and consequently to increase their performance, and to reduce their costs [59].
In the next subsection, we detail the different types of stochastic geometry process that can be used for wireless communication modeling.

2.2.1 Poison Point Process

Points present the basic elements of practical geometry applications. A collection of points randomly distributed in the space are described by point fields, random point patterns, or point processes which are equivalent mathematical terminologies. They are often found in studies into nature and technology [60].

In probability, statistics and related fields, a PPP or a Poisson process or a Poisson point field is a random object. In a mathematical space, it deals with points with random positions. The process, generally defined in Euclidean space, has convenient mathematical properties [61]. These properties allow PPP to be used as a mathematical model for evidently random processes in many applications, such as astronomy, biology, ecology, geology, physics, image processing, and telecommunications.

The PPP is characterized by a process with each point stochastically independent of all other points, distributed with density λ. Thus, it is sometimes called a purely or completely random process [62]. Based on that, the pdf of the distance to the n-th nearest neighbor, for 2-D models, is expressed as follow [63]

$$PR_n(r) = r^{2n-1}(\lambda\pi)^n \frac{2}{\Gamma(n)} \exp(-\lambda\pi r^2), r > 0. \tag{2.1}$$

For $n = 1$ (nearest neighbor), this is a Rayleigh distribution. The mean distance is $1/(2\sqrt{\lambda})$. It does not matter whether we measure from an arbitrary point of the plane or from a point of the process.

The Laplace functional $\mathcal{L}$ of a point process Φ is defined by the following formula

$$\mathcal{L}_{\Phi}(f) = \mathbb{E}\left[\exp\Big(-\int_{\mathcal{R}^d} f(x)\Phi(dx)\Big)\right]. \tag{2.2}$$

where f runs over the set of all non-negative functions on $\mathcal{R}^d$. Note that the Laplace functional completely characterizes the distribution of the point process. Indeed, the Laplace functional of the Poisson point process of intensity measure Λ is

$$\mathcal{L}_{\Phi}(f) = \exp\left(-\int_{\mathcal{R}^d}\Big(1-\exp(-f(x))\Big)\Lambda(dx)\right) \tag{2.3}$$

2.2.2 Matern Hard Core Process (MHCP)

An hard core point process (HCPP) is a repulsive point process where no two points of the process coexist with a separating distance less predifined hard core parameter.
This point process, introduced by B. Matern, is a typical example for models derived from PPP [64], the latter being an important basis for constructing more complicated point processes, random sets and fibre processes. It has been successfully applied to real data, it has been used in ecological and carrier sense multiple access (CSMA) network modeling, as well as geographical analysis. For MHCP, there are two different types that are detailed as follows.

2.2.2.1 MHCP of Type I

The first type of MHCP is obtained by deleting every point in the process with its nearest neighbor closer than a given hard-core distance. Two competing points of an underlying Poisson process can both be removed with some probability depending on a deterministic function [64].
Let X be stationary PPP with balls of fixed radius as marks, X_I is thinned process (overlapping grains removed) and X_I^o is the ground process after removing the grains. Hard-core processes have a guaranteed minimum distance d_{min} between all pairs of point [65]. As shown in Figure 2.1, the MHCP of type I X_I^o contains all points of X which have no neighbors in X, i. e. a retained point doesn't have any point in X at a distance of d_{min} or lesser [66].

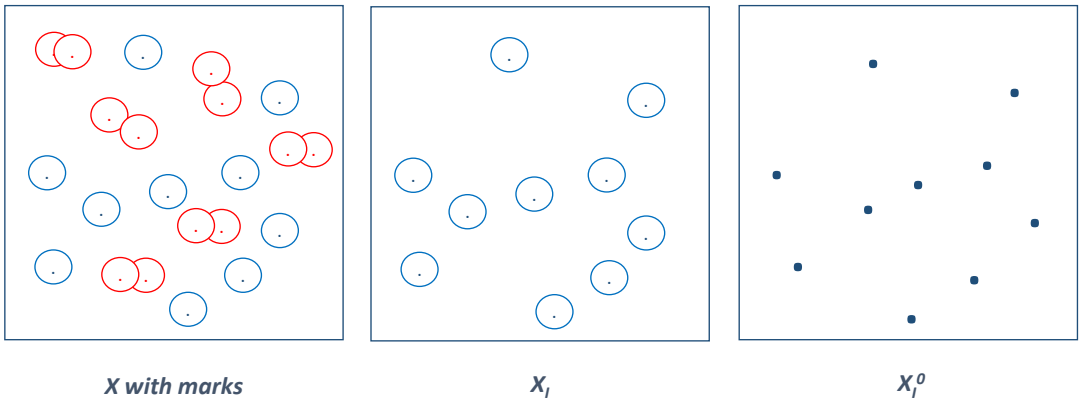

Figure 2.1: MHCP of type I

2.2.2.2 MHCP of type II

Concerning MHCP of type II, the weights are assigned to all the points and in a competition between two points only one of them, namely the point equipped with weight greater than or equal to the weight of the other one will be removed with some probability [64].

Figure 2.2 illustrates the points of X that are assigned independent marks (uniformly distributed in the interval [0, 1], usually interpreted as birth times). We can clearly see that only points, older than all their neighbors, survive in X_I^o [66].

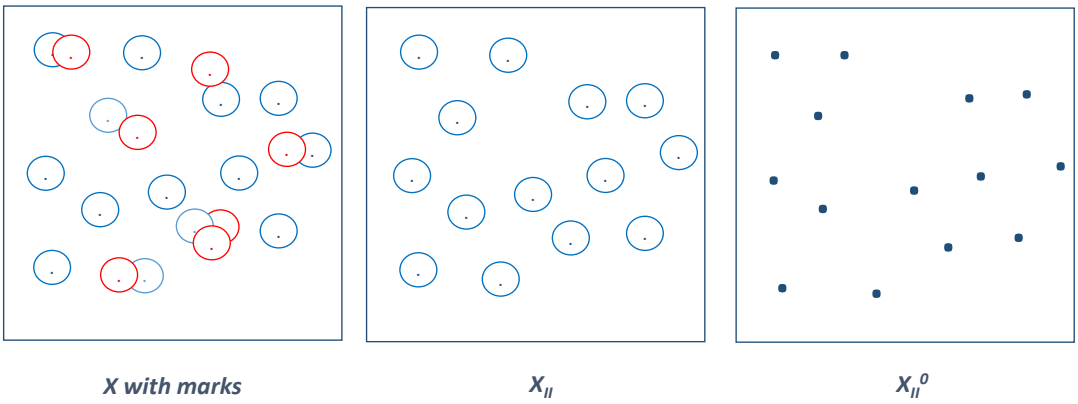

Figure 2.2: MHCP of type II

Accordingly, respecting a minimum distance, d_{min}, between each two BSs, the locations of BSs are distributed according to a MHCP of Type II, Φ, which is based on a parent PPP, Φ_p, of density λ_p. In MHCP of type II process, each node (from the parent nodes) has a random associated mark, and a node is not retained only if there is another

node within distance d_{min} with a smaller mark. Accordingly, and based on the correlation between the node retaining events, the probability that a given BS is retained, is derived in [67] and is equal to

$$Pr_{_q} = \frac{1 - \exp(-\frac{4}{3}\pi\lambda_{_p} d_{min}^{3})}{\frac{4}{3}\pi\lambda_{_p} d_{min}^{3}}. \tag{2.4}$$

The density λ of the new MHCP of Type II Φ is derived by weighting $Pr_{_q}$ with the PPP density $\lambda_{_p}$ [67], and is equal to

$$\lambda = \frac{1 - \exp(-\frac{4}{3}\pi\lambda_{_p} d_{min}^{3})}{\frac{4}{3}\pi d_{min}^{3}}. \tag{2.5}$$

For the 2-D case, the expression of $\lambda_{_{2D}}$ is as follows,

$$\lambda_{_{2D}} = \frac{1 - \exp(-\pi\lambda_{_p} d_{min}^{2})}{\pi d_{min}^{2}} \tag{2.6}$$

2.3 Fading in Wireless Communications

The wireless signal characteristics change while they move from the transmitter to the receiver antenna. They depend upon the distance between the two antennas, the path(s) taken by the signal, and the environment (buildings and other objects) around the path [68, 69]. If we have a model of the medium between the transmitter and the receiver, we can predict the received signal profile from that of the transmitted one. The channel model is this model of the medium [70].

Thus, the transmitted signal x, after propagation through the channel h, is transformed to y, which can be presented as follows

$$y(f) = h(f)\, x(f)\, + n(f), \tag{2.7}$$

Where $h(f)$ is channel response, and $n(f)$ is the noise. x, y, H, and n are all functions of the signal frequency f. As shown in the figure 2.3, the key components of the channel response are path loss, shadowing, multipath, and material penetration.

2.3.1 Path Loss

When there is no object that blocks the link between the transmitter and the receiver, the free space line of sight channel is consider. By supposing this case, once the energy is

spread spherically around the transmitting antenna, the signal attenuates and the received power can be expressed as follow [70, 71]:

$$P_r = P_t \left[\frac{\sqrt{G_l}\,\lambda}{4\pi d} \right]^2 , \tag{2.8}$$

where, P_t is the transmit power, G_l is the product of the transmit and receive antenna field radiation patterns, λ is the wavelength, and d is the distance. Compared to theory, where the power decreases with the squared distance, the power decreases rapidly, in practice, almost third or fourth power of distance. The ground may produce some of the waves, which reflect and attain the receiver. Having a phase shift of $180°$, these reflected waves can affect the net received power. Thus, the received power is given by [71],

$$P_r = P_t \frac{G_t G_r h_t^2 h_r^2}{d^4} \tag{2.9}$$

Where, h_t and h_r are the antenna heights of the transmitter and receiver, respectively. Here, the antenna heights and the wavelength are assumed to be neglected. Another formula for path loss is given by,

$$P_r = P_t P_0 \left(\frac{d_0}{d} \right)^{\alpha} , \tag{2.10}$$

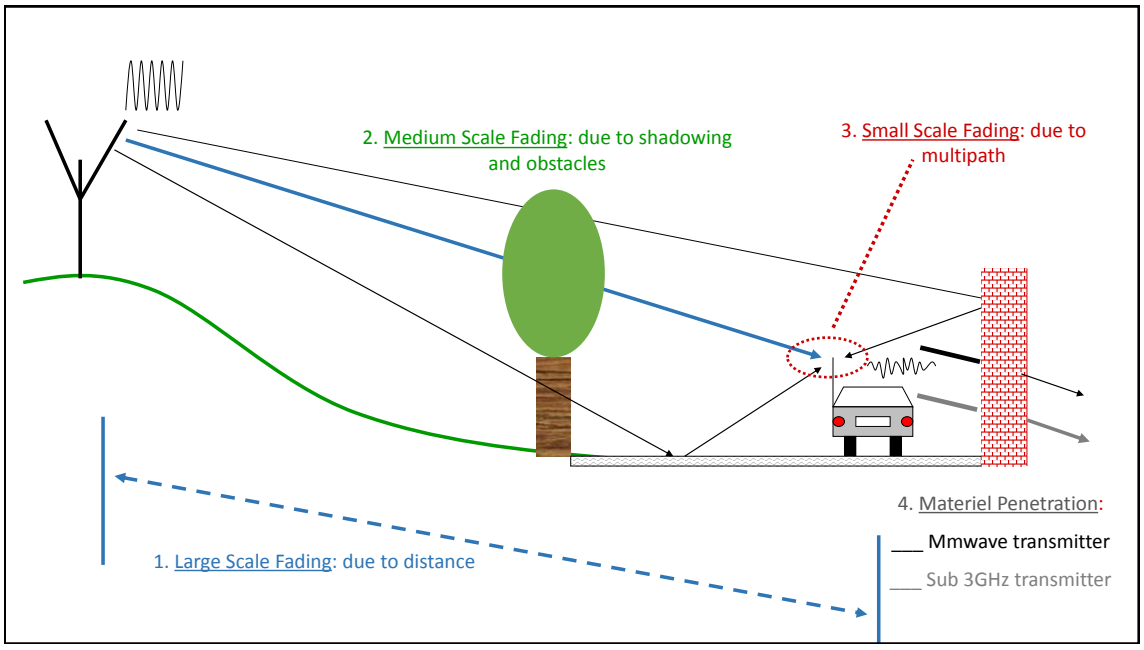

Figure 2.3: The wireless channel response components [70].

where, P_0 is the power at a distance d_0 and α is the path loss exponent. The path loss is given by:

$$PL(d)_{[dB]} = PL(d_0) + 10\alpha \log\left(\frac{d}{d_0}\right), \tag{2.11}$$

Here, $PL(d_0)$ is the mean path loss in dB at distance d_0. Figure 2.4 shows the received power is depending on the distance between the transmitter and the receiver.

2.3.2 Shadowing

The existence of objects (such buildings or trees), in the signal path, may affect the signal. This is due to absorption, reflection, scattering, and diffraction, called also shadowing. The shadowing is, when the middle building cast a shadow on the received antenna. Thus, the path loss expression is given by [71],

$$PL(d)_{[dB]} = PL(d_0) + 10\alpha \log\left(\frac{d}{d_0}\right) + \chi, \tag{2.12}$$

where, χ is a normally (Gaussian) distributed random variable (in dB) with standard deviation σ. χ is the shadowing effect. Once the shadowing affects the signal, the received power will be different for the points at the same distance d from the transmitter. This power has a log-normal distribution. This phenomenon is lognormal shadowing.

2.3.3 Multipath

The receiver may receive reflected waves produced by objects around the path of the wireless signal. These reflected signals has different amplitudes and phases by taking a different path. These multiple signals influence the received power by increasing or decreasing it at the receiver. The total received power and the signals are sensitive to the UE's positions [70].

We can clearly see the three components of the channel response in Figure 2.4. The lognormal shadowing changes the total loss. In addition, signal strength variations due to multipath change at distances in the range of the signal wavelength.

2.3.4 Material Penetration

The radio wave propagation characteristics differ from one frequency band to another. As presented in figure 2.5, compared to signals at lower frequencies, mmWaves are more vul-

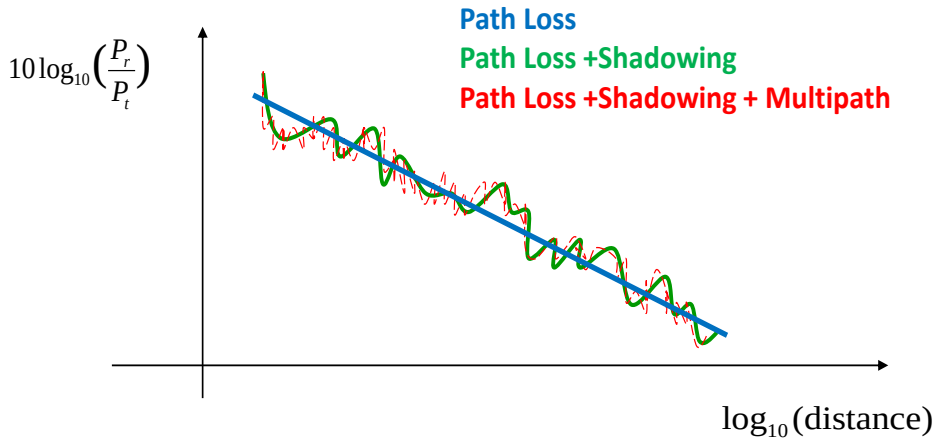

Figure 2.4: Path loss, shadowing, and multipath [71].

nerable both to atmospheric effects and to human shadowing and cannot propagate well through most materials [72]. Thus, these effects cannot be neglected in the modeling process. The high penetration loss of signals arriving from outdoors in indoor environments limits the range of the covered area and emphasizes the need for HetNet in providing coverage for the obstructed environments. Explicitly, HetNets would allow a wireless system to communicate with a user suffering from an obstructed mmWave link through a different wireless technology, such as the existing legacy wireless systems operating in lower frequency bands.

2.4 3-D System and Channel Modeling without Blockage Effects

In this subsection, a 3-D HetNet in the context of a high-rise building environment is considered, where K-tiers of BSs are randomly located, with densities λ_k ($\lambda_p = \sum_{k=1}^{K} \lambda_k$), and transmit powers P_k, $k \in \{1, 2, .., K\}$. Each tier is different in terms of average transmit power, and BS density. Fig. 2.6 presents the 3-D space system model, with the case of $K = 3$, and a side length $2R = 100$ m. The density λ_{BS} of the new MHCP of Type II,

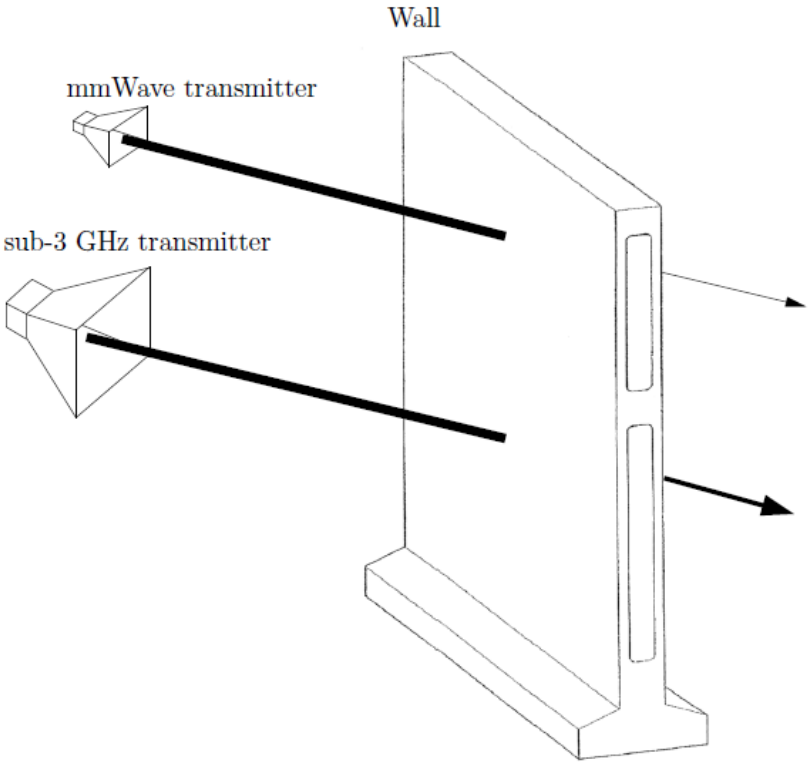

Figure 2.5: Material penetration for mmWave transmitter and a sub-3 GHz transmitter [72].

Φ, is derived by weighting q with the PPP density λ_p [67], and is equal to

$$\lambda_{\text{BS}} = \frac{1 - \exp(-\frac{4}{3}\pi\lambda_p d_{min}^3)}{\frac{4}{3}\pi d_{min}^3}. \tag{2.13}$$

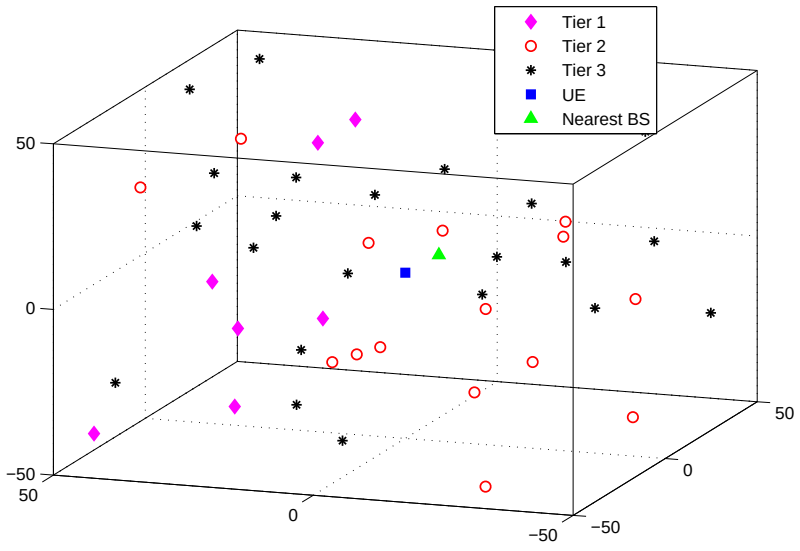

Figure 2.6: 3-D model of a 3-tiers HetNet.

By considering an independent collection of user equipments (UEs), each active UE, located according to a PPP, Φ_u, with density λ_u, communicates with its nearest BS. The nearest BS, that can be one of the three tiers type, is the closest BS to the UE. As the cells' density is usually smaller than that of UEs, we assume that the cells are active at the same time, and the UEs are active with a given access probability. Each cell is only able to communicate with one active user via a given access channel at the same time. Also, all the channels are assumed to be independent Rayleigh fading, and the noise is an additive white Gaussian noise with zero mean and power $N_{_0}$. Let us consider a target UE that is located at the origin of the coordinates within a distance r from its nearest BS, $c_{_o}$. Based on this system model, we detail in the following, some fundamental expressions that are needed for the performance analysis of wireless communication systems.

2.4.1 Path Loss Models

The above presented system model has been used to study the communication between an active user and its target BS in two frequency bands, namely Ultra High Frequency (UHF) bands and mmWave ones.

2.4.1.1 UHF Path Loss Model

Regarding the low and high frequency bands, the Devasirvatham model is widely used in literature to explain the effect of the presence of huge number of obstacles (walls and/or floors) [73], such as,

$$PL_{_{UHF}}(r) = PL_{_{UHF}}(r_{_0}) + 10\ \alpha\ \log_{10}\left(\frac{r}{r_{_0}}\right) + 10\ \log_{10}\left(\mu r\right), \tag{2.14}$$

where, $PL_{_{UHF}}(r_{_0})$ is the path loss at distance $r_{_0}$, α is the path loss exponent, and μ is a constant attenuation per unit of path length. Depending on the surroundings, μ extends from 0.2 to 0.7 [dB/m] [73].

2.4.1.2 Millimeter Waves Path Loss Model

The path-loss model expression for mmWave bands is given by [74]

$$PL_{_{mmWave}}(r) = FSPL + S \tag{2.15}$$

with,

$$FSPL = \tau\ 10\ \alpha\ \log_{10}\left(\frac{r}{r_{_0}}\right) + PL_{_{mmWave}}(r_{_0}), \tag{2.16}$$

where, τ is the mean slope correction factor (unit-less), which is obtained directly from experiments, and $PL_{_{mmWave}}(r_{_0})$ presents the free space path loss in dB at a close-in reference distance $r_{_0}$, which is expressed as [74]

$$PL_{_{mmWave}}(r_{_0}) = 20\ \log_{10}\left(\frac{4\pi r_{_0}}{\nu}\right), \tag{2.17}$$

Where, $\nu = \frac{C}{f_c}$ is the carrier wavelength in meters, C is the celerity of light, f_c is the carrier frequency, and S is the typical log-normal random shadowing variable with 0 dB mean, and standard deviation σ $(8.2 < \sigma < 10.6)$ in dB [74].

Therefore, and based on (2.14-2.17), we express the signal attenuation, depending on the path loss, and floor attenuation factor, in a general expression for both UHF and mmWave communications as follows

$$A_{_{M1}}\ r^{-\beta}, \tag{2.18}$$

where, $A_{_{M1}}$ is a coefficient that is defined by,

$$A_{_{M1}} = \frac{r_{_0}^{\beta}}{\gamma\ 10^{^{PL_0/10}}}, \tag{2.19}$$

and,

$$(\beta, \gamma, PL_{_0}) = \begin{cases} (\alpha+1, \mu, PL_{_{UHF}}(r_{_0})) & \text{for UHF bands,} \\ (\tau\alpha, 10^{\frac{S}{10}}, PL_{_{mmWave}}(r_{_0})), & \text{for mmWave bands.} \end{cases} \tag{2.20}$$

2.4.2 Signal-to-Interference-plus-Noise Ratio

For both transmission bands under consideration, we assume that the same frequency bands are used at the same time by the different BSs, and hence the power of total interference, for a specified receiver, is calculated by collecting power received from all small cells excluding the home station power. Let $h \sim \mathcal{CN}(0, \Omega_h)$, and $g_i \sim \mathcal{CN}(0, \Omega_g)$ be the complex channel fading gains of the links between the BS i , $i \in \Phi\backslash\{c_{_o}\}$, and u, respectively. Accordingly, the SINR at u can be expressed as

$$\text{SINR} = \frac{P_{_{\text{BS}}} H A_{_{M1}} r^{-\beta}}{\eta I + N_{_0}}, \tag{2.21}$$

where,

$$I = \sum_{i \in \Phi \setminus \{c_o\}} q P_i G_i A_{M1} r_i^{-\beta}, \tag{2.22}$$

where, $H = \|h\|^2$, $G_i = \|g_i\|^2$, r_i is the distance between the BS i and u, $P_i(P_{\text{BS}})$ is the transmit power of BS $i(c_o)$ which can be the transmit power of any tier k, i.e., $P_i(P_{\text{BS}}) \in \{P_1, P_2, ..., P_K\}$, and η, $0 \leq \eta \leq 1$, denotes the interference management efficiency, i.e., $\eta = 0$ means that we have a total interference cancellation (IC), and $\eta = 1$ means that there is no interference management (IM). P_{BS} is the transmit power of BS that can be femtocell or picocell with a transmission probability q.

2.4.3 Probability Density Function

In this subsection, we derive the PDF of the distance r, which is denoted by f. The expression of f is essential to derive the performance analysis expressions. The probability that r is larger than a distance R is the probability that no BS exists in the sphere of volume $\frac{4}{3}\pi\lambda_{\text{BS}}R^3$. Based on [34], an approximate expression of this probability can be written as follows,

$$\Pr\{R < r\} \approx \exp\left(-\frac{4}{3}\pi\lambda_{\text{BS}}R^3\right), \tag{2.23}$$

This is the complementary cumulative distribution function (CCDF) of r. Based on that, the approximate expression of the PDF, f, is given by

$$f(r) \approx 4\pi\lambda_{\text{BS}}r^2 \exp\left(-\frac{4}{3}\pi\lambda_{\text{BS}}r^3\right). \tag{2.24}$$

2.5 3-D System and Channel Modeling with Blockage Effects

As shown in Figure. 2.7, a 3-D model in the context of a high-rise buildings environment is considered, where BSs are randomly located according to PPP, with densities λ_{BS}, transmit power P_{BS}, and height H_{BS}. We use a Boolean scheme of random rectangles to model randomly located blockages. Based on that, random shape theory, which is a branch of advanced geometry that formalizes random objects in space [60, 75], the centers of the rectangles C_K form a homogeneous PPP of density λ_{BL}, the lengths L_K, widths W_K of

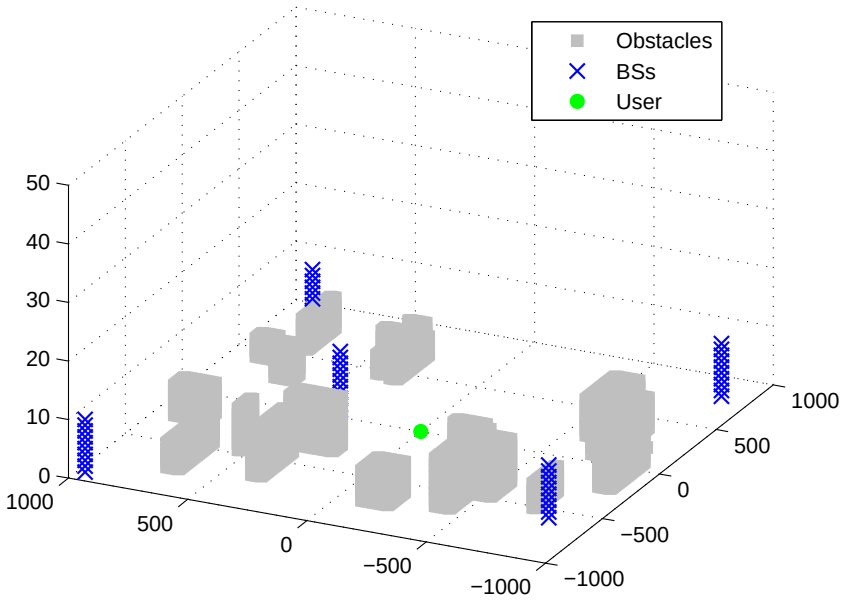

Figure 2.7: The system model when taking into consideration blockages.

the rectangles, and the height H_{K} of blockages are assumed to be distributed according to given probability density functions $f_{L}(x)$, $f_{W}(x)$, $f_{H}(x)$ respectively. Each UE, with height H_{UE}, communicates with its nearest BS. Here, we assume that each cell is only able to communicate with one active user via a given access channel at the same time. Let us consider a target user u that is located at the origin of the coordinates within a distance r from its nearest BS c_{o}.

2.5.1 Path Loss Models

Considering the blockages effect, Rayleigh and Rice fading are assumed for UHF communications, while the Nakagami-m fading assumption is made in the case of mmWave communications.

2.5.1.1 UHF Path Loss Model

For low frequency bands, we assume Devasirvatham model as presented in section 2.3.2.1. Thus, the path loss is expressed as in (2.14), and A_{M2} is expressed as follows,

$$A_{M2} = \frac{r_{0}^{\alpha+1}}{\mu\, 10^{PL_{UHF}(r_{0})/10}}, \tag{2.25}$$

2.5.1.2 MmWave Path Loss Model

The authors in [35, 76, 77] have proposed path loss with different value of path loss exponent and random shadowing for each environment (LOS or NLOS). Moreover, based on [78], which is considering random fading and shadowing effects impairing the wireless transmission, and which is focusing on the determination of LOS and NLOS environments, the general path-loss model, for mmWave communications with blockages effects is presented as follows,

$$PL_{\xi[\text{dB}]} = FSPL_{\xi[\text{dB}]} + S_{\xi[\text{dB}]} + F_{\xi[\text{dB}]}, \tag{2.26}$$

where, ξ is a parameter equal to one (two) for the LOS (NLOS) case [35,76,77], $FSPL_{\xi[\text{dB}]}$ is the free space path-loss (FSPL), which is expressed as [74],

$$FSPL_{\xi[\text{dB}]} = 20\ \log_{10}\left(\frac{4\pi f_c}{C}\right) + 10\ \alpha_\xi \log_{10}(r), \tag{2.27}$$

with, α_ξ is the path loss exponent, $S_{\xi[\text{dB}]}$, and $F_{\xi[\text{dB}]}$ are the random shadowing and small-scale fading factors, respectively.

The A_{M2} attenuation factor is expressed as follows

$$A_{M2} = \left[\frac{C}{4\pi f_c}\right]^2, \tag{2.28}$$

2.5.2 Signal-to-Noise Ratio

Based on this system, we detail in the following, the SNR expressions for UHF and Mmwaves bands, that are needed for the performance analysis of wireless communication considering blockage effects.

2.5.2.1 UHF Communication

For these frequency bands, we consider a noise limited system, where the effect of interference signals is ignored either because the system is not affected by interference, where orthogonal frequencies are used for example, or perfect interference cancellation is conducted. Accordingly, the SNR at u can be expressed as

$$\text{SNR} = \frac{P_{\text{BS}} H A_{M2} r^{-(\alpha+1)}}{N_0}, \tag{2.29}$$

2.5.2.2 MmWave Communication

Based on the path loss expression presented in the above section, the value of the instantaneous received SNR at a given user can be expressed as follows,

$$\text{SNR} = \sum_{\xi=1}^{2} \frac{p_{\xi}\ P_{\text{BS}}\ A_{M2}\ s_{\xi}\ f_{\xi}\ r^{-\alpha_{\xi}}}{N_0}. \tag{2.30}$$

The remaining parameters are given in the LOS $(\xi = 1)$ and NLOS $(\xi = 2)$ cases, such as $p_1(p_2)$ is the probability of LOS (NLOS). s_{ξ} is the log-normal shadowing power in Watts, which is expressed as

$$s_{\xi} = 10^{-\frac{S_{\xi[\text{dB}]}}{10}}, \tag{2.31}$$

where, $S_{\xi[\text{dB}]}$ is normally distributed with zero mean, and variance σ_{ξ}^2, and f_{ξ} is the power in Watts of the small-scale fading, which is assumed to be Nakagami-m distributed. As the squared of Nakagami random variable is a gamma random one, the distribution of f_{ξ} is expressed as follows [79]:

$$p_{f_{\xi}}(f) = \Big[\frac{m_{\xi}}{\Omega}\Big]^{m_{\xi}} \frac{f^{m_{\xi}-1}}{\Gamma(m_{\xi})} \exp\Big(-\frac{m_{\xi}}{\Omega} f\Big), \tag{2.32}$$

where, $\Gamma(x)$ is the Gamma function which is expressed as

$$\Gamma(x) = \int_0^{+\infty} t^{x-1}\ \exp(-t)\ dt. \tag{2.33}$$

If x is a positive integer, $\Gamma(x) = (x-1)!$.

2.5.3 Probability Density Function

Let $f^{(\text{NBS})}$ be the PDF of r, the distance between the user and the nearest BS (NBS). $f^{(\text{NBS})}$ is expressed as follows,

$$f^{(\text{NBS})}(r) = 2\pi\lambda_{\text{BS}} r \exp\Big(-\pi\lambda_{\text{BS}}\Big[r^2 - (H_{\text{BS}} - H_{\text{UE}})^2\Big]\Big). \tag{2.34}$$

In fact, the probability that r is larger than a distance R, is given by

$$\begin{aligned} &\Pr\{r \le R\} = 1 - \Pr\{R < r\} \qquad (2.35)\\ &= 1 - \Pr\{R^2 < h_r^2 + (H_{\text{BS}} - H_{\text{UE}})^2\}\\ &= 1 - \Pr\{\sqrt{R^2 - (H_{\text{BS}} - H_{\text{UE}})^2} < h_r\}, \forall R \ge (H_{\text{BS}} - H_{\text{UE}}). \end{aligned}$$

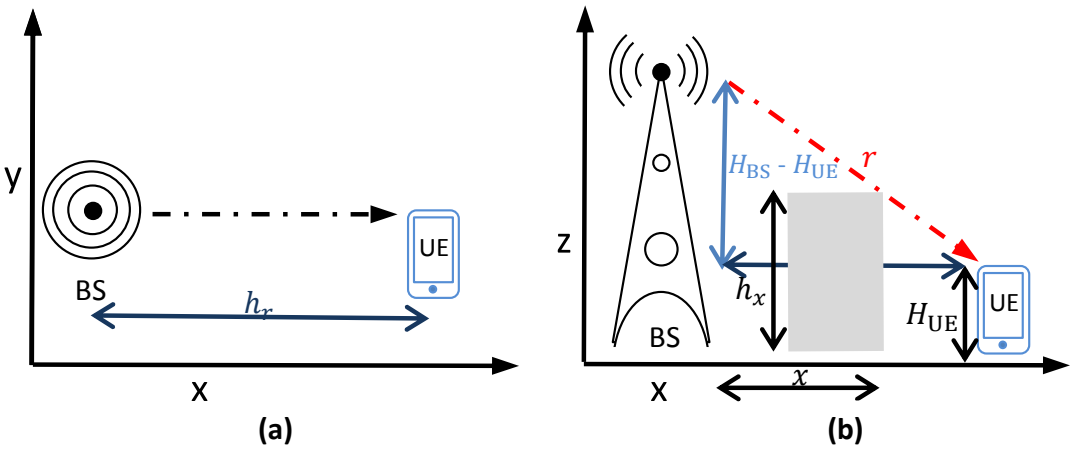

Figure 2.8: Closest BS: X-Y, and X-Z modeling

As h_r presents the horizontal distance between a given UE and its nearest BS (as shown in Figure2.8), $\Pr\{\sqrt{R^2-(H_{\text{BS}}-H_{\text{UE}})^2} < h_r\}$ can be evaluated as the probability that no BS exists in the disc of radius $\sqrt{R^2-(H_{\text{BS}}-H_{\text{UE}})^2}$. Based on PPP's properties, the probability of finding exactly n particles within a given volume V [80] is expressed as follows

$$P_n \approx \frac{(\lambda_{\text{BS}} \times V)^n}{n!} \exp(-\lambda_{\text{BS}} \times V), \tag{2.36}$$

Consequently, $\Pr\{\sqrt{R^2-(H_{\text{BS}}-H_{\text{UE}})^2} < h_r\}$ can be written as follows

$$\Pr\{\sqrt{R^2-(H_{\text{BS}}-H_{\text{UE}})^2} < h_r\} = \exp\left(-\pi\lambda_{\text{BS}}\left[R^2-(H_{\text{BS}}-H_{\text{UE}})^2\right]\right), \tag{2.37}$$

By substituting (2.37) in (2.35), and after taking the derivative of the CDF expression, the PDF of r is expressed as in (2.34).

Let $f^{(\text{SBS})}$ be the PDF expression of the distance to the strongest BS (SBS). The expression of $f^{(\text{SBS})}(r)$ can be approximated as follows

$$f^{(\text{SBS})}(r) \approx f^{(\text{NBS})}(r), \tag{2.38}$$

Fig. 2.9 presents the simulated probability density function of the distance to the strongest BS compared to the PDF expression of the distance to the nearest one. This figure confirms the accuracy of the approximate expression in (2.38), for simuation values presented in table 4.1.

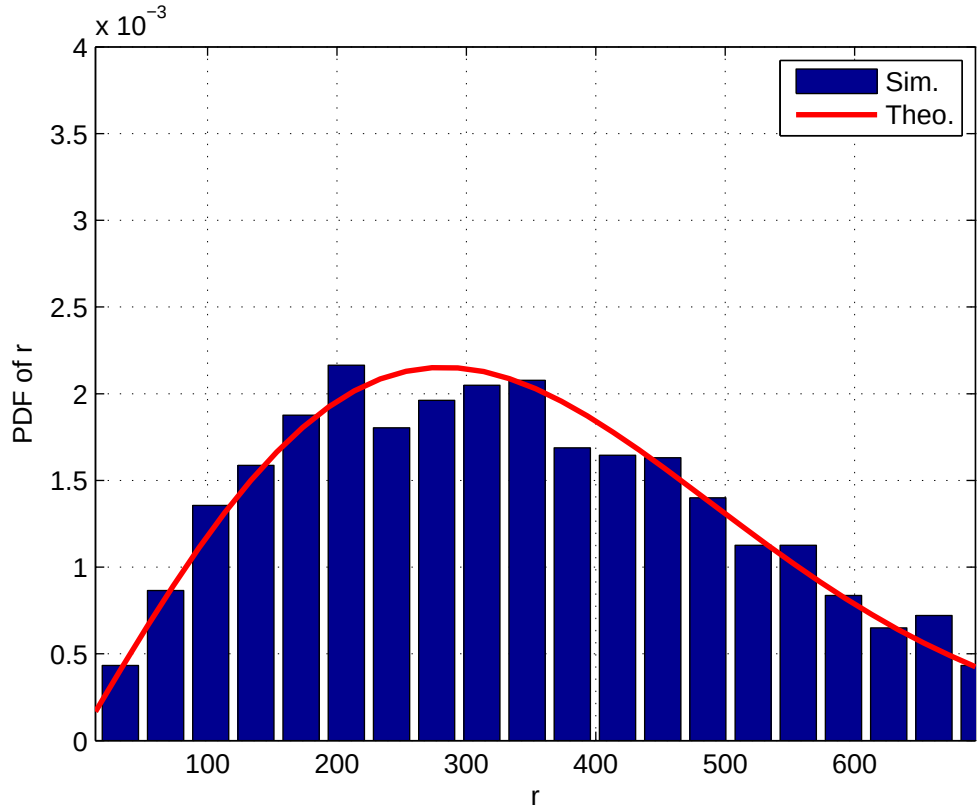

Figure 2.9: Histogram for simulating the PDF of the distance to the strongest BS as compared to the PDF expression of the distance to nearest one

Based on that, in mmWave based communication networks, we can conclude that the BS that offers the strongest received signal strength to a given UE is highly probable the nearest BS to this UE.

2.6 Conclusion

In this chapter, we have proposed two 3-D models, of cellular networks operating in two frequency bands, namely UHF and mmWave bands. The first model considers a 3-D HetNet in the context of a high-rise building environment, where K-tiers of BSs are randomly located.

Afterwards, the wireless networks are modeled taking into consideration the presence of blockages by employing a PPP and a Boolean scheme of rectangles in order to, respectively, describe the positions of different BSs and the geometry of blockages.

Finally, we derive the expressions of the corresponding probability density function and

the SINR/SNR of the two proposed models, for both, UHF and mmWave bands.

Chapter 3

Performance Analysis of 3-D Wireless Communication Networks

3.1 Introduction

5G wireless cellular networks can use UHF signals or mmWave signals. The UHF band is between 300 MHz and 3GHz for the high frequency [74]. UHF has different penetrations through the buildings walls depending on the frequency. It has been used, since earlier days, as one of the line-of-sight communications in hilly remote areas, where other means of wired communication can't be installed. It can provide a coverage for long distances. Actually, the UHF band is expected to support widespread coverage across urban, suburban and rural areas and help support IoT services.

For mmWave based communications, the band is between 30 Ghz and 300 Ghz [74]. MmWave communications have been defined as a flexible solution for the 5G networks [81]. Indeed, it provides a large bandwidth, thereby supports Gigabit wireless services. These systems offer a highly directional communication relying on narrow beams. Consequently, they achieve a high beamforming gain, and eliminate the interference coming from adjacent cells [82]. MmWave BSs, for a fixed array aperture, pack more antennas to achieve an important array gain into a given space. In addition, they offer analogical and low complicated beamforming/precoding schemes. This is because, they experience, at high frequencies, hardware qualifications [83]. Unlike other communication systems, the path-loss of mmWave bands is increasing with great orders of magnitude [84]. Con-

sequently, mmWave frequency bands are only adapted for short-range systems.

In this chapter, based on the presented system models in chapter II, we detail performance analysis of wireless communication system for different scenarios where UHF and mmWaves are used. We present two comparative studies. For each study, we derive the analytical expressions, and we evaluate and confirm them by the numerical results.

3.2 Performance Analysis of 2-D and 3-D based HetNets

In this section, we derive the average coverage probability expressions in interference plus noise environment (INE), and interference limited environment (ILE), with 2-D and 3-D space modeling. We consider a 3-D cellular network model that is deploying picocells and femtocells with maximum densities λ_{pc} and λ_{fc}, respectively. For this study, we consider mmWave communications ($\beta = \tau\alpha$) and $\eta = 1$ In the rest of the document, we use these two notations, coverage probability or successful transmission, to present the event when the corresponding communication channel supports a target SINR γ_{th}. For INE, the coverage probability is defined as $P_C \triangleq \text{P}\{\text{SINR} \geq \gamma_{\text{th}}\}$, with γ_{th} is a predefined SINR threshold.

Let r be the distance from the target UE to the nearest small cell. The average coverage probability can be derived as follows,

$$\begin{aligned}\bar{P}_C &= \mathbb{E}\left[\text{P}\{\text{SINR} \geq \gamma_{\text{th}} \mid r\}\right] \\ &= \int_{r\geq 0} \text{P}\Big\{H \geq \gamma_{\text{th}} P_{\text{BS}}^{-1} A_{M1}^{-1} r^{\tau\alpha}(I + N_0)\Big\} f(r)\, dr, \end{aligned} \tag{3.1}$$

By using the PDF expression of r as introduced in (2.24), and the exponential PDF expression of H, (3.1) can be rewritten as follows,

$$\begin{aligned}\bar{P}_C = \int_{r\geq 0} 4\pi\lambda_{\text{BS}} r^2 \exp\Big(-\frac{4}{3}\pi\lambda_{\text{BS}} r^3\Big) \int_{P_{\text{BS}}\geq 0}\int_{I\geq 0} \exp\Big(-\gamma_{\text{th}} P_{\text{BS}}^{-1} A_{M1}^{-1} r^{\tau\alpha}\Big(I + N_0\Big)\Big) \\ f_I(I)\, f_P(P_{\text{BS}})\, dI\, dP_{\text{BS}}\, dr, \end{aligned} \tag{3.2}$$

where, f_I, and f_P are the PDFs of I and P_{BS}, respectively.

According to the definition of Laplace transform (2.2) and based on (3.2), $\bar{P}_C$ can be

rewritten as

$$\bar{P}_{C} = \int_{r\geq 0} 4\pi\lambda_{\text{BS}} r^{2} \exp\Big(-\frac{4}{3}\pi\lambda_{\text{BS}} r^{3}\Big) \times \mathbb{E}_{P_{\text{BS}}}\Big[\exp\Big(-\gamma_{\text{th}} P_{\text{BS}}^{-1} A_{M1}^{-1} r^{\tau\alpha} N_{0}\Big)\mathcal{L}_{I}\Big[\gamma_{\text{th}} P_{\text{BS}}^{-1} A_{M1}^{-1} r^{\tau\alpha}\Big]\Big] dr, \tag{3.3}$$

where, $\mathcal{L}_{I}[.]$ is the Laplace transform of the random variables I.

According to the independence of G_{i} as defined in (2.22),

$$\begin{aligned}\mathcal{L}_{I}[s] &= \mathbb{E}_{\{\Phi,G_i,P_i\}}\Bigg[\exp\Bigg(-s\sum_{i\in\Phi\setminus\{c_o\}} qP_{i}G_{i}A_{M1}l_{i}^{-(\tau\alpha)}\Bigg)\Bigg] \\ &= \mathbb{E}_{\Phi}\Bigg[\prod_{i\in\Phi\setminus\{c_o\}}\mathbb{E}_{\{G_i,P_i\}}\Big[\exp\Big(-s\,qP_{i}G_{i}A_{M1}l_{i}^{-(\tau\alpha)}\Big)\Big]\Bigg].\end{aligned} \tag{3.4}$$

Using the probability generating functional of the PPP [60], (3.4) can be expressed as follows

$$\mathcal{L}_{I}[s] = \exp\Bigg(-4\pi\lambda_{\text{BS}}\int_{r}^{\infty}\mathbb{E}_{\{G_i,P_i\}}\Big[1-\exp\Big(-s\,qP_{i}G_{i}A_{M1}v^{-(\tau\alpha)}\Big)\Big]v^{2}dv\Bigg). \tag{3.5}$$

By using the PDF expressions of G_{i}, $\mathcal{L}_{I}$ [s] can be expressed as follows

$$\mathcal{L}_{I}[s] = \exp\Bigg(-4\pi\lambda_{\text{BS}}\int_{r}^{\infty}\mathbb{E}_{G_i}\Big[1-\frac{1}{1+s\,qP_{i}G_{i}A_{M1}v^{-\tau\alpha}}\Big]v^{2}dv\Bigg). \tag{3.6}$$

Let $\rho_{\text{pc}} = \frac{\lambda_{\text{pc}}}{\lambda_{\text{pc}}+\lambda_{\text{fc}}}$ ($\rho_{\text{fc}} = \frac{\lambda_{\text{fc}}}{\lambda_{\text{pc}}+\lambda_{\text{fc}}}$) the probability that $P_{j} = P_{\text{pc}}(P_{\text{fc}}), \forall j \in \Phi$, where we suppose that the UE are located according to independent stationary point processes. By letting $s = \gamma_{\text{th}} P_{\text{BS}}^{-1} A_{M1}^{-1} r^{\tau\alpha}$, (3.6) can be rewritten as

$$\begin{aligned}\mathcal{L}_{I_{\text{pc}}}\Big[\gamma_{\text{th}} P_{\text{BS}}^{-1} A_{M1}^{-1} r^{\tau\alpha}\Big] = \exp\Bigg(-4\pi\lambda_{\text{BS}} \times \int_{r}^{\infty}\Bigg(\rho_{\text{pc}}\Big[1-\frac{1}{1+q\gamma_{\text{th}} P_{\text{BS}}^{-1} P_{\text{pc}} r^{\tau\alpha} v^{-\tau\alpha}}\Big] \\ + \rho_{\text{fc}}\Big[1-\frac{1}{1+q\gamma_{\text{th}} P_{\text{BS}}^{-1} P_{\text{fc}} r^{\tau\alpha} v^{-\tau\alpha}}\Big]\Bigg)v^{2}dv\Bigg).\end{aligned} \tag{3.7}$$

By employing the change in variables:
$a = (q\gamma_{\text{th}} P_{\text{BS}}^{-1} P_{\text{pc}})^{\frac{-3}{\tau\alpha}} (\frac{v}{r})^{3}$, and $b = (q\gamma_{\text{th}} P_{\text{BS}}^{-1} P_{\text{fc}})^{\frac{-3}{\tau\alpha}} (\frac{v}{r})^{3}$, the expression (3.7) can be further simplified to be

$$\begin{aligned}\mathcal{L}_{I_{\text{pc}}}\Big[\gamma_{\text{th}} P_{\text{BS}}^{-1} A_{M1}^{-1} r^{\tau\alpha}\Big] = \exp\Bigg(-4\pi\lambda_{\text{BS}} r^{3} \times \Bigg[\rho_{\text{pc}}(q\gamma_{\text{th}} P_{\text{BS}}^{-1} P_{\text{pc}})^{\frac{3}{\tau\alpha}} \int_{(q\gamma_{\text{th}} P_{\text{BS}}^{-1} P_{\text{pc}})^{\frac{-3}{\tau\alpha}}}^{\infty} \frac{1}{1+a^{\frac{\tau\alpha}{3}}} da \\ + \rho_{\text{fc}}(q\gamma_{\text{th}} P_{\text{BS}}^{-1} P_{\text{fc}})^{\frac{3}{\tau\alpha}} \int_{(q\gamma_{\text{th}} P_{\text{BS}}^{-1} P_{\text{fc}})^{\frac{-3}{\tau\alpha}}}^{\infty} \frac{1}{1+b^{\frac{\tau\alpha}{3}}} db\Bigg]\Bigg).\end{aligned} \tag{3.8}$$

Finally, based on (3.8) and by employing the change in variables $x = r^3$, the coverage probability expression in INE is given by

$$\bar{P}_C^{\text{INE}} = \frac{4}{3}\pi\lambda_{\text{BS}}\left[\rho_{\text{pc}}\int_0^{\infty}\exp\left(-\frac{4}{3}\pi x(\lambda_{\text{BS}} + \Im_{\text{pc}}) - \gamma_{\text{th}}P_{\text{pc}}^{-1}A_{M1}^{-1}N_0\, x^{\frac{\tau\alpha}{3}}\right)dx + \rho_{\text{fc}}\int_0^{\infty}\exp\left(-\frac{4}{3}\pi x(\lambda_{\text{BS}} + \Im_{\text{fc}}) - \gamma_{\text{th}}P_{\text{fc}}^{-1}A_{M1}^{-1}N_0\, x^{\frac{\tau\alpha}{3}}\right)dx\right], \tag{3.9}$$

where,

$$\Im_{\text{pc}} = \rho_{\text{pc}}(q\gamma_{\text{th}})^{\frac{3}{\tau\alpha}}\int_{(q\gamma_{\text{th}})^{\frac{-3}{\tau\alpha}}}^{\infty}\frac{1}{1+a^{\frac{\tau\alpha}{3}}}da + \rho_{\text{fc}}(q\gamma_{\text{th}}P_{\text{pc}}^{-1}P_{\text{fc}})^{\frac{3}{\tau\alpha}}\int_{(q\gamma_{\text{th}}P_{\text{pc}}^{-1}P_{\text{fc}})^{\frac{-3}{\tau\alpha}}}^{\infty}\frac{1}{1+b^{\frac{\tau\alpha}{3}}}db, \tag{3.10}$$

and,

$$\Im_{\text{fc}} = \rho_{\text{pc}}(q\gamma_{\text{th}}P_{\text{fc}}^{-1}P_{\text{pc}})^{\frac{3}{\tau\alpha}}\int_{(q\gamma_{\text{th}}P_{\text{fc}}^{-1}P_{\text{pc}})^{\frac{-3}{\tau\alpha}}}^{\infty}\frac{1}{1+a^{\frac{\tau\alpha}{3}}}da + \rho_{\text{fc}}(q\gamma_{\text{th}})^{\frac{3}{\tau\alpha}}\int_{(q\gamma_{\text{th}})^{\frac{-3}{\tau\alpha}}}^{\infty}\frac{1}{1+b^{\frac{\tau\alpha}{3}}}db. \tag{3.11}$$

For (ILE), where the noise effect is ignored ($N_0 \approx 0$) because the interference is significantly larger than the noise, the coverage probability, can be expressed as follows

$$\bar{P}_C^{\text{ILE}} = \frac{\rho_{\text{pc}}}{1+\Im_{\text{pc}}} + \frac{\rho_{\text{fc}}}{1+\Im_{\text{fc}}}. \tag{3.12}$$

In order to verify the aforementioned analytical derivations, simulations results are used based on the Table 3.1. Without loss of generality, the frequency is set to be 28 GHz, and $S = 0$ dB [74]. We consider a high-rise building in a dense urban area, where many picocells and femtocells are deployed. We focus on a 3-D space region ($R \times R \times R$), with $R = 100$ m, and the transmit powers of picocells and femtocells are respectively set to be 0.25 W, and 0.02 W. To make a fair comparison, in the 2-D model, the small cells are deployed into a square area ($R \times R$), whereas the density is equal to $\lambda_{2D} = \frac{1-\exp(-\pi(\lambda_{\text{pc}}+\lambda_{\text{fc}})d_{min}^2)}{\pi d_{min}^2}$.

Fig 3.1 shows the coverage probability as a function of SINR threshold, γ_{th}, for the new 3-D cellular model and the traditional 2-D model in INE and ILE, for different values

Table 3.1: Simulation Parameters

Parameter	**Value**
$PL(r_0)$	61.3849
μ	0.5 dB/m
r_0	$1m$
λ_{pc}	$2e-5\text{m}^{-3}$
λ_{fc}	$2e-4\ \text{m}^{-3}$
N_0	-145 dBm
d_{min}	5 m

of path loss exponent α, $q = 0.5$, and $\tau = 0.88$. As this figure shows, by increasing the values of α, the coverage probability for the two models is increasing too. This is due to the little impact of increasing α on the desired signal compared to its impact on the interference. In fact, the power of the desired signal is based mainly on the distance

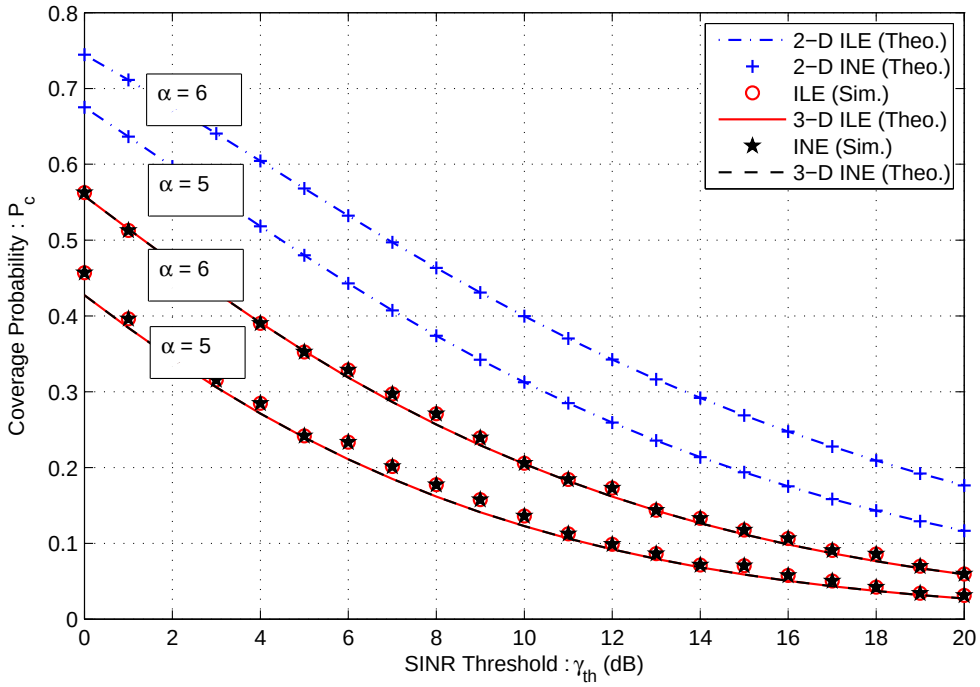

Figure 3.1: Coverage probability vs. SINR threshold for 2-D and 3-D models for different α values, $q = 0.5$, and $\tau = 0.88$.

between the corresponding cell and the receiver. However, because of the obstacles and the long distances between the interferer and the corresponding receiver, the interference signals attenuation increases with α, and the level of the total interference decreases which causes an enhancement of the SINR level and the coverage probability. We can notice also that the theoretical results of the 3-D model are more accurate than the theoretical results of the 2-D one for both INE and ILE when compared to their corresponding simulations results. These results are justified by the fact that the distance between a transmitter and a receiver in the 2-D model is a projection of an actual distance which makes the calculation of the SINR not accurate. However, the new general 3-D model uses the actual distance which is more realistic. It is clear that the results are almost the same for the INE and ILE. The main reason is that the interference is significantly larger than the noise, and the noise effect is ignored.

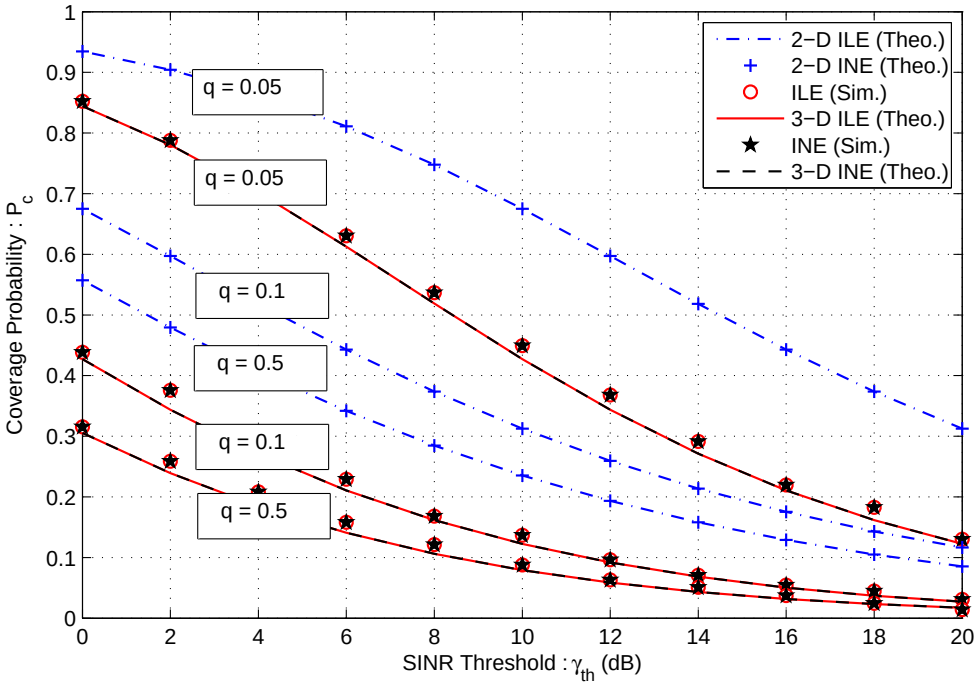

Figure 3.2: Coverage probability vs. SINR threshold for 2-D and 3-D models for different q values, $\alpha = 5$, and $\tau = 0.88$.

Figure 3.2 presents the variations of the coverage probability versus SINR threshold for the two models for different values of transmission probability q, $\alpha = 5$, and $\tau = 0.88$. We can clearly see that the coverage probability is increasing with the decreased values

of the transmission probabilities. This is because more the transmission probability is smaller, less interference nodes are transmitting. Thus, the SINR level and the coverage probability increase.

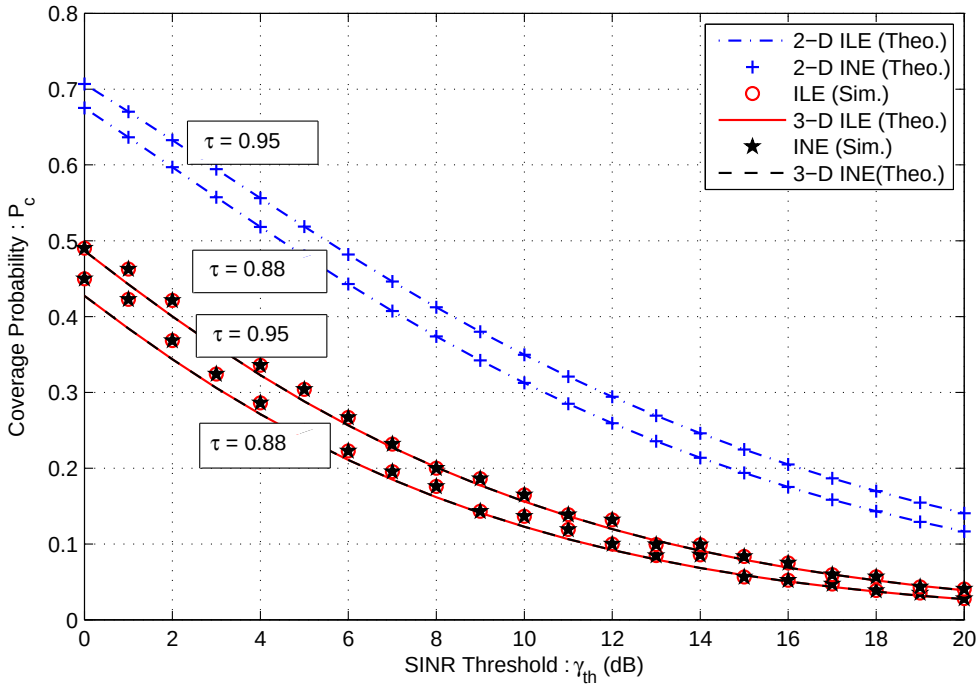

Figure 3.3: Coverage probability vs. SINR threshold for 2-D and 3-D models for different τ, $\alpha = 5$, and $q = 0.5$.

For $\alpha = 5$ and $q = 0.5$, Figure 3.3 illustrates the coverage probability as a function of the SINR threshold for the two models for different values of the mean slope correction factor τ. According to equation (2.21), the SINR is proportional to τ, where the signal power decrease but the interference decrease too by rising τ values. This can explain why the coverage probability does increase when the the value of the correction factor is larger as it is obvious in Figure 3.3.

3.3 Performance analysis of UHF & MmWave based 3-D cellular networks

In this section, we present a comparative study between the performance of mmWaves and UHF based communications systems. We derive the successful transmission proba-

bility, the average throughput, and BER expressions for the two scenarios. To confirm the analytical results, simulations are done to analyze the performance of the 3-D HetNets for the different transmission bands under consideration. For the simulation environment, we consider a 3-D space region ($R \times R \times R$) in a dense urban area, where three types of small cells are distributed in the 3-D space region (3-tier cellular network) with densities $\lambda_p = \sum_{k=1}^{3} \lambda_k$. The simulation parameters are set as the Table 3.2.

Table 3.2: Simulation Parameters

Parameter	**Value**
λ_1	$1e-5$/m^3
λ_2	$2e-5$/m^3
λ_3	$3e-5$/m^3
P_1	300 mW
P_2	100 mW
P_3	20 mW
R	100 m
d_{min}	4 m
N_0	-110 dBm
$PL_{UHF}(1)$	40 dB
$PL_{Mm}(1)$	61.3849 dB
μ	0.5 dB/m
τ	0.88

3.3.1 Successful Transmission Probability

The expressions of the average successful transmission probability (STP) for the different bands are derived as follows.

Based on (2.19,2.20), the general expression for STP can be written as

$$\begin{aligned} STP &= \mathbb{E}_{\{r\}}\Big[\Pr\Big\{\text{SINR} \geq \gamma_{\text{th}}|r\Big\}\Big] \\ &= \Pr\left\{H \geq \gamma_{\text{th}} P_{\text{BS}}^{-1} A_{M1}^{-1} r^{\beta} \left(\eta I + N_0\right)\right\}, \end{aligned} \tag{3.13}$$

By using the exponential PDF expression of H, (3.13) can be rewritten as follows

$$STP = \int_{I\geq 0} \exp\Big(-\gamma_{\text{th}} P_{\text{BS}}^{-1} A^{-1} r^{\beta}\Big(\eta I + N_0\Big)\Big) f_I\, dI$$
$$= \int_{r\geq 0} f(r) \times \mathbb{E}\Bigg[\exp\Big(-\gamma_{\text{th}} P_{\text{BS}}^{-1} A_{M1}^{-1} r^{\beta} N_0\Big)\, \mathcal{L}_{I_r}\Big[\eta\gamma_{\text{th}} P_{\text{BS}}^{-1} A_{M1}^{-1} r^{\beta}\Big]\Bigg] dr, \qquad (3.14)$$

where, $\mathcal{L}_I\,[.]$ is the Laplace transform of the random variables I. According to the independence of H, and P_i

$$\mathcal{L}_I\,[s] = \mathbb{E}_{\{\Phi,H,P_i\}}\Bigg[\exp\Bigg(-s\sum_{i\in\Phi\setminus\{R\}} P_i H A_{M1} r_i^{-(\beta)}\Bigg)\Bigg]$$
$$= \mathbb{E}_{\Phi}\Bigg[\prod_{i\in\Phi\setminus\{R\}} \mathbb{E}_{\{H,P_i\}}\Big[\exp\Big(-sP_i H A_{M1} r_i^{-\beta}\Big)\Big]\Bigg]. \qquad (3.15)$$

Using the probability generating functional [60], $\mathcal{L}_I\,[s]$ can be rewritten as follows

$$\mathcal{L}_I\,[s] = \exp\Bigg(-4\pi\lambda_{\text{BS}} \times \int_r^{\infty} \mathbb{E}_{\{H,P_i\}}\Big[1-\exp\Big(-sP_i H A_{M1} v^{-\beta}\Big)\Big] v^2 dv\Bigg). \qquad (3.16)$$

Using the exponential PDF expression of H, (3.16) becomes

$$\mathcal{L}_I\,[s] = \exp\Bigg(-4\pi\lambda_{\text{BS}} \times \int_r^{\infty} \mathbb{E}_{\{P_i\}}\Big[1-\int_0^{\infty}\exp\Big(-H(1+sP_i A_{M1} v^{-\beta})\Big) dH\Big] v^2 dv\Bigg)$$
$$= \exp\Bigg(-4\pi\lambda_{\text{BS}} \int_r^{\infty} \mathbb{E}_{\{P_i\}}\Big[1-\frac{1}{1+sP_i A_{M1} v^{-\beta}}\Big] v^2 dv\Bigg). \qquad (3.17)$$

Let $\rho_k\ (=\frac{\lambda_k}{\lambda_p})$ denotes the probability that $P_i = P_k, \forall\, i \in \Phi$. Based on that, the $\mathcal{L}_I\,[s]$ expression is given by

$$\mathcal{L}_I\,[s] = \exp\Bigg(-4\pi\lambda_{\text{BS}} \int_r^{\infty} \sum_{k=1}^{K} \rho_k \Big[1-\frac{1}{1+sP_k A_{M1} v^{-\beta}}\Big] v^2 dv\Bigg)$$
$$= \exp\Bigg(-4\pi\lambda_{\text{BS}} \sum_{k=1}^{K} \rho_k \int_r^{\infty} \Big[1-\frac{1}{1+sP_k A_{M1} v^{-\beta}}\Big] v^2 dv\Bigg). \qquad (3.18)$$

By letting $s = \eta\gamma_{\text{th}} P_{\text{BS}}^{-1} A_{M1}^{-1} r^{\beta}$, and by using the change in variables: $a = (\eta\gamma_{\text{th}} P_{\text{BS}}^{-1} P_k)^{\frac{-3}{\beta}} (\frac{v}{r})^3$ (3.18) can be further simplified to

$$\mathcal{L}_I\Big[\eta\gamma_{\text{th}} P_{\text{BS}}^{-1} A_{M1}^{-1} r^{\beta}\Big] = \exp\Bigg(-\frac{4}{3}\pi\lambda_{\text{BS}} r^3 \qquad (3.19)$$
$$\times \sum_{k=1}^{K}\Bigg\{\rho_k (\eta\gamma_{\text{th}} P_{\text{BS}}^{-1} P_k)^{\frac{3}{\beta}} \int_{(\eta\gamma_{\text{th}} P_{\text{BS}}^{-1} P_k)^{\frac{-3}{\beta}}}^{\infty} \frac{1}{1+a^{\frac{\beta}{3}}}\, da\Bigg\}\Bigg).$$

Based on (2.24), (3.14) and (3.19), the expression of STP is given by

$$STP = \int_{r\geq 0} 4\pi\lambda_{\text{BS}} r^2 \exp\left(-\frac{4}{3}\pi\lambda_{\text{BS}} r^3\right) \times \mathbb{E}\Bigg[\exp\Big(-\gamma_{\text{th}} P_{\text{BS}}^{-1} A_{M1}^{-1} r^{\beta} N_0\Big) \times \exp\left(-\frac{4}{3}\pi r^3 \sum_{k=1}^{K}\left\{\rho_k(\eta\gamma_{\text{th}} P_{\text{BS}}^{-1} P_k)^{\frac{3}{\beta}} \times \int_{(\eta\gamma_{\text{th}} P_{\text{BS}}^{-1} P_k)^{\frac{-3}{\beta}}}^{\infty} \frac{1}{1+a^{\frac{\beta}{3}}}\, da\right\}\right)\Bigg] dr. \tag{3.20}$$

Now, using the probabilities ρ_k, and by employing a variable change $x = \frac{4}{3}\pi\lambda_{\text{BS}} r^3$ in (3.20), the average coverage probability of the proposed scheme is expressed as follows,

$$STP = \int_0^{\infty} \exp(-x) \times \sum_{k'=1}^{K}\Bigg\{\rho_{k'} \exp\Bigg(-\gamma_{\text{th}} P_{k'}^{-1} A_{M1}^{-1}\Big(\frac{3x}{4\pi\lambda_{\text{BS}}}\Big)^{\frac{\beta}{3}} N_0 - x\sum_{k=1}^{K}\Big\{\rho_k(\eta\gamma_{\text{th}} P_{k'}^{-1} P_k)^{\frac{3}{\beta}} \int_{(\eta\gamma_{\text{th}} P_{k'}^{-1} P_k)^{\frac{-3}{\beta}}}^{\infty} \frac{1}{1+a^{\frac{\beta}{3}}}\, da\Big\}\Bigg)\Bigg\} dx. \tag{3.21}$$

The STP expression can be further simplified using the following Theorem

Theorem 1. *Let $f(x)$ be a given function defined for all real numbers x. Then*

$$\int_0^{\infty} f(x)\exp(-x)\, dx = \sum_{n=1}^{N} f(x_n) w_n + R_N, \tag{3.22}$$

where, x_n, w_n, and R_N are the n^{th} abscissa (root), weight, and remainder of the N^{th} order Laguerre polynomial, respectively [85].

The Laguerre Polynomial of order N, is expressed as follow

$$L_N(x) = \sum_{k=0}^{N} \frac{(-1)^k}{k!} \binom{n}{k} x^k. \tag{3.23}$$

and, w_n is given by

$$w_n = \frac{x_n}{(N+1)^2 (L_{N+1}(x_n))^2}, \tag{3.24}$$

Based on Theorem 1, (3.21) can be expressed as,

$$STP = \sum_{n=1}^{N}\Bigg\{\sum_{k'=1}^{K}\Bigg\{\rho_{k'} \exp\Bigg(-\gamma_{\text{th}} P_{k'}^{-1} A_{M1}^{-1}\Big(\frac{3x_n}{4\pi\lambda_{\text{BS}}}\Big)^{\frac{\beta}{3}} N_0 - x_n \sum_{k=1}^{K}\Big\{\rho_k(\eta\gamma_{\text{th}} P_{k'}^{-1} P_k)^{\frac{3}{\beta}} \times \int_{(\eta\gamma_{\text{th}} P_{k'}^{-1} P_k)^{\frac{-3}{\beta}}}^{\infty} \frac{1}{1+a^{\frac{\beta}{3}}}\, da\Big\}\Bigg)\Bigg\} w_n\Bigg\} + R_N, \tag{3.25}$$

Finally, assuming that $R_N \approx 0$, $\Im(u,b) = u\int_b^{\infty} \frac{1}{1+x^{\beta/3}}\,dx$, and $u = (\eta\gamma_{\text{th}}P_k/P_{k'})^{\frac{3}{\beta}}$, the final average coverage probability expression is given by (3.26).

$$STP = \sum_{n=1}^{N}\left\{w_n \sum_{k'=1}^{K}\left\{\rho_{k'}\exp\Big(-\Big[\frac{\gamma_{\text{th}}N_0}{P_{k'}A_{M1}}\Big]\Big[\frac{3x_n}{4\pi\lambda_{\text{BS}}}\Big]^{\frac{\beta}{3}} - x_n\sum_{k=1}^{K}\Big\{\rho_k\Im(u,1/u)\Big\}\Big)\right\}\right\}. \tag{3.26}$$

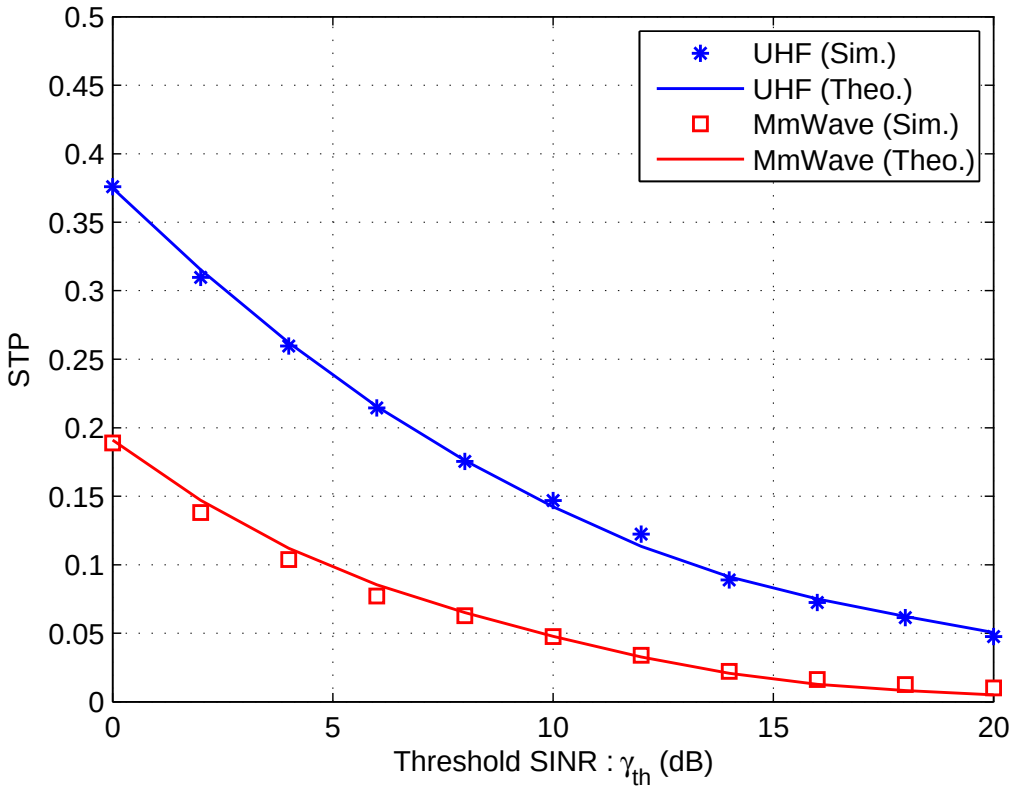

Figure 3.4: Average successful transmission probability vs. γ_{th} for different values of α, and $\eta = 0.3$.

The analytical expression in (3.26) and the simulation results are represented in Figure 3.4. This figure depicts the successful transmission probability in communication systems based on the two considered bands as a function of γ_{th}. Under the above mentioned simulation parameters, a UHF transmission is more probable to be successful that of a mmWave transmission. The main reason for this phenomenon is that the UHF offer a low path loss, compared to mmWaves, and hence a better performance in term of successful transmission probability.

3.3.2 Average Throughput

The average throughput expression is denoted by $\bar{D}$ =B$\bar{C}$, where $\bar{C}$ is the ergodic capacity which is expressed in the following equation,

$$\bar{C} = \mathbb{E}\left[\log_2(1+\text{SINR})\right] = \frac{1}{\ln(2)}\mathbb{E}\left[\ln(1+\text{SINR})\right], \tag{3.27}$$

and B is the bandwidth, which is expressed as follows

$$B = \begin{cases} B_{_{UHF}} & \text{for UHF transmission,} \\ B_{_{MW}} & \text{for mmWave transmission.} \end{cases} \tag{3.28}$$

$\bar{C}$ expression can be derived by using the following Theorem.

Theorem 2. *Let W and I be arbitrary non-negative random variables. Then, based on [86] we have*

$$\mathbb{E}\left[\ln\left(1+\frac{W}{I+N_{_0}}\right)\right] = \int_0^\infty \left(\frac{1-\mathcal{L}_W\left(\frac{y}{N_{_0}}\right)}{y}\right)\mathcal{L}_{_I}\left(\frac{y}{N_{_0}}\right)\exp(-y)\,dy. \tag{3.29}$$

Based on Theorem 2, the upper bound expression of the average ergodic capacity can be evaluated as follows

$$\bar{C} \approx \frac{1}{ln(2)}\left(\sum_{n=1}^{N}\left\{\left(1-\mathcal{L}_{_W}\left(\frac{x_n}{N_{_0}}\right)\right)\mathcal{L}_{_I}\left(\frac{x_n}{N_{_0}}\right)\frac{w_n}{x_n}\right\} + R_N\right), \tag{3.30}$$

where,

$$W = P_{_{\text{BS}}} H A_{_{M1}} r^{-\beta}. \tag{3.31}$$

We used the PDF expression of H to derive $\mathcal{L}_{_W}\left(\frac{x_n}{N_{_0}}\right)$ as follows

$$\begin{aligned}
&\mathcal{L}_{_W}\left(\frac{x_n}{N_{_0}}\right) = \mathbb{E}\left[\exp\left(\frac{-x_n W}{N_{_0}}\right)\right] \\
&= \mathbb{E}_{\{P_{_{\text{BS}}},r,H\}}\left[\exp\left(\frac{-x_n P_{_{\text{BS}}} H A_{_{M1}}\, r^{-\beta}}{N_{_0}}\right)\right] \\
&= \mathbb{E}_{\{P_{_{\text{BS}}},r\}}\left[\int_0^\infty \exp\left(-H\left(1+\frac{x_n P_{_{\text{BS}}} A_{_{M1}}\, r^{-\beta}}{N_{_0}}\right)\right)dH\right] \\
&= \mathbb{E}_{\{P_{_{\text{BS}}}\}}\left[\int_0^\infty \frac{N_0 4\pi\lambda_{_{\text{BS}}} r^2}{N_{_0}+x_n P_{_{\text{BS}}} A_{_{M1}}\, r^{-\beta}} \exp\left(-\frac{4}{3}\pi\lambda_{_{\text{BS}}} r^3\right)\, dr\right].
\end{aligned} \tag{3.32}$$

By using the change in variable : $v = \frac{4}{3}\pi\lambda_{\text{BS}} r^3$, $\mathcal{L}_W\left(\frac{x_n}{N_0}\right)$ can be rewritten as

$$\mathcal{L}_W\left(\frac{x_n}{N_0}\right) = \mathbb{E}_{\{P_{\text{BS}}\}}\left[\int_0^{\infty} \frac{N_0 \exp(-v)}{N_0 + x_n P_{\text{BS}} A_{M1}\left(\frac{3v}{4\pi\lambda_{\text{BS}}}\right)^{-\frac{\beta}{3}}} dv\right]. \tag{3.33}$$

Based on Theorems 1 and 2, the $\mathcal{L}_W\left(\frac{x_n}{N_0}\right)$ can be further simplified to

$$\mathcal{L}_W\left(\frac{x_n}{N_0}\right) = \mathbb{E}_{\{P_{\text{BS}}\}}\left[\sum_{m=1}^{M} \frac{N_0 w_m}{N_0 + x_n P_{\text{BS}} A_{M1}\left(\frac{3\ x_m}{4\pi\lambda_{\text{BS}}}\right)^{-\frac{\beta}{3}}} + R_M\right]. \tag{3.34}$$

By using the ρ_k probability, (5.32) can be evaluated as follows

$$\mathcal{L}_W\left(\frac{x_n}{N_0}\right) = \sum_{k=1}^{K}\left\{\rho_k\left(\sum_{m=1}^{M} \frac{N_0 w_m}{N_0 + x_n P_k A_{M1}\left(\frac{3\ x_m}{4\pi\lambda_{\text{BS}}}\right)^{-\frac{\beta}{3}}} + R_M\right)\right\}, \tag{3.35}$$

Based on (3.19), Theorem 1, and by using the change in variable : $x_q = \frac{4}{3}\pi\lambda_{\text{BS}} r^3$, $\mathcal{L}_I\left(\frac{x_n}{N_0}\right)$ can be expressed as

$$\mathcal{L}_I\left(\frac{x_n}{N_0}\right) = \sum_{q=0}^{Q}\left\{\exp\left(-\frac{4}{3}\pi\lambda_{\text{BS}} \sum_{k=1}^{K}\left\{\rho_k \Im(a,b)\right\}\right) w_q\right\} + R_q, \tag{3.36}$$

where, $\Im(a,b) = a\int_b^{\infty} \frac{1}{1+x^{\beta/3}}\, dx$, $a = \left(\eta\frac{x_n}{N_0} P_k A_{M1}\right)^{\frac{3}{\beta}}$, and $b = \left(\frac{\eta x_n}{N_0} P_k A_{M1}\right)^{\frac{-3}{\beta}} \frac{3x_q}{4\pi\lambda_{\text{BS}}}$. Finally, Based on (3.30) and (3.35 - 3.36), the final average throughput expression for the both transmission bands is given by (3.37)

$$\begin{aligned}\bar{D} = \frac{B}{ln(2)}\Bigg[\sum_{n=1}^{N}\Bigg\{\frac{w_n}{x_n}\Bigg(1 - \sum_{k=1}^{K}\Big\{\rho_k\Big(\sum_{m=1}^{M} \frac{w_m}{1 + \frac{x_n}{N_0} P_k A_{M1}\left(\frac{3\ x_m}{4\pi\lambda_{\text{BS}}}\right)^{-\frac{\beta}{3}}} + R_M\Big)\Big\}\Bigg) \\ \times \Bigg(\sum_{q=0}^{Q}\Big\{w_q \exp\Big(-\frac{4}{3}\pi\lambda_{\text{BS}} \sum_{k=1}^{K}\rho_k \Im(a,b)\Big)\Big\} + R_q\Bigg)\Bigg\} + R_N\Bigg],\end{aligned} \tag{3.37}$$

where, $a = \left(\frac{\eta x_n}{N_0} P_k A_{M1}\right)^{\frac{3}{\beta}}$, and $b = \left(\frac{\eta x_n}{N_0} P_k A_{M1}\right)^{\frac{-3}{\beta}} \frac{3x_q}{4\pi\lambda_{\text{BS}}}$.

The average throughput is evaluated based on simulations and on analytical expression in (3.37), the results are depicted in Figure 3.5. We can clearly see that the average throughput of mmWave communications is higher and it increases when the bandwidth is larger. This represents the advantage of mmWave systems where a wider frequency bands can be used when compared to UHF systems.

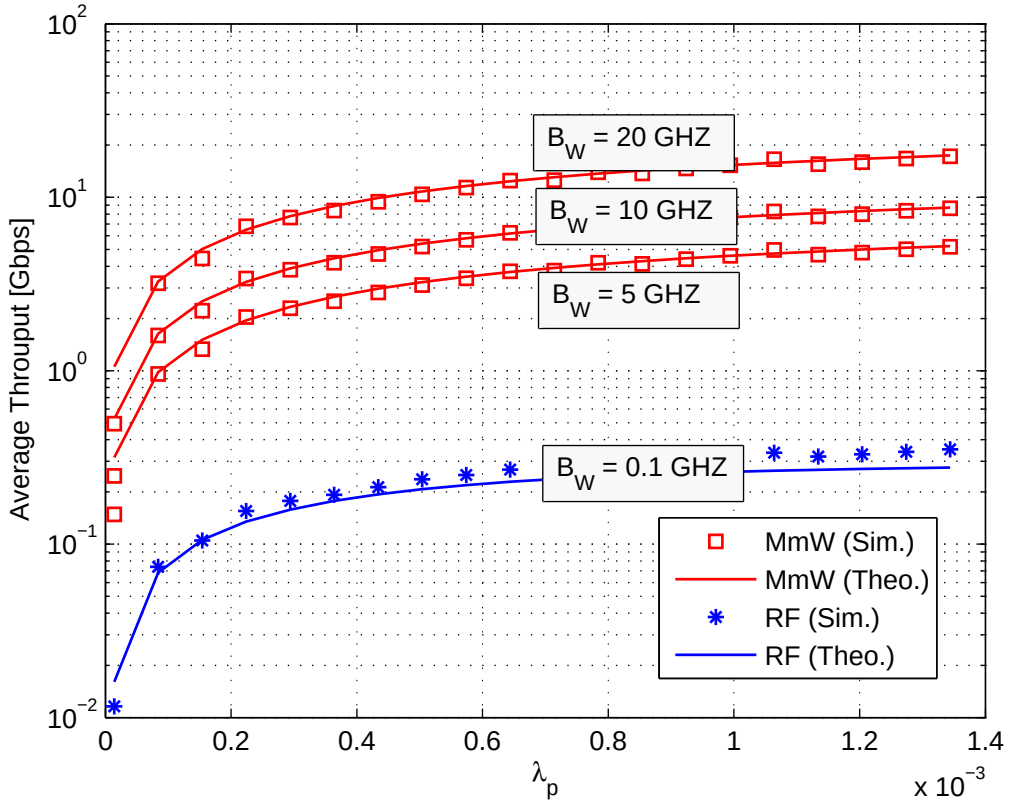

Figure 3.5: Average throughput vs. the total density of cells λ_p for different values of B_w, and $\eta = 0.1$.

3.3.3 Average Bit Error Rate

The average BER is derived by using the following Theorem:

Theorem 3. *Let H be a unit-mean exponential random variable, and let I be an arbitrary random variable which is independent of H, Then*

$$\mathbb{E}\left[g\left(\frac{H}{I+N_0}\right)\right] = g(0) + \int_0^\infty g_1(z)\mathcal{L}_I(z)\exp(-zN_0)\,dz, \tag{3.38}$$

with,

$$g_1(z) = \frac{d}{dz}g(z), \tag{3.39}$$

and

$$z = \frac{H}{I+N_0}. \tag{3.40}$$

Proof. See [86].

The average BER for general PSK modulation, denoted by $\bar{P}_e$, can be expressed as

follows [71]

$$\bar{P}_e = \mathbb{E}\left[\eta_m \, \mathrm{Q}\left(\sqrt{\theta \, \mathrm{SINR}}\right)\right]. \tag{3.41}$$

Let $g(z)$ be expressed as

$$\begin{aligned} g(z) &= \eta_m \, \mathrm{Q}\left(\sqrt{\theta P_{\text{BS}} A_{M1} \, r^{-(\beta)} z}\right) \\ &= \frac{\eta_m}{\sqrt{2\pi}} \int_{\sqrt{\frac{\theta P_{\text{BS}} A_{M1} z}{r^{\beta}}}}^{\infty} \exp\left(\frac{-t^2}{2}\right) dt \end{aligned} \tag{3.42}$$

Consequently,

$$\begin{aligned} g_1(z) &= \frac{d}{dz} g(z) \\ &= -\frac{\eta_m}{\sqrt{2\pi}} \exp\left(\frac{-\theta P_{\text{BS}} A_{M1} z}{2r^{\beta}}\right) \frac{d}{dz} \sqrt{\theta P_{\text{BS}} A_{M1} \, r^{-\beta} z} \\ &= -\frac{\eta_m}{2} \sqrt{\frac{\theta P_{\text{BS}} A_{M1}}{2\pi z r^{\beta}}} \exp\left(\frac{-\theta P_{\text{BS}} A_{M1} z}{2r^{\beta}}\right). \end{aligned} \tag{3.43}$$

According to Theorem 1 and Theorem 3, $\bar{P}_e$ can be expressed as,

$$\begin{aligned} \bar{P}_e &= \mathbb{E}_{\{P,r\}} \left[\frac{\eta_m}{2} - \frac{\eta_m}{2} \sqrt{\frac{\theta P_{\text{BS}} A_{M1}}{2\pi r^{\beta}}} \int_0^{\infty} \frac{1}{\sqrt{z}} \exp\left(\frac{-\theta P_{\text{BS}} A_{M1} z}{2r^{\beta}}\right) \mathcal{L}_I(z) \exp(-z N_0) \, dz \right] \\ &= \mathbb{E}_{\{P\}} \Bigg[\frac{\eta_m}{2} - \frac{\eta_m}{2} \int_{r>0} f(r) \sqrt{\frac{\theta P_{\text{BS}} A_{M1}}{2\pi r^{\beta} N_0}} \\ &\times \left(\sum_{n=1}^{N} \left\{ \frac{1}{\sqrt{x_n}} \exp\left(\frac{-\theta P_{\text{BS}} A_{M1} x_n}{2r^{\beta} N_0}\right) \mathcal{L}_I\left(\frac{x_n}{N_0}\right) w_n \right\} + R_N \right) dr \Bigg]. \end{aligned} \tag{3.44}$$

By analogy with (3.19), $\mathcal{L}_I\left(\frac{x_n}{N_0}\right)$ can be expressed as

$$\mathcal{L}_I\left(\frac{x_n}{N_0}\right) = \exp\left(-\frac{4}{3}\pi\lambda_{\text{BS}} \times \sum_{k=1}^{K} \left\{ \rho_k \left(\frac{x_n A P_k}{N_0}\right)^{\frac{3}{\beta}} \int_{\left(\frac{x_n A_{M1} P_k}{N_0} r^{\beta}\right)^{\frac{-3}{\beta}}}^{\infty} \frac{1}{1 + a^{\frac{\beta}{3}}} \, da \right\} \right), \tag{3.45}$$

Now, by substituting (3.45) in (3.44), and by using the probability $\rho_{k'}$, $\bar{P}_e$ is given by,

$$\begin{aligned} \bar{P}_e = \frac{\eta_m}{2} - \frac{\eta_m}{2} \int_{r>0} 4\pi\lambda_{\text{BS}} r^2 \exp\left(-\frac{4}{3}\pi\lambda_{\text{BS}} r^3\right) \sqrt{\frac{\theta P_{\text{BS}} A_{M1}}{2\pi r^{\beta} N_0}} \Bigg[\sum_{n=1}^{N} \Bigg\{ \frac{1}{\sqrt{x_n}} \exp\left(\frac{-\theta P_{\text{BS}} A_{M1} x_n}{2r^{\beta} N_0}\right) - \\ \times \frac{4}{3}\pi\lambda_{\text{BS}} \sum_{k=1}^{K} \left\{ \rho_k \left(\frac{x_n A_{M1} P_k}{N_0}\right)^{\frac{3}{\beta}} \int_{\left(\frac{x_n A_{M1} P_k}{N_0 r^{\beta}}\right)^{\frac{-3}{\beta}}}^{\infty} \frac{1}{1 + a^{\frac{\beta}{3}}} \, da \right\} \Bigg) w_n \Bigg\} + R_N \Bigg] dr. \end{aligned} \tag{3.46}$$

Finally, by using the change in variable : $x_q = \frac{4}{3}\pi\lambda_{\text{BS}} r^3$, and Theorem 1, $\bar{P}_e$ is expressed as in (3.47), where $\omega_{k'} = \sqrt{\frac{\theta P_{k'} A_{M1}}{2\pi N_0 \left(\frac{3x_q}{4\pi\lambda_{\text{BS}}}\right)^{\frac{\beta}{3}}}}$.

$$\bar{P}_e = (\eta_m/2) - (\eta_m/2) \sum_{k'=1}^{K} \left\{ \rho_{k'} \left(\sum_{q=1}^{Q} w_q \omega_{k'} \left[\sum_{n=1}^{N} \frac{w_n}{\sqrt{x_n}} \right.\right.\right. \\ \left.\left.\left. \times \exp\left(-\pi x_n \omega_{k'}^2 - \frac{4}{3}\pi\lambda_{\text{BS}} \sum_{k=1}^{K} \rho_k \mathfrak{I}(a,b) \right) + R_N \right] + R_q \right) \right\}. \quad (3.47)$$

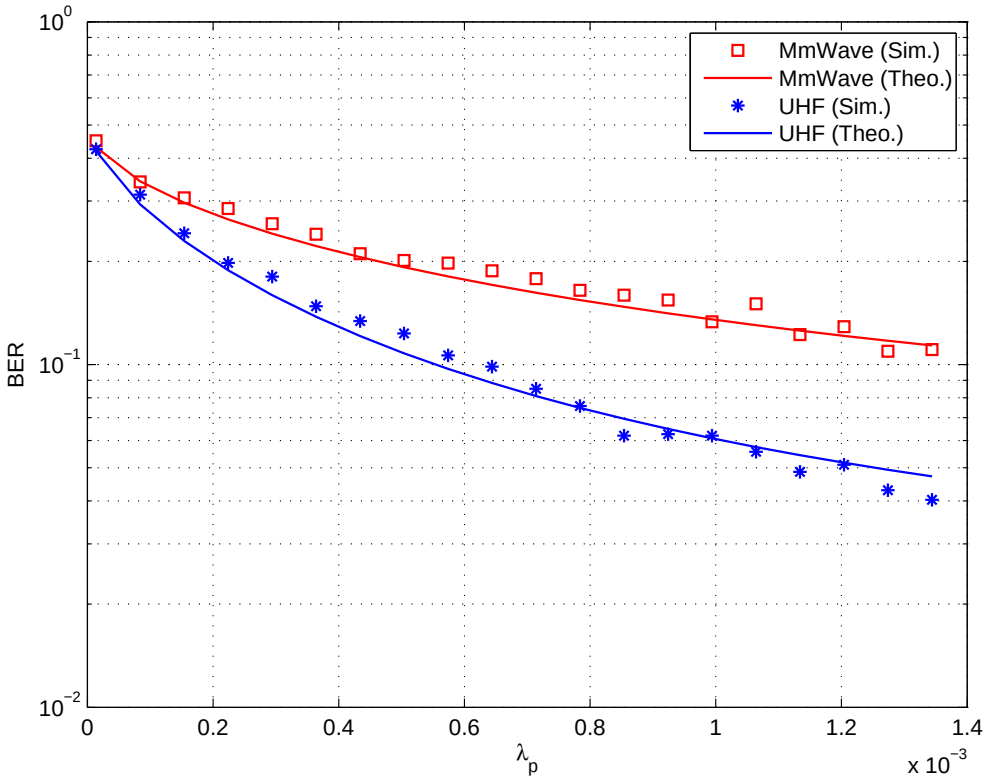

Figure 3.6: Average BER vs. λ_p with $\eta = 0.1$.

Simulations and analytical expression in (3.47) are used to evaluate the BER, where $\theta = 2$ and $\eta_m = 1$, the results are illustrated in Figure 3.6. This figure shows the average BER for mmWave and UHF transmissions vs. λ_p with $N_0 = -110$ dBm, and $\alpha = 5$. The BER is lower when increasing the value of λ_p, which means that the network performance is better when the density of BSs is larger since this will allow to achieve a better coverage. In addition, we can see that UHF performance is better than mmWave performance despite the wider frequency bands of mmWave systems. This is because of their larger pass loss attenuation.

3.4 Conclusion

In this chapter, the performance analysis of the model without blockage effects, as proposed in chapter 2, is introduced. First, we have derived the average coverage probability expression of a down-link HetNet. Simulations results have been compared to the analytical ones in order to highlight the advantage of the proposed 3-D model when compared to the traditionnel 2-D one. Then, based on a 3-D model for K-tier heterogeneous cellular networks, a fair comparison between UHF and mmWave communication systems has been proposed. We have derived the expressions of the successful transmission probability, the average throughput, and the BER for the two transmission bands. The obtained simulation results shows that UHF based communications provide a better coverage and BER due to their lower path loss, while mmWave based communications offer a better throughput due to the higher transmission bandwidth.

Chapter 4

Analysis of Blockage Effects on Urban Cellular Networks

4.1 Introduction

In recent years, several advances in wireless communications played an important role in the development of future 5G networks. However, understanding the wireless propagation channel is very essential to improve the exchange of information between communicating entities. The densely located buildings impact penetration losses and troubles the coverage prediction of cellular networks in urban zones [87]. Such blockage effects become more severe, and may limit the performance of communication systems. Blockage effects are usually integrated into the shadowing model, along with reflections, scattering, and diffraction [88]. All these phenomena are often modeled by employing a log-normal distribution which parameters are determined from measurements. Unfortunately, this model does not describe the distance-dependence of blockage effects, that is the longer the distance between the transmitter and the receiver, the more buildings are likely to intersect the wireless link, hence more shadowing is likely to be experienced [36]. This explains the importance of proposing more sophisticated models of the wireless propagation channel in a dense urban area to capture all its characteristics especially the blockage. This will allow enhancing the performance of 5G networks [89]. In this chapter, we analysis the blockage effects on urban cellular networks under UHF bands. Actually, we derive the probability of LOS, and the coverage probability expression. Numerical results are presented to confirm and discuss the derived analytical expressions. The conducted simulations are based on Monte Carlo simulation using MatLab software, where a channel object is used to represent Rice fading channels with a specific sampling time (T_s), a specific maximum Doppler frequency shift ($f_{\max}$), and a specific

Rician factor $K_{\text{Rice}} = 10^{(K_{\text{Rice}}[dB]/10)}$. Without loss of generality, the used simulation parameters are presented in the Table 4.1.

Table 4.1: Simulation Parameters

Parameter	Value
$Simulation\ Time$ [s]	100
T_s [s]	$1e-4$
N_s	$1e6$
M [dB]	50
N	10
N_{o}	-130 dBm
λ_{BS}	$1e-6$
λ_{BL}	$4e-6$
H_{BS}	30 m
H_{UE}	1 m
$H_{\text{BDG}}^{(\text{max})}$	$1.5H_{\text{BS}}$
$H_{\text{BDG}}^{(\text{min})}$	H_{UE}
R	1000 m
μ	0.5 dB/m
α	2.5
$PL(r_{\text{0}})$	40 dB

4.2 Probability of LOS

In this section, based on the model previously presented in Chapter 2, we derive the probability of LOS expression, the probability that the link between the transmitter and the receiver is line of sight, for different scenarios: 2-D and 3-D cases.

4.2.1 2-D Case

For the 2-D modeling, we denote the point process that is formed by centers of the rectangles C_K with lengths in $(l, l+dl)$, widths in $(w, w+dw)$, and orientations in $(\theta, \theta+d\theta)$ as $\phi(l, w, \theta)$.

Note that $\Phi(l, w, \theta)$ is a subset (partition) of the center point process $\{C_K\}$, and is a PPP with the density of $\lambda_{l,w,\theta} = \lambda_{BL} f_L(l) dl f_W(w) dw f_\Theta(\theta) d\theta$.

The work in [36] has defined a collection of blockages as $B(l, w, \theta) = \{(C_K, L_K, W_K, \Theta_K), C_K \in \Phi(l, w, \theta)\}$. $J(l, w, \theta)$ is supposed to be the number of blockages, which belong to the subset $B(l, w, \theta)$ and cross the link OX. $J(l, w, \theta)$ is a Poisson random variable with mean $E[J(l, w, \theta)] = \lambda_{l,w,\theta}(Rl|\sin(\theta)| + Rw|\cos(\theta)| + lw)$, where R is the length of the link OX.

As shown in Figure 4.1, OX is the link of distance R. P, Q, S, T, U, and V are the centers of the corresponding rectangles. A rectangle from $B(l, w, \theta)$ intersects the link OX if and only if its center falls in the region PQSTUV, which is made up of parallelogram QSUV and right triangles PQV and TSU. Hence $J(l, w, \theta)$ equals the number of points of $\Phi(l, w, \theta)$ falling in the region PQSTUV. Let the area of region PQSTUV be $S(l, w, \theta)$. The number of points of $\Phi(l, w, \theta)$ falling in the region PQSTUV is a Poisson variable with mean $\lambda_{l,w,\theta} S(l, w, \theta)$. Consequently,

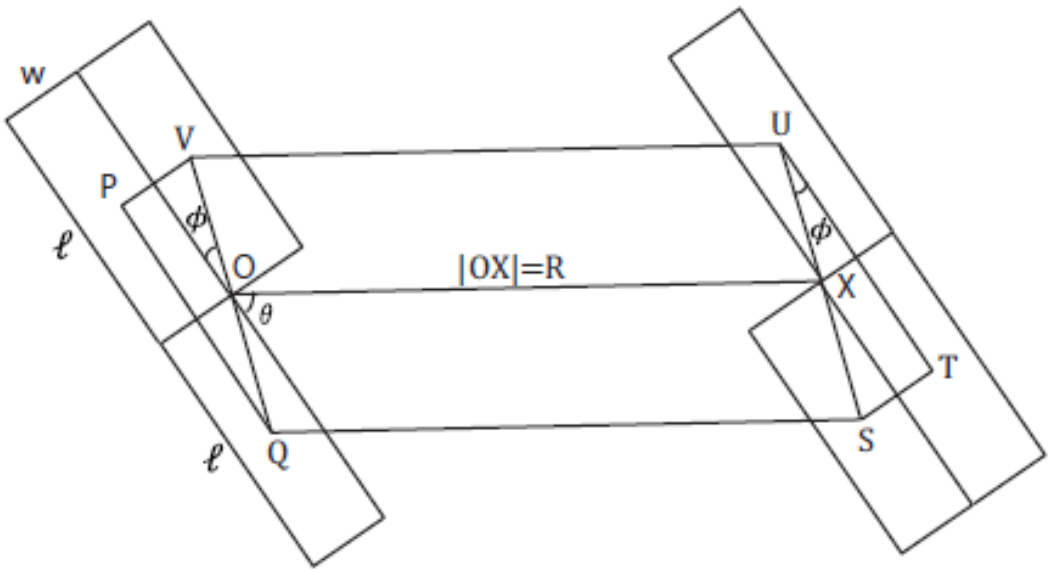

Figure 4.1: Probability of LOS: The link between the transmitter and the receiver [36]

.

$J(l, w, \theta)$ is a Poisson variable with mean

$$
\begin{aligned}
J(l,w,\theta) &= \lambda_{l,w,\theta} S(l,w,\theta) \\
S(l,w,\theta) &= \Big(\text{air of QSUV} + \text{air of PQV} + \text{air of TSU}\Big) \\
&= \Big(R \times \text{height of QSUV} + PQ \times \frac{PV}{2} + TU \times \frac{TS}{2}\Big) \\
&= \Big(R|\sin(\theta+\psi)| \times QV + l \times \frac{w}{2} + l \times \frac{w}{2}\Big) \\
&= \Big(R\big[|\sin(\theta)\cos(\psi) + \cos(\theta)\sin(\psi)|\big] \times \sqrt{l^2+w^2} + lw\Big) \\
&= \Big(R\big[|\sin(\theta)|\frac{l}{\sqrt{l^2+w^2}} + |\cos(\theta)|\frac{w}{\sqrt{l^2+w^2}}\big] \times \sqrt{l^2+w^2} + lw\Big) \\
&= \Big(Rl|\sin(\theta)| + Rw|\cos(\theta)| + lw\Big).
\end{aligned}
$$

Based on [36], we assume that K_{BL} is the number of buildings that blocks a link between a BS and a user. K_{BL} is a Poisson distributed random variable with the mean $\beta R + p$, where $\beta = 2\frac{\lambda_{BL}}{\pi}\Big(E[W] + E[L]\Big)$, and $p = \lambda_{BL} E[L]E[W]$.
Thus, the probability that a link of length r admits line-of-sight propagation, i.e., no blockages cross the link, is expressed as follow [36]

$$P_{\text{LOS}}^{(2D)} = \exp(\beta r + p) \tag{4.1}$$

4.2.2 3-D Case

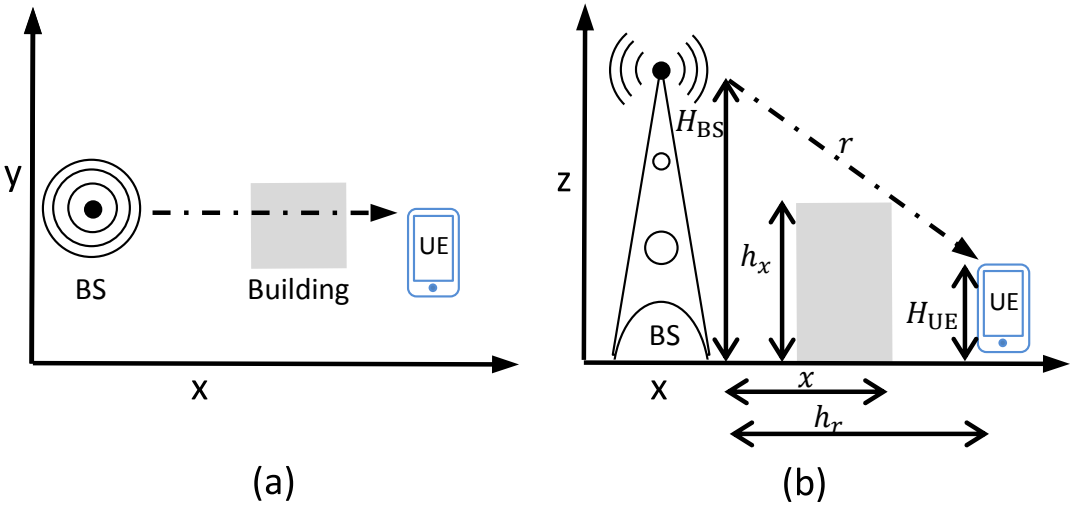

Figure 4.2: LOS: a) X-Y modeling, and b) X-Z modeling

The 3-D model takes into consideration the height of UE, BS, and buildings, which must improve the probability of having a LOS link between an active user and its serving BS. As shown

in Figure 4.2, some buildings blocks the wireless link in 2-D model (a), while allowing the communication between the user and its base station when taking into account the 3-D representation (b). Let us consider a building intersecting the link between the user and the BS in the X-Y plane (a) and located at a distance x away from the BS. As depicted in Figure4.2 (b), the building blocks the direct propagation path only if its height $h > h_{x}$, where h_{x} can be computed as

$$h_{x} = \frac{x\, H_{\text{UE}} + (h_{r} - x) H_{\text{BS}}}{h_{r}} \tag{4.2}$$

Accordingly, it is clear that when $x = 0, h_{x} = H_{\text{BS}}$. Based on that, the probability of LOS is expressed as follow

$$\begin{aligned} P_{\text{LOS}}^{(\text{3D})} &= P_{\text{LOS}}^{(\text{2D})} + (1 - P_{\text{LOS}}^{(\text{2D})}) P(h < h_{x}) \\ &= P_{\text{LOS}}^{(\text{2D})} + (1 - P_{\text{LOS}}^{(\text{2D})}) \int_{0}^{h_{r}} \frac{1}{h_{r}} \int_{H_{\text{BDG}}^{(\text{min})}}^{h_{x}} \frac{1}{H_{\text{BDG}}^{(\text{max})} - H_{\text{BDG}}^{(\text{min})}} \text{d}h\, \text{d}x \\ &= P_{\text{LOS}}^{(\text{2D})} + \frac{\left(1 - P_{\text{LOS}}^{(\text{2D})}\right)\left(H_{\text{BS}} - H_{\text{BDG}}^{(\text{min})}\right)}{2\left(H_{\text{BDG}}^{(\text{max})} - H_{\text{BDG}}^{(\text{min})}\right)}, \end{aligned} \tag{4.3}$$

where H_{BDG} is the height of buildings which is varying between $H_{\text{BDG}}^{(\text{max})}$ and $H_{\text{BDG}}^{(\text{min})} (H_{\text{UE}} \approx H_{\text{BDG}}^{(\text{min})})$.

Figure4.3 presents the probability of LOS for 2-D modeling and 3-D modeling. As shown in this figure, the probability of 3-D model outperforms that of the 2-D one, and the difference between them increase by increasing the distance r. The main reason for this phenomenon is that some blockages can intersect the link between the BS and the target user in the in 2-D, but, when considering the height of blockages, the connection can be established since the height of buildings is not sufficient to block the direct link. This makes the probability of LOS in 3-D better.

Figure 4.4 presents the probability of LOS for 2-D modeling and 3-D modeling with different buildings dimensions. As shown in this figure, by increasing the values of $E[L]$ and $E[W]$, the probability of LOS is decreasing because bigger buildings may limit more the propagation and may block the transmission.

4.3 Coverage probability

In this section, we derive the coverage probability expressions.

The successful transmission is the event when the corresponding communication channel supports a target SNR higher then a given threshold γ_{th}. The general expression for P_{C} can be written

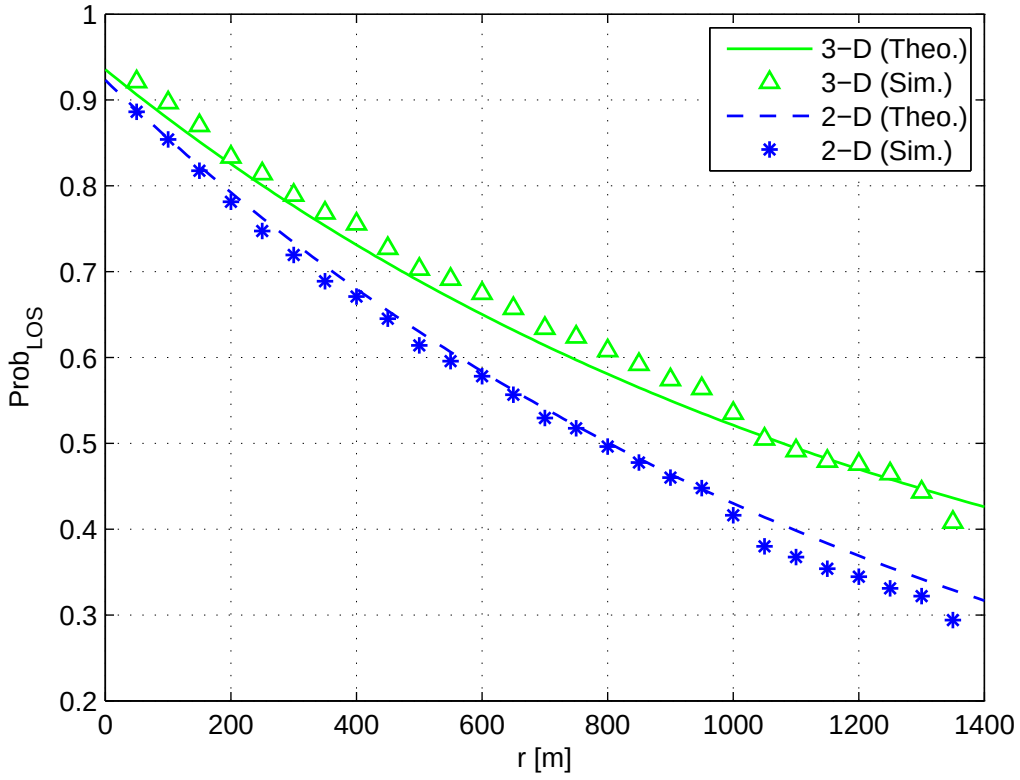

Figure 4.3: Probability of LOS: 2-D modeling vs. 3-D modeling.

as

$$P_{\mathrm{C}} = \mathbb{E}_{\{r\}}\Big[\Pr\Big\{\mathrm{SNR} \geq \gamma_{\mathrm{th}} | r\Big\}\Big] \,. \tag{4.4}$$

The coverage probability under the Rayleigh, the Rice and the hybrid fading assumptions is respectively denoted by $P_{\mathrm{C}}^{(\mathrm{Rayleigh})}$, $P_{\mathrm{C}}^{(\mathrm{Rice})}$, and $P_{\mathrm{C}}^{(\mathrm{Hybrid})}$. In the following, the different expressions of the coverage probability are derived.

4.3.1 Rayleigh Fading Assumption

In this subsection, we derive the expression of the $P_{\mathrm{C}}^{(\mathrm{Rayleigh})}$, which is given by

$$P_{\mathrm{C}}^{(\mathrm{Rayleigh})} = \mathbb{E}_{\{r\}}\Big[\Pr\Big\{\mathrm{SNR} \geq \gamma_{\mathrm{th}} | r\Big\}\Big] \tag{4.5}$$

Based on equation (2.29), $P_{\mathrm{C}}^{(\mathrm{Rayleigh})}$ is expressed as follow,

$$P_{\mathrm{C}}^{(\mathrm{Rayleigh})} = \Pr\left\{H \geq \gamma_{\mathrm{th}} P_{\mathrm{BS}}^{-1} A_{M2}^{-1} r^{\beta} \left(N_0\right)\right\}, \tag{4.6}$$

By using the exponential PDF expression of H, (4.6) can be rewritten as follows

$$P_{\mathrm{C}}^{(\mathrm{Rayleigh})} = \int_{r\geq 0} f(r) \times \mathbb{E}\Big[\exp\Big(-\gamma_{\mathrm{th}} P_{\mathrm{BS}}^{-1} A_{M2}^{-1} r^{\beta} N_0\Big)\Big] dr, \tag{4.7}$$

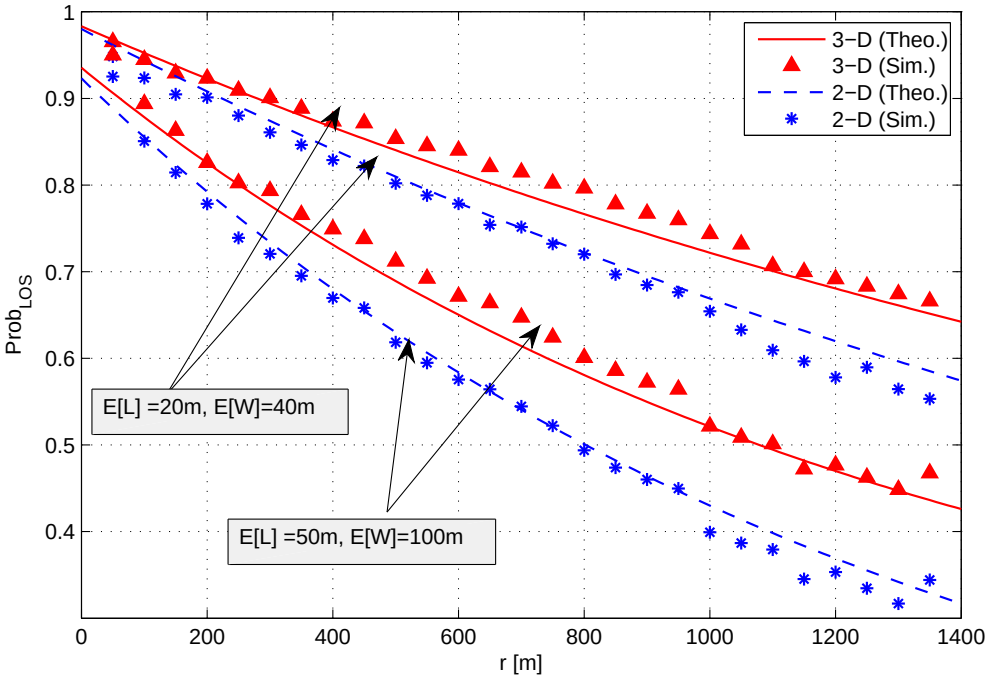

Figure 4.4: Probability of LOS: 2-D modeling vs. 3-D modeling with different $E[L]$ and $E[W]$.

The $P_{\text{C}}^{(\text{Rayleigh})}$ expression can be further simplified using the following Theorem

Theorem 1. *Let $f(x)$ be a given function defined for all real numbers x. Then*

$$\int_0^{\infty} f(x)\exp(-x)\,dx = \sum_{n=1}^{N} f(x_n)w_n + R_N, \tag{4.8}$$

where, x_n, w_n, and R_N are the n^{th} abscissa (root), weight, and remainder of the N^{th} order Laguerre polynomial, respectively [85].

The Laguerre Polynomial of order N, is expressed as follow

$$L_N(x) = \sum_{k=0}^{N} \frac{(-1)^k}{k!}\binom{n}{k}x^k. \tag{4.9}$$

and, w_n is given by

$$w_n = \frac{x_n}{(N+1)^2(L_{N+1}(x_n))^2}, \tag{4.10}$$

Based on Theorem 1, and by employing a variable change $x = \frac{4}{3}\pi\lambda_{\text{BS}}r^3$, the average coverage probability is expressed as follows,

$$P_{\text{C}}^{(\text{Rayleigh})} = \sum_{n=1}^{N}\left\{w_n \times \exp\left(\frac{\gamma_{\text{th}}N_{\text{o}}}{P_{\text{BS}}A_{M2}}\left[\frac{x_n}{\pi\lambda_{\text{BS}}} + (H_{\text{BS}} - H_{\text{UE}})^2\right]^{\alpha+1}\right)\right\}, \tag{4.11}$$

where, x_n and w_n are the n^{th} abscissa (root) and weight of the N^{th} order Laguerre polynomial, respectively.

4.3.2 Rice Fading Assumption

In this subsection, we derive the coverage probability expression under rice fading assumption. Here, the received signals are assumed to be subject to the Rician type of fading, where the corresponding PDF of the channel gain squared amplitude with unit mean is expressed as follows [90]

$$p_{\text{Rice}}(x) =(K_{\text{Rice}}+1)\exp\left(-K_{\text{Rice}}\right)\exp\Big(-(K_{\text{Rice}}+1)x\Big)\times \mathrm{I}_0\Big(2\sqrt{K_{\text{Rice}}\,(K_{\text{Rice}}+1)x}\Big), \quad (4.12)$$

where K_{Rice} is the Rician factor.
To simplify the analytical derivations of the corresponding coverage probability expression, and based on the alternative expression of $\mathrm{I}_0(.)$ [91, Eq. (8.445)], a tight approximation of (4.12) is given by,

$$\begin{aligned} p_{\text{Rice}}(x) \approx&(K_{\text{Rice}}+1)\exp\left(-K_{\text{Rice}}\right)\exp\Big(-(K_{\text{Rice}}+1)x\Big)\\ &\times\sum_{m=0}^{M}\Big[K_{\text{Rice}}(K_{\text{Rice}}+1)\Big]^m\frac{x^m}{m!\,\Gamma(m+1)}, \end{aligned} \quad (4.13)$$

where, $M >> 1$ is a large integer.

To confirm the accuracy of the approximate expression in (4.13), we present in Figure 4.5 empirical PDF of the Rice channel gain squared amplitude as well as the exact and approximate PDF expressions in (4.12) and (4.13), respectively, with $K_{\text{Rice}} = 1$. As shown in this figure, there is an excellent fit between the exact and the approximate expressions, where an average error of less than $1\text{e}{-12}$ (for $M = 50$) is observed.

Now, based on the PDF approximate expression in (4.13) and on [91, Eq. $(3.351.1)$], the coverage probability, under Rice assumption, denoted by $P_{\text{C}}^{(\text{Rice})}$, is derived as follows

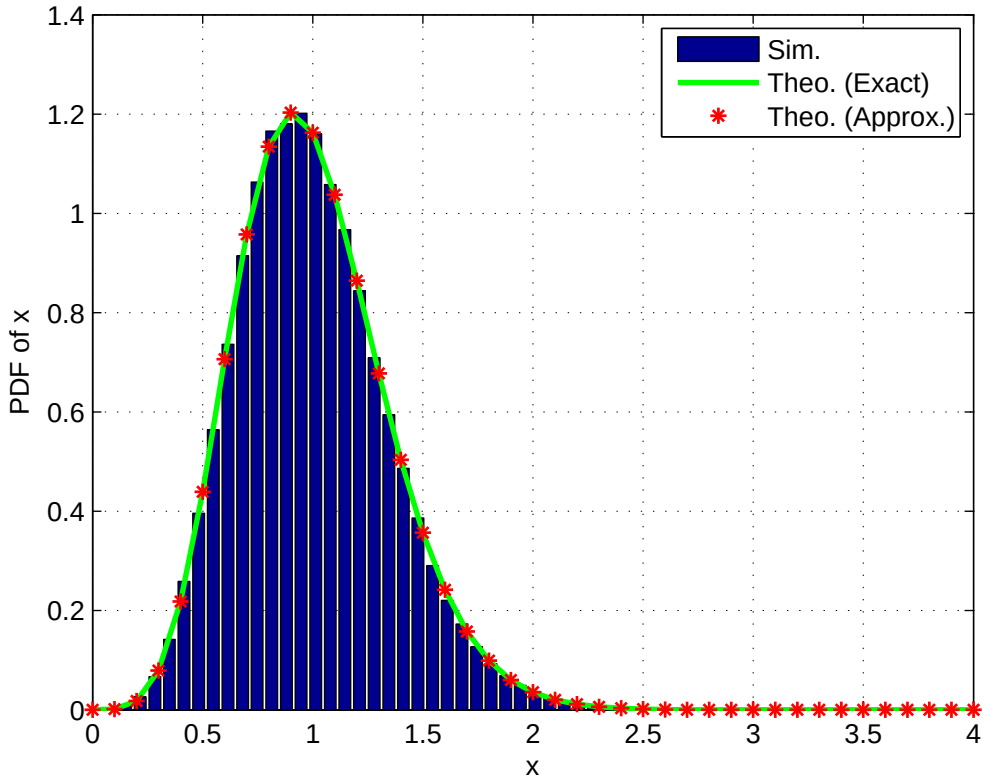

Figure 4.5: Empirical PDF of the Rice channel gain squared amplitude as compared to the exact and approximate expressions in (4.12) and (4.13), respectively, with $K_{\text{Rice}}[dB] = 12$ dB.

$$
\begin{aligned}
P_{\text{C}}^{(\text{Rice})} &= 1 - Pr(\text{SNR} < \gamma_{\text{th}}) \\
&= 1 - \int_0^{\infty} f(r) \int_0^{\frac{\gamma_{\text{th}} N_{\text{o}} r^{\alpha+1}}{P_{\text{BS}} A_{M2}}} p_{\text{Rice}}(x)\, \mathrm{d}x\, \mathrm{d}r \\
&\approx 1 - (K_{\text{Rice}}+1) \exp\left(-K_{\text{Rice}}\right) \int_0^{\infty} f(r) \sum_{m=0}^{M} \left\{ \left[K_{\text{Rice}}(K_{\text{Rice}}+1)\right]^m \frac{1}{\Gamma(m+1)} \right. \\
&\left. \left(\left[K_{\text{Rice}}+1\right]^{-m-1} - \sum_{l=0}^{m} \frac{y^l}{l!} \exp\Big(-y\,(K_{\text{Rice}}+1)\Big) \left[K_{\text{Rice}}+1\right]^{l-m-1} \right) \right\} \mathrm{d}r, \quad (4.14)
\end{aligned}
$$

with, $y = \frac{\gamma_{\text{th}} N_{\text{o}} r^{\alpha+1}}{P_{\text{BS}} A_{M2}}$. By applying a change of variables: $x = \lambda_{\text{BS}} \pi \left[r^2 - (H_{\text{BS}} - H_{\text{UE}})^2\right]$, and based on Laguerre Theorem (theorem 1), the final expression of $P_{\text{C}}^{(\text{Rice})}$ is given by,

$$P_{\mathrm{C}}^{(\mathrm{Rice})} \approx 1 - (K_{\mathrm{Rice}}+1)\exp\left(-K_{\mathrm{Rice}}\right)\sum_{m=0}^{M}\left\{\frac{\left[K_{\mathrm{Rice}}(K_{\mathrm{Rice}}+1)\right]^{m}}{\Gamma(m+1)} \times \left(\left[K_{\mathrm{Rice}}+1\right]^{-m-1} - \sum_{n=1}^{N} w_n \sum_{l=0}^{m}\frac{z_n^{l}}{l!}\,\exp\Big(-z_n\,(K_{\mathrm{Rice}}+1)\Big)\left[K_{\mathrm{Rice}}+1\right]^{l-m-1}\right)\right\}, \tag{4.15}$$

with, $z_n = \frac{\gamma_{\mathrm{th}} N_{\mathrm{o}}}{P_{\mathrm{BS}} A}\left[\frac{x_n}{\pi\lambda_{\mathrm{BS}}} + (H_{\mathrm{BS}} - H_{\mathrm{UE}})^2\right]^{\frac{\alpha+1}{2}}$.

4.3.3 Hybrid Fading Assumption

In this subsection, we derive the coverage probability expression under hybrid fading assumption. The link between a user and its serving BS could be established in two scenarios: LOS and NLOS. The NLOS links are traditionally modeled by Rayleigh fading channels, while the Rice fading channels represent usually the LOS links. Here, we will try to capture the two scenarios since their probability of occurrence is already calculated in equation (4.3). However, the two above sections are dedicated to the derivation of the coverage probability under the two fading assumptions. Hence, when combining the two probabilities under the hybrid assumption, the coverage probability is given by,

$$P_{\mathrm{C}}^{(\mathrm{Hybrid})} = P_{\mathrm{LOS}}^{(\mathrm{3D})}\, P_{\mathrm{C}}^{(\mathrm{Rice})} + (1 - P_{\mathrm{LOS}}^{(\mathrm{3D})})\, P_{\mathrm{C}}^{(\mathrm{Rayleigh})}. \tag{4.16}$$

Figure 4.6 shows the variations of the coverage probability under the different assumptions as a function of the SNR Threshold. Analytical and simulations results are identical which confirm the accuracy of the expressions derived as above. We can clearly see that the Rice fading assumption has the best coverage probability due to the fact that it is suitable for LOS environments and Rayleigh fading assumption is adequate for NLOS environments. For a 3-D more realistic network, the hybrid assumption is combining the two scenarios which is better than the most useful channel assumption (Rayleigh) in research papers.

Figure 4.7 shows the variations of the coverage probabilities under the different assumptions vs. SNR Threshold for different K_{Rice}. Coverage probabilities under Rice assumption and hybrid assumption are decreasing with the decreasing value of the Rician factor, which is the ratio of signal power in dominant component over the (local-mean) scattered power, and become closer to the Rayleigh fading coverage probability. This is because the common Rayleigh fading is a special case of the rice fading with $K_{\mathrm{Rice}} = 0$.

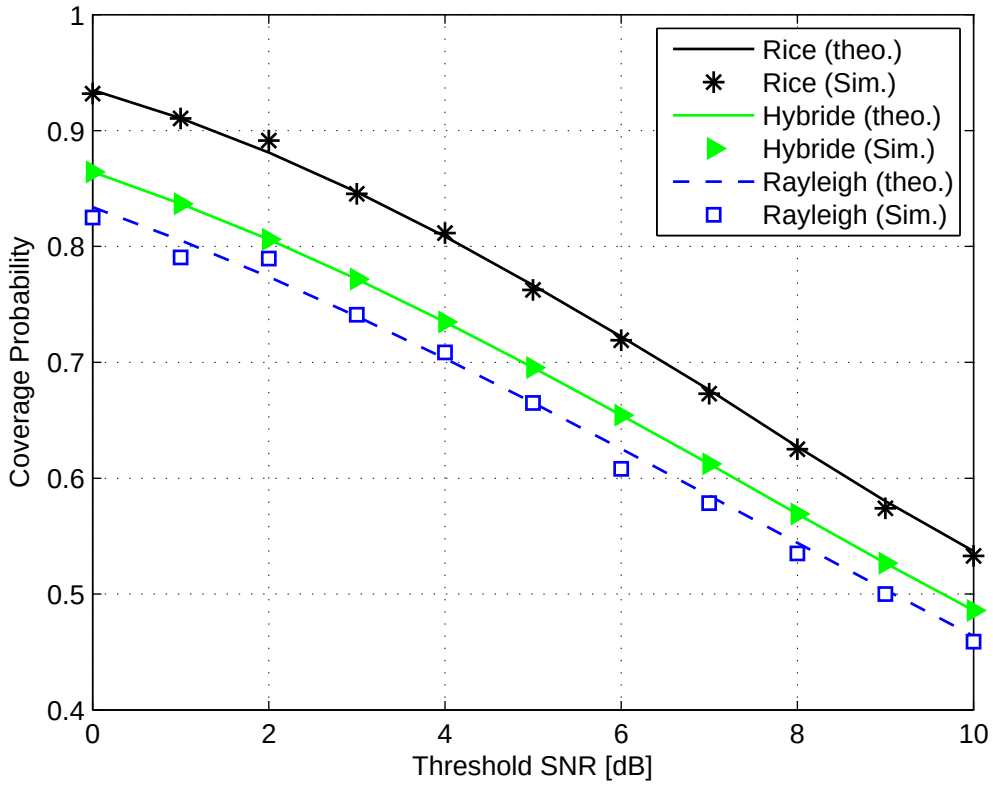

Figure 4.6: Coverage Probabilities for the different assumptions.

4.4 Conclusion

In this chapter, a hybrid fading assumption is proposed when a 3-D model of wireless communication networks is employed. We have derived the expressions of the probability of LOS for 2-D and 3-D cases, and, the coverage probability under different assumptions. The simulation results show that the probability of 3-D model outperforms that of the 2-D one. In fact, some blockages can intersect the link between the BS and the target user in the in 2-D, but, when considering the height of blockages, the connection can be established since the height of buildings is not sufficient to block the direct link. This makes the probability of LOS in 3-D better.

Besides, simulation results are presented to highlight the advantage of the hybrid fading assumption under which the system performance is the more realistic. For a 3-D network, the hybrid assumption is combining the two scenarios (LOS/NLOS) which is better than the most useful channel assumption (Rayleigh) in research papers.

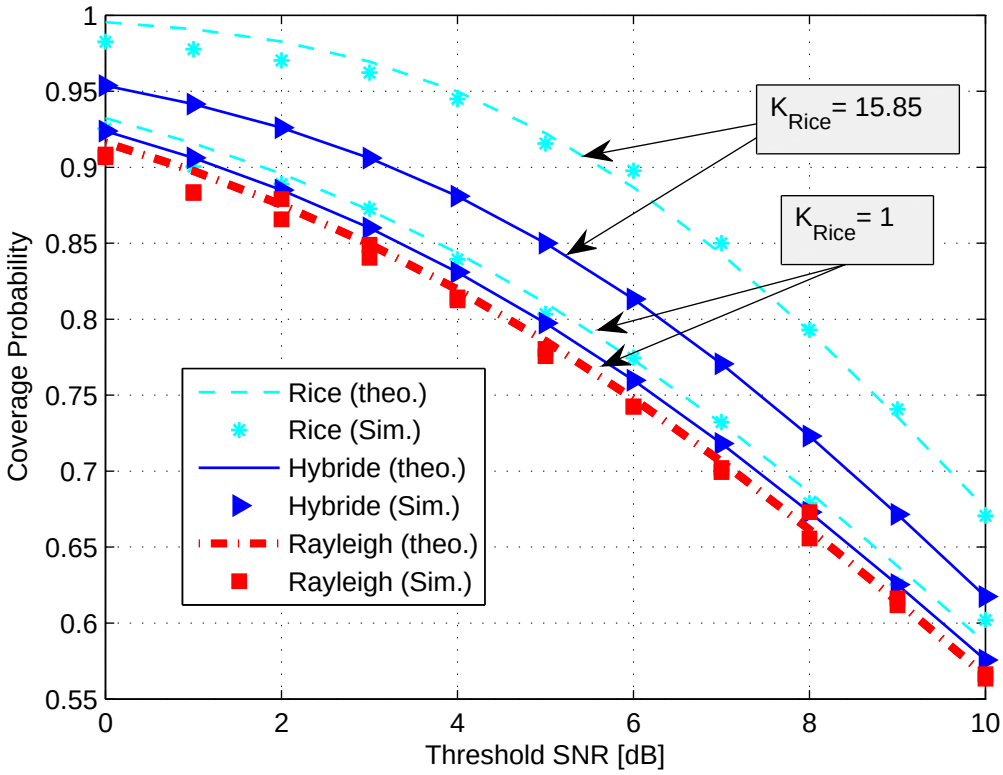

Figure 4.7: Coverage Probabilities for the different assumptions with different K_{Rice}.

Chapter 5

Energy Harvesting Based Scheme for 3-D Cellular Network

5.1 Introduction

Thanks to energy harvesting, BSs and devices are becoming self-sustaining. This technology can improve the efficiency of wireless communication networks [92], and can prolong the durability of batteries [93]. BSs and users may harvest energy by two ways [81]. The environment, such as solar energy or wind energy [94], presents the first renewable energy. However, these natural sources are volatile, and liable to change rapidly and unpredictably, which can impact on the quality of service. On the other hand, BSs and users can harvest energy from ambient radio signals, relying on RF energy harvesting [51]. Based on that, power transfer is envisaged as a promising technology for 5G mobile networks.

This chapter presents an energy harvesting based scheme for 3-D cellular networks in order to enhance communications system performance. The proposed scheme is based on the energy harvesting to reduce the transmission delay and to enhance the ergodic capacity. That is why, the average transmission delay and the ergodic capacity expressions are detailed and derived. Using numerical results, the analytical derived expressions are evaluated, and the advantages of the proposed scheme are investigated.

5.2 Energy Harvesting based Transmission (EHT)

In this section, we propose a new communication scheme for 3-D cellular networks. A new algorithm is proposed to enhance the average delay of transmission, and systematically, enhance

the ergodic capacity.

As shown in Algorithm 1, the standard scheme is used when the SNR can't reach a predefined level γ_{th}. Then, the communication between the transmitter and the receiver is successfully established.

Algorithm 1 : Standard Scheme

$P = P_{\text{BS}}, k = 1$: The initial number of time slot
while $(SNR < \gamma_{\text{th}})$ & $(k \leq TS_{\text{max}})$ **do**
    $k++$.
    Updating the channel state information.
    Updating SNR
Endwhile
delay = k

To improve the previously introduced 3-D model without blockage effects, we propose the following transmission scheme:

Algorithm 2 : The Energy Harvesting Transmission (EHT) Scheme Algorithm

$P = P_{\text{BS}}, k = 1$: The initial number of time slot
while $(SNR < \gamma_{\text{th}})$ & $(k \leq TS_{\text{max}})$ **do**
    $k++$.
    Updating the channel state information.
    if (Harvesting Condition) **then**
        The BS harvest and update its power P
        $P = P + \nu_{\text{EH}} P_{\text{BS}}$ (ν_{EH} is the $\%$ of power added)
        Updating SNR
    Endif
Endwhile
delay = k

This algorithm improves the SNR by allowing the BSs to harvest energy and increase the transmission power. For a given user, a BS is able to increase the SNR by a certain rate, ν_{EH}, each time slot provided that it exists at least one BS (different of the serving BS) in the harvesting zone. Accordingly, the serving BS continues harvesting the energy until the SNR reach a predefined level γ_{th}. However, the number maximal of time slots is given by TS_{max} which will limit the delay. When the required level of SNR γ_{th} is reached, the transmission is ensured which will enhance the average delay of transmission.

5.3 Performance Analysis

In this section, we detail the general expression of the average delay of transmission, and ergodic capacity expressions. Here, we assume that a perfect interference cancellation is performed.
For the simulation environment, we consider a 3-D space region ($R \times R \times R$) in a dense urban area under UHF bands. Simulations results are based on the Table 5.1.

Table 5.1: Simulation Parameters

Parameter	Value
λ_{BS}	$2e-4$/m^3
P_{BS}	200 mW
R	100 m
d_{min}	5 m
r_{EH}	10 m
N_0	-120 dBm
$PL_{RF}(1)$	40 dB
μ	0.5 dB/m
ν_{EH}	0.3

5.3.1 Average Delay of Transmission

5.3.1.1 Standard Scheme

Here, the standard scheme is when the BS does not harvest any energy. Hence, the algorithm looks like the above one only without updating the energy value. In general, the expression of the average delay is derived as follow

$$\bar{D} = \sum_{k=1}^{TS_{\max}} k\, P_k, \tag{5.1}$$

where, P_k, is the probability that the successful transmission is ensured at time slot k, and systematically, is the probability that the BS couldn't transmit in the $k-1$ time slots. This can be explained by the fact the the distance betwenn the mobile user and the BS can change,

$$P_k = STP_0\,(1-STP_0)^{k-1}, \tag{5.2}$$

where, STP_0 is the successful transmission probability, which is given by

$$STP_0 = \mathbb{E}_{\{r\}}\Big[\Pr\Big\{SNR_0 \geq \gamma_{\text{th}}|r\Big\}\Big] \tag{5.3}$$

Thus, STP_0 is expressed as follow,

$$STP_0 = \Pr\left\{H \geq \gamma_{\text{th}} P_{\text{BS}}^{-1} A_{M1}^{-1} r^{\beta} N_0\right\}, \tag{5.4}$$

By using the exponential PDF expression of H, (5.4) can be rewritten as follows

$$STP_0 = \int_{r\geq 0} f(r) \times \mathbb{E}\Big[\exp\Big(-\gamma_{\text{th}} P_{\text{BS}}^{-1} A_{M1}^{-1} r^{\beta} N_0\Big)\Big] dr, \tag{5.5}$$

The STP_0 expression can be further simplified using the following Theorem

Theorem 1. *Let $f(x)$ be a given function defined for all real numbers x. Then*

$$\int_0^{\infty} f(x)\exp(-x)\,dx = \sum_{n=1}^{N} f(x_n)w_n + R_N, \tag{5.6}$$

where, x_n, w_n, and R_N are the n^{th} abscissa (root), weight, and remainder of the N^{th} order Laguerre polynomial, respectively [85].

The Laguerre Polynomial of order N, is expressed as follow

$$L_N(x) = \sum_{k=0}^{N} \frac{(-1)^k}{k!}\binom{n}{k}x^k. \tag{5.7}$$

and, w_n is given by

$$w_n = \frac{x_n}{(N+1)^2(L_{N+1}(x_n))^2}, \tag{5.8}$$

Based on Theorem 1, and by employing a variable change $x = \frac{4}{3}\pi\lambda_{\text{BS}} r^3$, the average coverage probability of the proposed scheme is expressed as follows,

$$STP_0 = \sum_{n=1}^{N}\left\{w_n \exp\Big(-\Big[\frac{\gamma_{\text{th}} N_0}{P_{\text{BS}} A_{M1}}\Big]\Big[\frac{3x_n}{4\pi\lambda_{\text{BS}}}\Big]^{\frac{\beta}{3}}\Big)\right\}. \tag{5.9}$$

5.3.1.2 Energy Harvesting based Scheme

Now, based on the proposed algorithm, and on (5.1), we derive the delay expression. Using the new algorithm, the serving BS have to search for another BS in the harvesting zone in order to harvest, at the current time slot. Thus, we can see in the derivation above that we have to consider the two cases (if the BS harvest or not). Based on that, we can derive the probability P_k as follow,

$$\begin{cases} \text{ts= 1} \;\; \mathrm{P}_1 = STP_0, \\ \text{ts= 2} \;\; \mathrm{P}_2 = (1 - STP_0)\,(P_{EH}\; STP_1 + (1 - P_{\text{EH}})\; STP_0), \\ \text{ts= 3} \;\; \mathrm{P}_3 = (1 - STP_0)\; P_{\text{EH}}\; (1 - STP_1) \times (P_{\text{EH}}\; STP_2 + (1 - P_{\text{EH}})\; STP_1) \\ \qquad\quad + (1 - STP_0)\; (1 - P_{\text{EH}})\; (1 - STP_0) \times (P_{\text{EH}}\; STP_1 + (1 - P_{\text{EH}})\; STP_0), \end{cases}$$

where P_{EH}, the probability that another BS is in the harvesting zone and the serving BS can harvest, is expressed as follows:

$$P_{\text{EH}} = 1 - \exp(\frac{-4}{3}\;\pi\;\;(r_{EH}^3)), \tag{5.10}$$

STP_k is the successful transmission probability, when the power is increased for k times (ν_{EH} is the percentage to be added to the transmit power when the BS harvest.), which is given by

$$STP_k = \mathbb{E}_{\{r\}}\Big[\Pr\Big\{SNR_k \geq \gamma_{\text{th}} | r\Big\}\Big]\,. \tag{5.11}$$

Thus, STP_k is expressed as follow,

$$STP_k = \Pr\Big\{H \geq \gamma_{\text{th}}(1 + \nu_{\text{EH}} k) P_{\text{BS}}^{-1} A_{M1}^{-1} r^{\beta}\;(N_0)\Big\}, \tag{5.12}$$

By using the exponential PDF expression of H, (5.12) can be rewritten as follows

$$STP_k = \int_{r\geq 0} f(r) \times \mathbb{E}\Big[\exp\Big(-\gamma_{\text{th}}(1 + \nu_{\text{EH}} k) P_{\text{BS}}^{-1} A_{M1}^{-1} r^{\beta} N_0\Big)\Big] dr, \tag{5.13}$$

Based on Theorem 1, and by employing a variable change $x = \frac{4}{3}\pi\lambda_{\text{BS}} r^3$, the average coverage probability of the proposed scheme is expressed as follows,

$$STP_k = \sum_{n=1}^{N} \Bigg\{ w_n \exp\Big(- \Big[\frac{\gamma_{\text{th}} N_0}{(1 + \nu_{\text{EH}} k) P_{\text{BS}} A_{M1}}\Big]\Big[\frac{3x_n}{4\pi\lambda_{\text{BS}}}\Big]^{\frac{\beta}{3}}\Big)\Bigg\}, \tag{5.14}$$

and, r_{EH} is the rayon of the spherical harvesting zone.

Based on the first three time slots, the expression of P_k is generalized as

$$P_{k>1} = (1 - STP_0) \sum_{n_2=0}^{1} \Bigg\{ (1 - STP_{n_2}) \times \sum_{n_3=n_2}^{n_2+1} \{ \\ (1 - STP_{n_3}) \ldots \sum_{n_k=n_{k-1}}^{n_{k-1}+1} \{STP_{n_k}\; P_{\text{EH}}^{n_k} (1 - P_{\text{EH}})^{k-1-n_k}\}\} \Bigg\} \tag{5.15}$$

Fig. 5.1 presents the average successful transmission probability vs. γ_{th} for different values of time slot k. As shown in this figure, increasing the time slot k offer a better performance in term of successful transmission probability. This because that the SNR is increasing when the BS

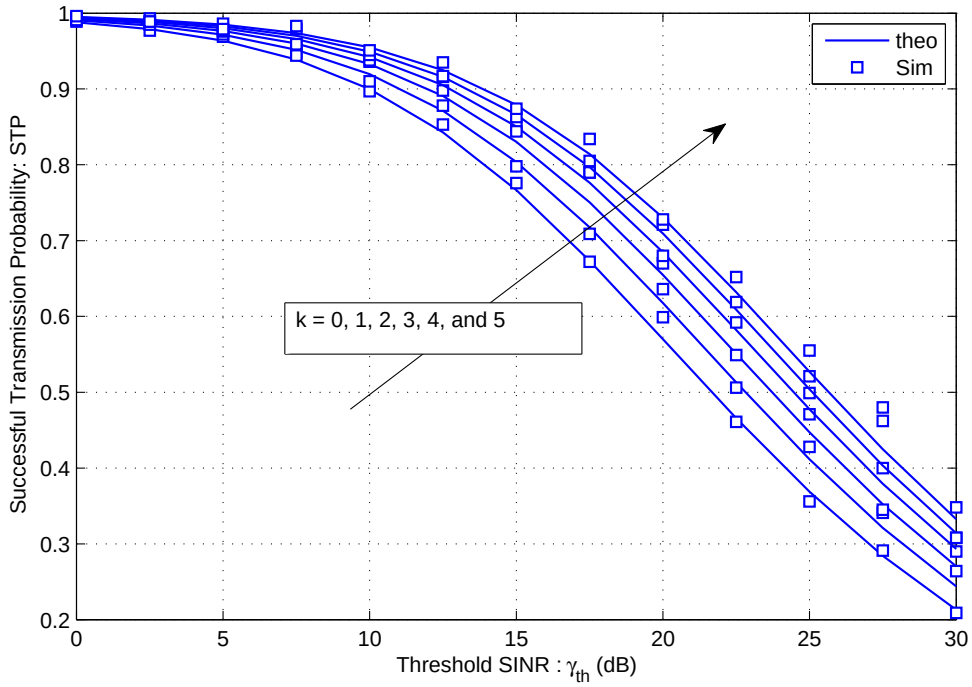

Figure 5.1: Average successful transmission probability vs. γ_{th} with different values of time slots k.

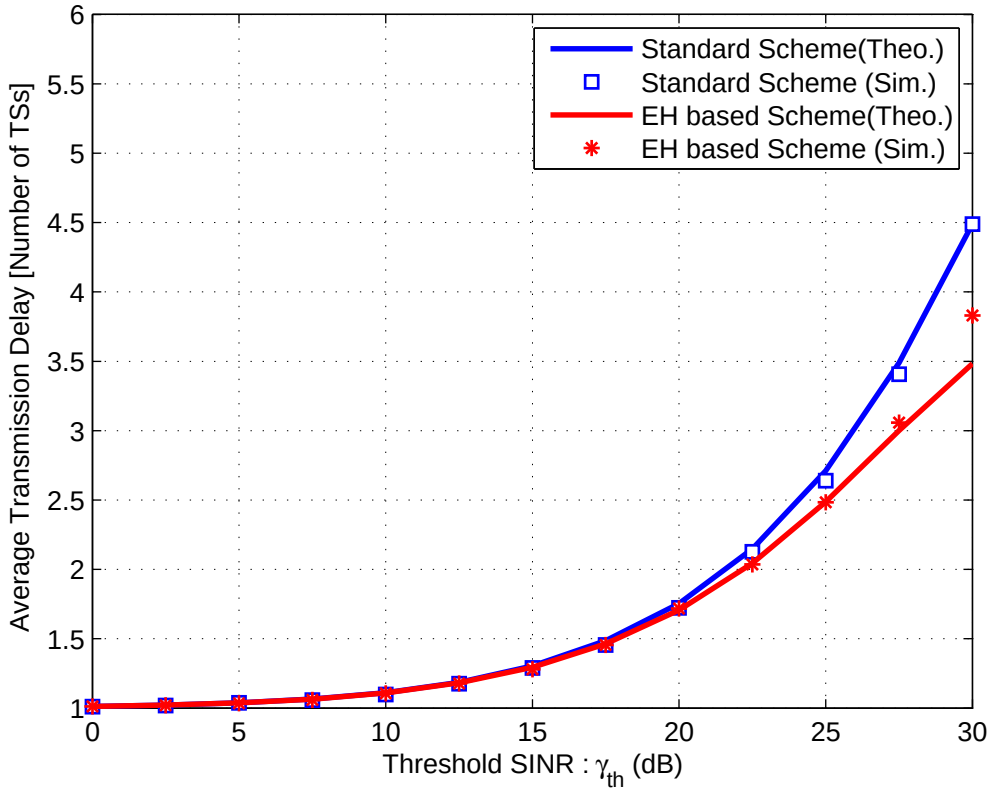

Figure 5.2: Average transmission delay vs. γ_{th} with $P_{\text{BS}} = 0.2W$, $TS_{\text{max}} = 20$, and $\nu_{\text{EH}} = 0.3$.

harvest more energy, at each time slot.

Fig. 5.2 presents the average transmission delay vs. γ_{th} when $P_{\text{BS}} = 0.2W$, $TS_{\max} = 20$ and $\nu_{\text{EH}} = 0.3$. This figure shows that the delay increases when increasing the value of γ_{th} for the two schemes. Also, the proposed algorithm reduces the delay when γ_{th} is higher than 20 dB. The main reason for this phenomenon is that the energy harvesting enhance the SNR, which in turn improves the performance in term of successful transmission probability and consequently in terms of delay.

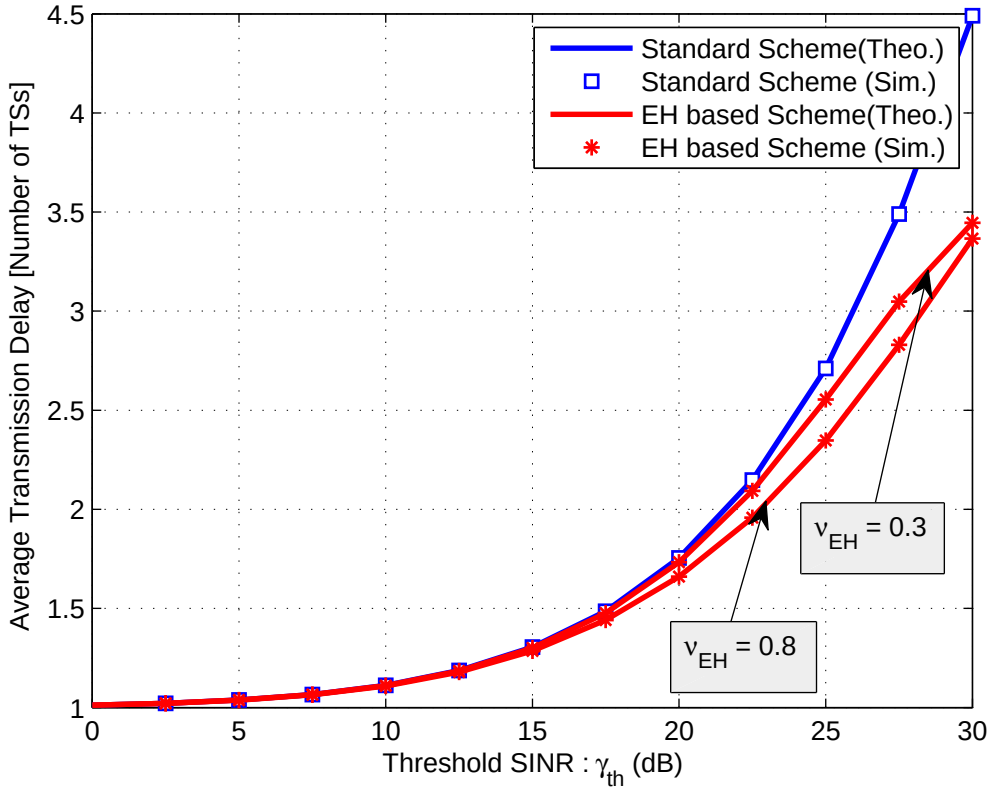

Figure 5.3: Average transmission delay vs. γ_{th} for different values of ν_{EH}.

Fig. 5.3 presents the average transmission delay vs. γ_{th} for different values of the percentage of power added, ν_{EH} when $P_{\text{BS}} = 0.2W$. This figure shows that the delay decreases when increasing the value of ν_{EH}. This can be explain by the fact that more the BS harvest with an important percentage more the SNR reach the predefined threshold rapidly.

5.3.2 Ergodic Capacity

In this section, we derive the ergodic capacity expression for the standard scheme and the EH scheme.

5.3.2.1 Standard Scheme

The general expression of the average ergodic capacity is presented as follow

$$\bar{C} = \sum_{k=1}^{TS_{\max}} \frac{C_k}{k}, \tag{5.16}$$

where,

$$C_k = EC_0 \, (1 - STP_0)^{k-1}. \tag{5.17}$$

EC_0 is the ergodic capacity at the moment of transmission and is derived as follows

$$\begin{aligned} EC_0 =& \mathbb{E}\left[\log_2(1+SNR)\right] \\ =& \frac{1}{ln(2)} \mathbb{E}\left[\ln(1+SNR)\right]. \end{aligned} \tag{5.18}$$

EC_0 expression can be derived by using the Theorem 2.

Theorem 2. *Let W and I be arbitrary non-negative random variables. Then, based on [86] we have*

$$\mathbb{E}\left[\ln\left(1+\frac{W}{I+N_0}\right)\right] = \int_0^\infty \left(\frac{1-\mathcal{L}_W\left(\frac{y}{N_0}\right)}{y}\right) \mathcal{L}_I\left(\frac{y}{N_0}\right) \exp(-y)\, dy. \tag{5.19}$$

Based on Theorem 2, the upper bound expression of the average ergodic capacity can be evaluated as follows

$$EC_0 \approx \frac{1}{ln(2)} \left(\sum_{n=1}^{N} \left\{ \left(1 - \mathcal{L}_W\left(\frac{x_n}{N_0}\right)\right) \frac{w_n}{x_n} \right\} + R_N \right), \tag{5.20}$$

where,

$$W = P_{\text{BS}} H A_{M1} r^{-\beta}. \tag{5.21}$$

We used the PDF expression of H to derive $\mathcal{L}_W\left(\frac{x_n}{N_0}\right)$ as follows

$$\begin{aligned} \mathcal{L}_W\left(\frac{x_n}{N_0}\right) &= \mathbb{E}\left[\exp\left(\frac{-x_n W}{N_0}\right)\right] \\ &= \mathbb{E}_{\{r,H\}}\left[\exp\left(\frac{-x_n P_{\text{BS}} H A_{M1}\, r^{-\beta}}{N_0}\right)\right] \\ &= \mathbb{E}_{\{r\}}\left[\int_0^\infty \exp\left(-H\left(1+\frac{x_n P_{\text{BS}} A_{M1}\, r^{-\beta}}{N_0}\right)\right) dH\right]. \end{aligned} \tag{5.22}$$

Thus, $\mathcal{L}_{W}\left(\frac{x_n}{N_0}\right)$ is expressed as follows

$$\mathcal{L}_{W}\left(\frac{x_n}{N_0}\right) = \int_0^{\infty} \frac{N_0 4\pi\lambda_{\text{BS}} r^{2}}{N_0 + x_n P_{\text{BS}} A_{M1}\, r^{-\beta}} \exp\left(-\frac{4}{3}\pi\lambda_{\text{BS}} r^{3}\right)\, dr. \tag{5.23}$$

By using the change in variable : $v = \frac{4}{3}\pi\lambda_{\text{BS}} r^{3}$, $\mathcal{L}_{W}\left(\frac{x_n}{N_0}\right)$ can be rewritten as

$$\mathcal{L}_{W}\left(\frac{x_n}{N_0}\right) = \int_0^{\infty} \frac{N_0 \exp\left(-v\right)}{N_0 + x_n P_{\text{BS}} A_{M1} \left(\frac{3v}{4\pi\lambda_{\text{BS}}}\right)^{-\frac{\beta}{3}}} dv. \tag{5.24}$$

Based on Theorems 1 and 2, the $\mathcal{L}_{W}\left(\frac{x_n}{N_0}\right)$ can be further simplified to

$$\mathcal{L}_{W}\left(\frac{x_n}{N_0}\right) = \sum_{m=1}^{M} \frac{N_0 w_m}{N_0 + x_n P_{\text{BS}} A_{M1} \left(\frac{3}{4\pi\lambda_{\text{BS}}} \frac{x_m}{}\right)^{-\frac{\beta}{3}}} + R_{M}. \tag{5.25}$$

Finally, by supposing that the reminder $R_N \approx 0$, the expression of the ergodic capacity for a successful transmission at the time slot $k = 0$ is expressed as follow

$$EC_{0} \approx \frac{1}{ln(2)} \sum_{n=1}^{N} \frac{w_n}{x_n} \left(1 - \sum_{m=1}^{M} \frac{w_m}{1 + \frac{x_n}{N_0} P_{\text{BS}} A_{M1} \left(\frac{3}{4\pi\lambda_{\text{BS}}} \frac{x_m}{}\right)^{-\frac{\beta}{3}}}\right). \tag{5.26}$$

5.3.2.2 Energy Harvesting based Scheme

In this section, using the proposed algorithm in the section above, we derived the expression of the ergodic capacity. Based on (5.16), the general expression is detailed as follow

$$\begin{cases} C_{1} = & EC_{0} \\ C_{k>1} = & (1 - STP_{0}) \sum_{n_2=0}^{1} \Big\{ (1 - STP_{n_2}) \times \sum_{n_3=n_2}^{n_2+1} \big\{ (1 - STP_{n_3}) \ldots \\ & \sum_{n_k=n_{k-1}}^{n_{k-1}+1} \{ EC_{n_k}\, P_{\text{EH}}^{n_k} (1 - P_{\text{EH}})^{k-1-n_k} \} \big\} \Big\}, \end{cases}$$

where EC_{k}, is the ergodic capacity for a successful transmission at the time slot k.

Unlike to EC_{0}, EC_{k} uses the updating transmit power after a k time slot and is expressed as follow

$$\begin{aligned} EC_{k} =& \mathbb{E}\left[\log_2(1 + SNR_{k})\right] \\ =& \frac{1}{ln(2)} \mathbb{E}\left[\ln(1 + SNR_{k})\right]. \end{aligned} \tag{5.27}$$

Based on Theorem 2, the upper bound expression of the average ergodic capacity can be evaluated as follows

$$EC_{k} \approx \frac{1}{ln(2)} \left(\sum_{n=1}^{N} \left\{ \left(1 - \mathcal{L}_{W} \left(\frac{x_n}{N_0} \right) \right) \frac{w_n}{x_n} \right\} + R_N \right), \tag{5.28}$$

where,

$$W = (1 + \nu_{\text{EH}} k) P_{\text{BS}} H A_{M1} r^{-\beta}. \tag{5.29}$$

We used the PDF expression of H to derive $\mathcal{L}_{W} \left(\frac{x_n}{N_0} \right)$ as follows

$$\begin{aligned}
&\mathcal{L}_{W} \left(\frac{x_n}{N_0} \right) = \mathbb{E} \left[\exp \left(\frac{-x_n W}{N_0} \right) \right] \\
&= \mathbb{E}_{\{r,H\}} \left[\exp \left(\frac{-x_n (1 + \nu_{\text{EH}} k) P_{\text{BS}} H A_{M1} \, r^{-\beta}}{N_0} \right) \right] \\
&= \mathbb{E}_{\{r\}} \left[\int_0^{\infty} \exp \left(-H \left(1 + \frac{x_n (1 + \nu_{\text{EH}} k) P_{\text{BS}} A_{M1} \, r^{-\beta}}{N_0} \right) \right) dH \right] \\
&= \int_0^{\infty} \frac{N_0 4\pi \lambda_{\text{BS}} r^{2}}{N_0 + x_n (1 + \nu_{\text{EH}} k) P_{\text{BS}} A_{M1} \, r^{-\beta}} \exp \left(-\frac{4}{3} \pi \lambda_{\text{BS}} r^{3} \right) \, dr.
\end{aligned} \tag{5.30}$$

By using the change in variable : $v = \frac{4}{3} \pi \lambda_{\text{BS}} r^{3}$, $\mathcal{L}_{W} \left(\frac{x_n}{N_0} \right)$ can be rewritten as

$$\mathcal{L}_{W} \left(\frac{x_n}{N_0} \right) = \int_0^{\infty} \frac{N_0 \exp(-v)}{N_0 + x_n (1 + \nu_{\text{EH}} k) P_{\text{BS}} A_{M1} \left(\frac{3v}{4\pi \lambda_{\text{BS}}} \right)^{-\frac{\beta}{3}}} dv. \tag{5.31}$$

Based on Theorems 1 and 2, the $\mathcal{L}_{W} \left(\frac{x_n}{N_0} \right)$ can be further simplified to

$$\mathcal{L}_{W} \left(\frac{x_n}{N_0} \right) = \sum_{m=1}^{M} \frac{N_0 w_m}{N_0 + x_n (1 + \nu_{\text{EH}} k) P_{\text{BS}} A_{M1} \left(\frac{3 \, x_m}{4\pi \lambda_{\text{BS}}} \right)^{-\frac{\beta}{3}}} + R_M. \tag{5.32}$$

Finally, by supposing that the reminder $R_N \approx 0$, the expression of the ergodic capacity for a successful transmission at the time slot k is expressed as follow

$$EC_{k} \approx \frac{1}{ln(2)} \sum_{n=1}^{N} \frac{w_n}{x_n} \left(1 - \sum_{m=1}^{M} \frac{w_m}{1 + \frac{x_n}{N_0} (1 + \nu_{\text{EH}} k) P_{\text{BS}} A_{M1} \left(\frac{3 \, x_m}{4\pi \lambda_{\text{BS}}} \right)^{-\frac{\beta}{3}}} \right). \tag{5.33}$$

The numerical results are interpreted to evaluate the performance analysis of the 3-D cellular network with the proposed algorithm.

Fig. 5.4 shows the variations of the average ergodic capacity for RF transmission bands as a function of P_{BS} when $\gamma_{\text{th}} = 20$ dB, and $\nu_{\text{EH}} = 0.3$. We can clearly see that the ergodic capacity of EH based scheme is higher. This is due to the fact that the energy harvesting increases the transmit power, which consequently improves the capacity.

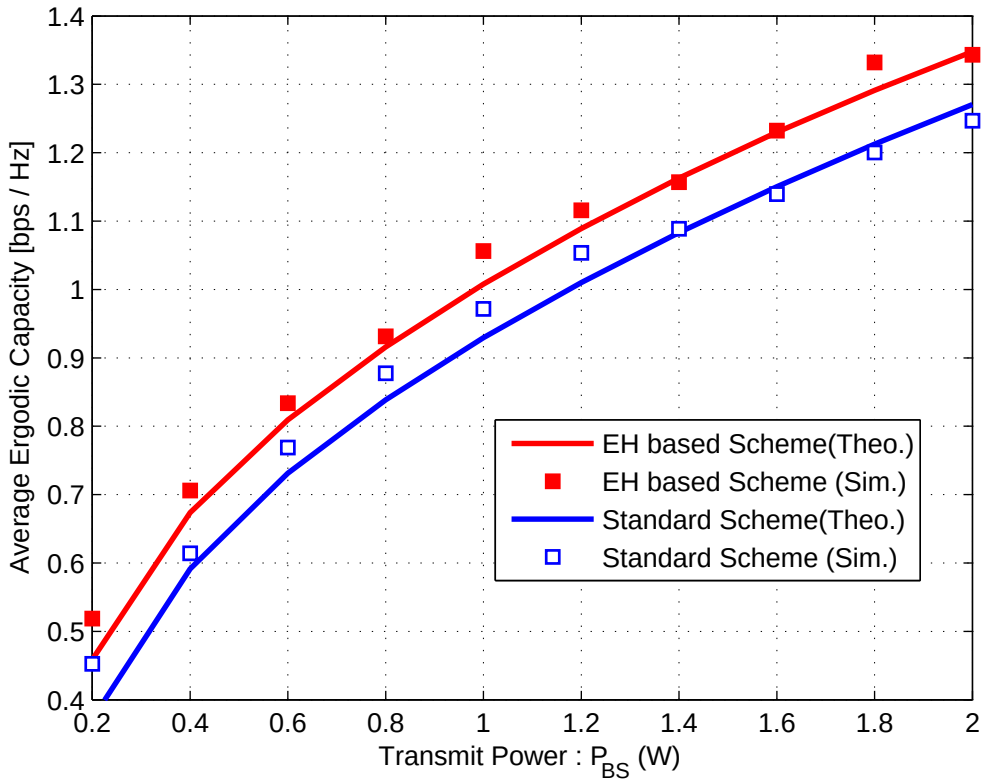

Figure 5.4: Average Ergodic Capacity vs. P_{BS} with $\gamma_{\text{th}} = 20$ dB, and $\nu_{\text{EH}} = 0.3$.

5.4 Conclusion

In this chapter, the energy-harvesting based transmission algorithm has been proposed in ordre to enhance the performance of the 3-D cellular network. This algorithm takes advantage of the harvested energy to improve the SNR, and consequently to improve the delay and the capacity. We have derived the expressions of the average transmission delay, and the average ergodic capacity. The evaluation of the obtained results are exploited to highlight the advantage of the algorithm proposed when compared to the standard scheme. The results confirm that EH based scheme provides more interesting performance in term of the delay of transmission and the average ergodic capacity.

Chapter 6

Relay Selection Scheme for D2D based 3-D Millimeter-Wave Cellular Networks

6.1 Introduction

Dense areas for cellular networks may cause problems of penetration losses and coverage predictions. In higher frequencies systems [95, 96], blockage effects become a serious problem that can limit the performance of emerging mmWave cellular networks [97, 98]. MmWave has been defined as a carrier frequency for the fifth generation (5G) cellular networks [99–104]. Unfortunately, unlike to low-frequency bands, mmWave are more sensitive to blockage effects. This is because of some obstacles (such as walls) which systematically generate important penetration loss [105].

In this chapter, we propose a new min/max scheme to enhance the successful transmission probability. This scheme is based on selected UE relay that can assist the transmission from the BS to the target UE. Based on the proposed 3-D model, we derive the expressions of probability density function (PDF), and average successful transmission probability for the different considered schemes. Based on conducted simulation results, we interpret the analytical results, and investigate the advantages of the proposed min/max based scheme, when compared to direct link, best DL, and best UL based scheme.

6.2 Min/Max Transmission Scheme

We consider the proposed 3-D model, introduced in the previous section 2.5. In addition, we assume that N_{RL}, a number of available relays are randomly located according to a PPP with density

λ_{RL} and height H_{RL}, and that all the links between the different nodes experience Nakagami-m fadings. We consider decode-and-forward (DF) relaying, which offers a better quality of service (QoS) when compared to amplify-and-forward (AF) relaying [106, 107]. In this section, a new algorithm is proposed, and its probability density function is derived.

6.2.1 Proposed Scheme Description

Based on the presented system model, we propose a new transmission scheme in order to enhance the successful transmission probability.

In the proposed Min/Max relay selection scheme, the base station can select the relay that offers the best ergodic capacity. In fact, the end-to-end communication between the BS and the user via the relay, has an ergodic capacity equal to to the minimum value between the ergodic capacities of the two hops. Thus, the best selected relay is the one that offers the maximum end-to-end capacity (minimum capacity of the both links), which is corresponding to the max-min (SNR). Based on that, as the SNR is inversely proportional to the distance, the best relay is selected based on the min-max distance of the two links. As presented in Algorithm 2, to enhance the SNR, the proposed scheme allows the BSs to search for available relays in order to ensure the communication between the transmitter and the receiver. If the SNR is less than a predefined level γ_{th}, the transmission will be switched from direct cellular mode to D2D relay mode. Accordingly, for each active relay, the maximum of the distance between this relay and the served user, and that between the same relay and the serving BS is retained. After that, we select the relay that provides the minimum distance among the retained maximum distances. The transmission is ensured only if the DL and UL SNRs reach the predefined threshold γ_{th}.

For the best DL (BDL) based scheme [47], relay selection is based on the minimum distance between the relays and the BS. On the other hand, the best UP (BUL) based scheme [45] selects the relay with the minimal distance to the UE. Concerning [42], the mmWave transmission is only possible when a LOS path exists, the above criterion indicates that the UE always associates with the nearest LOS BS in cellular mode or the nearest LOS candidate relay UE in mmWave D2D relay mode. As for [44], the selection of the most appropriate relay is based on the minimum sum of the distances from the D2D transmitter to the relay and the receiver to the relay respectively.

Algorithm 3 **Min/Max Relay Selection Scheme**

1: $r_{\text{UL}}(i)$**: the distance between the** i^{th} **relay and the receiver.**
2: $r_{\text{DL}}(i)$**: the distance between the selected BS and the** i^{th} **relay .**
3: **if** $(SNR \geq \gamma_{\text{th}})$ **then**
4: **Direct link transmission.**
5: **else**
6: **for** $i = 1$ to N_{RL} **do**
7: $y(i) = max(r_{\text{UL}}(i), r_{\text{DL}}(i))$
8: **Endfor**
9: Select the relay index k, where $\text{y}_{\text{k}}) = min(y)$
10: **Endif**
11: **if** $(SNR_{\text{DL}} \geq \gamma_{\text{th}})\&(SNR_{\text{UL}} \geq \gamma_{\text{th}})$ **then**
12: **D2D based Transmission.**
13: **Endif**

6.2.2 Probability Density Function

The CCDF and PDF of the distance to the n-th nearest neighbor are expressed, respectively, as follows [63]

$$CCDF_{DL} = \exp\big(-\pi\lambda_{\text{RL}}(r^2 - (H_{\text{BS}} - H_{\text{RL}})^2)\big) \sum_{k=0}^{n-1} \frac{(\pi\lambda_{\text{RL}}(r^2 - (H_{\text{BS}} - H_{\text{RL}})^2))^k}{k!}, \tag{6.1}$$

$$CCDF_{UL} = \exp\big(-\pi\lambda_{\text{RL}}(r^2 - (H_{\text{UE}} - H_{\text{RL}})^2)\big) \sum_{k=0}^{n-1} \frac{(\pi\lambda_{\text{RL}}(r^2 - (H_{\text{UE}} - H_{\text{RL}})^2))^k}{k!}, \tag{6.2}$$

and,

$$f_{DL} = (r^2 - (H_{\text{BS}} - H_{\text{RL}})^2)^{n-\frac{1}{2}} \frac{2}{\Gamma(n)} (\pi\lambda_{\text{RL}})^n \ \exp\big(-\pi\lambda_{\text{RL}}(r^2 - (H_{\text{BS}} - H_{\text{RL}})^2)\big), \tag{6.3}$$

$$f_{UL} = (r^2 - (H_{\text{UE}} - H_{\text{RL}})^2)^{n-\frac{1}{2}} \frac{2}{\Gamma(n)} (\pi\lambda_{\text{RL}})^n \ \exp\big(-\pi\lambda_{\text{RL}}(r^2 - (H_{\text{UE}} - H_{\text{RL}})^2)\big). \tag{6.4}$$

Let $y = max(r_{UL}, r_{DL})$

$$\begin{aligned} F_Y(y) &= P[max(r_{UL}, r_{DL}) \leq y] \\ &= P[r_{UL} \leq y]P[r_{DL} \leq y] \\ &= \text{CDF}_{UL}\text{CDF}_{DL}. \end{aligned} \tag{6.5}$$

Thus, the pdf of y is expressed as follows

$$f(y) = f_{UL}\text{CDF}_{UL} + f_{DL}\text{CDF}_{DL} \tag{6.6}$$

Let $u = min(x_1, x_2, .., x_{N_{\text{RL}}})$

$$\begin{aligned} F_U(u) &= P[min(x_1, x_2, .., x_{N_{\text{RL}}}) \leq u] \\ &= 1 - P[min(x_1, x_2, .., x_{N_{\text{RL}}}) \geq u] \\ &= 1 - P[x_1 \geq u]P[x_2 \geq u] \times ... \times P[x_{N_{\text{RL}}} \geq u] \\ &= 1 - (1 - F_1)(1 - F_2) \times ... \times (1 - F_{N_{\text{RL}}}). \end{aligned} \tag{6.7}$$

Based on (6.7), let $z = min(y_1, y_2, .., N_{\text{RL}})$,

$$F_z = \big[1 - \prod_{i}^{N_{\text{RL}}} (1 - F_i(y))\big] \tag{6.8}$$

After taking the derivative of the CDF expression, the PDF is expressed as follows

$$f_z = \sum_{n=1}^{N_{\text{RL}}} f_y \prod_{i=1, i\neq n}^{N_{\text{RL}}} (1 - F(y)) \tag{6.9}$$

$$f_{min/max} = \sum_{n=1}^{N_{\text{RL}}} \big[f_{UL}\text{CDF}_{UL} + f_{DL}\text{CDF}_{DL}\big] \times \prod_{i=1, i\neq n}^{N_{\text{RL}}} (1 - (\text{CDF}_{UL})^2). \tag{6.10}$$

where,

$$\prod_{i=1, i\neq n}^{N_{\text{RL}}} \big(1 - \text{CDF}_{UL}\text{CDF}_{DL}\big) = \big(1 - \text{CDF}_{UL}\text{CDF}_{DL}\big)^{N_{\text{RL}}-1} \tag{6.11}$$

Thus,

$$f_{min/max} = \sum_{n=1}^{N_{\text{RL}}} \big[f_{UL}\text{CDF}_{UL} + f_{DL}\text{CDF}_{DL}\big] \times \big(1 - \text{CDF}_{UL}\text{CDF}_{DL}\big)^{N_{\text{RL}}-1}. \tag{6.12}$$

Finally, the PDF of the corresponding distance within the proposed scheme is derived and expressed as follows

$$f_{min/max}(r) = N_{\text{RL}}\big[f_{UL}\text{CDF}_{UL} + f_{DL}\text{CDF}_{DL}\big] \times \big(1 - \text{CDF}_{UL}\text{CDF}_{DL}\big)^{N_{\text{RL}}-1}, \tag{6.13}$$

where, r is the minimum of the max values of the DL and UL distances for the corresponding relays. CDF_{DL} is the cumulative density function (CDF) of the distance between the BS and the selected relay UE, and given by

$$\text{CDF}_{DL} = 1 - \frac{1}{N_{\text{RL}}} \sum_{n=1}^{N_{\text{RL}}} \exp\big(-\pi\lambda_{\text{RL}}[r^2 - (H_{\text{BS}} - H_{\text{RL}})^2]\big) \sum_{k=0}^{n-1} \frac{(\pi\lambda_{\text{RL}}[r^2 - (H_{\text{BS}} - H_{\text{RL}})^2])^k}{k!}. \tag{6.14}$$

CDF_{UL} is the CDF of the distance between the selected relay UE and the served user UE, and expressed as,

$$\text{CDF}_{UL} = 1 - \frac{1}{N_{\text{RL}}} \sum_{n=1}^{N_{\text{RL}}} \exp\left(-\pi\lambda_{\text{RL}}[r^2 - (H_{\text{UE}} - H_{\text{RL}})^2]\right) \sum_{k=0}^{n-1} \frac{\left(\pi\lambda_{\text{RL}}[r^2 - (H_{\text{UE}} - H_{\text{RL}})^2]\right)^k}{k!}. \tag{6.15}$$

By deriving the CDF expressions, the PDF of r_{DL} and r_{UL} is expressed as follows,

$$f_{DL} = \frac{1}{N_{\text{RL}}} \sum_{n=1}^{N_{\text{RL}}} (r^2 - (H_{\text{BS}} - H_{\text{RL}})^2)^{n-\frac{1}{2}} \frac{2}{\Gamma(n_1)} (\pi\lambda_{\text{RL}})^{n_1} \exp\left(-\pi\lambda_{\text{RL}}[r^2 - (H_{\text{BS}} - H_{\text{RL}})^2]\right), \tag{6.16}$$

and,

$$f_{UL} = \frac{1}{N_{\text{RL}}} \sum_{n=1}^{N_{\text{RL}}} (r^2 - (H_{\text{BS}} - H_{\text{RL}})^2)^{n_1-\frac{1}{2}} \frac{2}{\Gamma(n_1)} (\pi\lambda_{\text{RL}})^{n} \exp\left(-\pi\lambda_{\text{RL}}[r^2 - (H_{\text{UE}} - H_{\text{RL}})^2]\right). \tag{6.17}$$

Figure 6.1 presents the simulated PDF of the corresponding distance within the proposed min/max scheme. This figure confirms the accuracy of the theoretical expression in (6.13), when compared to the simulation.

6.3 Performance Analysis

6.3.1 Probability of LOS/NLOS

The probability of LOS p_1, derived previously in equation (4.3) , is presented as

$$p_1 = P_1^{(2D)} + \frac{\left(1 - P_1^{(2D)}\right)\left(H_{\text{BS}} - H_{\text{BDG}}^{(\text{min})}\right)}{2\left(H_{\text{BDG}}^{(\text{max})} - H_{\text{BDG}}^{(\text{min})}\right)} \tag{6.18}$$

where $P_1^{(2D)}$ is the probability of LOS in 2-D environments as given in equation (4.1)

$$P_1^{(2D)} = \exp(-\beta r + p), \tag{6.19}$$

Accordingly, the probability of NLOS is expressed as follows

$$p_2 = 1 - p_1 \tag{6.20}$$

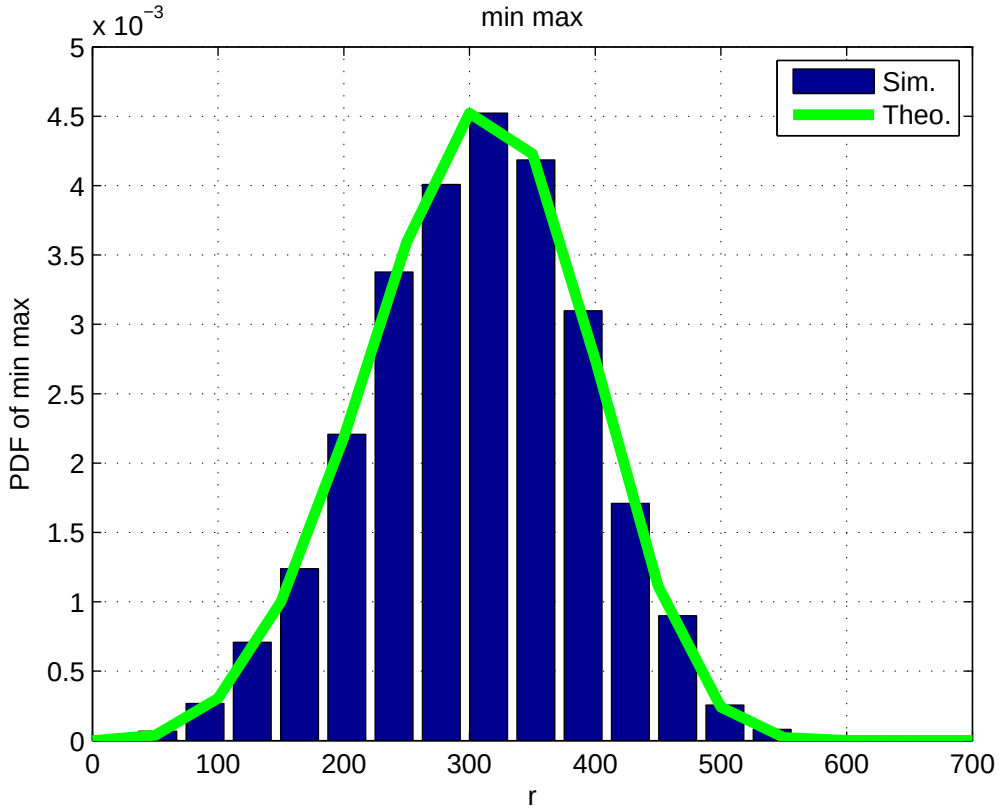

Figure 6.1: Theoretical and simulated PDFs of the corresponding distance within the proposed min/max scheme

6.3.2 Successful Transmission Probability

6.3.2.1 Direct Link

The successful transmission probability of the direct link scheme, based on equation (2.30), Pc_0 is derived as follow,

$$\begin{aligned} Pc_0 &= \int_0^R \Pr\left\{SNR_0 \geq \gamma_{\text{th}} \mid r\right\} f(r_0)\, dr_0 \\ &= \int_0^R \Bigg[p_1 \Pr\left\{ \frac{P_{\text{B}}\, A_{M2}\, s_1\, f_1\, r_0^{-\alpha_1}}{N_0} \geq \gamma_{\text{th}} \mid r_0 \right\} \\ &\quad + p_2 \Pr\left\{ \frac{P_{\text{B}}\, A_{M2}\, s_2\, f_2\, r_0^{-\alpha_2}}{N_0} \geq \gamma_{\text{th}} \mid r_0 \right\} \Bigg] f(r_0)\, dr_0 \end{aligned} \tag{6.21}$$

The general probability $\Pr\left\{ \frac{P_{\text{B}}\, A_{M2}\, s_\xi\, f_\xi\, r_0^{-\alpha_\xi}}{N_0} \geq \gamma_{\text{th}} \mid r_0 \right\}$ is derived as follows:

$$\begin{aligned} \Pr\left\{ \frac{P_{\text{B}}\, A_{M2}\, s_\xi\, f_\xi\, r_0^{-\alpha_\xi}}{N_0} \geq \gamma_{\text{th}} \mid r_0 \right\} &= \Pr\left\{ f_\xi \geq \frac{\gamma_{\text{th}}\, N_0\, r_0^{\alpha_\xi}}{P_{\text{B}}\, A_{M2}\, s_\xi} \mid r_0 \right\} \\ &= \int_0^{+\infty} p_{s_\xi}(s) \int_{v_\xi}^{+\infty} p_{f_\xi}(f)\, df\, ds, \end{aligned} \tag{6.22}$$

where, $v_{\xi} = \frac{\gamma_{\text{th}}\ N_0\ r_0^{\alpha_{\xi}}}{P_{\text{B}}\ A_{M2}\ 10^{-\frac{s}{10}}}$.

By substituting (2.32) into (6.22), and based on [91, (Eq. 3.381.3)], the integration with respect to f is evaluated and yields to

$$\Pr\left\{\frac{P_{\text{B}}\ A_{M2}\ s_{\xi}\ f_{\xi}\ r_0^{-\alpha_{\xi}}}{N_0} \geq \gamma_{\text{th}} \mid r_0\right\} = \frac{1}{\Gamma(m_{\xi})}\int_0^{+\infty} p_{s_{\xi}}(s)\ \Gamma\Big(m_{\xi}, \frac{m_{\xi}}{\Omega_{\xi}}\ v_{\xi}\Big)\ ds, \tag{6.23}$$

where, $\Gamma(.,.)$ is the incomplete gamma function [91, Eq. (8.350.2)], which can be expressed as [91, Eq. (8.352.2)]

$$\Gamma(k+1, x) = k!\ \exp(-x)\sum_{m=0}^{k}\frac{x^m}{m!}. \tag{6.24}$$

Now, as $S_{\xi[\text{dB}]}$ is normally distributed with zero mean, and variance σ_{ξ}^2, its PDF expression is given by

$$p_{S_{\xi[\text{dB}]}}(s) = \frac{1}{\sqrt{2\ \pi\ \sigma_{\xi}^2}}\exp\left(-\frac{s^2}{2\ \sigma_{\xi}^2}\right). \tag{6.25}$$

By using the expression of $p_{s_{\xi}}$, (6.23) is rewritten as follows:

$$\Pr\left\{\frac{P_{\text{B}}\ A_{M2}\ s_{\xi}\ f_{\xi}\ r_0^{-\alpha_{\xi}}}{N_0} \geq \gamma_{\text{th}} \mid r_0\right\} = \frac{1}{\Gamma(m_{\xi})\ \sqrt{2\ \pi\ \sigma_{\xi}^2}}\int_0^{+\infty}\exp\left(-\frac{s^2}{2\ \sigma_{\xi}^2}\right)\Gamma\Big(m_{\xi}, \frac{m_{\xi}}{\Omega_{\xi}}\ v_{\xi}\Big)\ ds. \tag{6.26}$$

By using the change in variables: $x = \frac{s^2}{2\ \sigma_{\xi}^2}$, and Laguerre theorem, the integration can be evaluated as follows:

$$\Pr\left\{\frac{P_{\text{B}}\ A_{M2}\ s_{\xi}\ f_{\xi}\ r_0^{-\alpha_{\xi}}}{N_0} \geq \gamma_{\text{th}} \mid r_0\right\} = \frac{1}{2\ \sqrt{\pi}\ \Gamma(m_{\xi})}\sum_{n=1}^{N}\frac{w_n}{\sqrt{x_n}}\ \Gamma\Big(m_{\xi}, \frac{m_{\xi}}{\Omega_{\xi}}\ v_{\xi,n}\Big)\ + R_N, \tag{6.27}$$

where,

$$v_{\xi,n} = \frac{\gamma_{\text{th}}\ N_0\ r_0^{\alpha_{\xi}}}{P_{\text{B}}\ A_{M2}}\ 10^{\frac{\sqrt{2\ \sigma_{\xi}^2\ x_n}}{10}}. \tag{6.28}$$

Finally, by using the change of variables:
$z = \pi\lambda_{\text{BS}}\Big[r_0^2 - (H_{\text{BS}} - H_{\text{UE}})^2\Big]$, the expression of p_{ξ}, and the Laguerre theorem, the final expression of successful transmission probability of the direct link scheme is given by,

$$Pc_0 = \sum_{k=1}^{N} w_k\ \sum_{\xi=1}^{2}\left\{\frac{p_{k,\xi}}{2\ \sqrt{\pi}\ \Gamma(m_{\xi})}\sum_{n=1}^{N}\left\{\frac{w_n}{\sqrt{x_n}}\Gamma\Big(m_{\xi}, \frac{m_{\xi}}{\Omega_{\xi}}\ v_{\xi,n}\Big)\ + R_N\right\}\right\}\ + R_k, \tag{6.29}$$

where,

$$v_{k,\xi,n} = \frac{\gamma_{\text{th}}\ N_0 \left[\frac{x_k}{\pi\lambda_{\text{BS}}} + \left(H_{\text{BS}} - H_{\text{UE}}\right)^2\right]^{\frac{\alpha_\xi}{2}}}{P_{\text{B}}\ A_{M2}}\ 10^{\frac{\sqrt{2\ \sigma_\xi^2\ x_n}}{10}}, \tag{6.30}$$

and,

$$p_{k,1} = 1 - p_{k,2} = P_{k,1}^{(\text{2D})} + \frac{\left(1 - P_{k,1}^{(\text{2D})}\right)\left(H_{\text{BS}} - H_{\text{BDG}}^{(\text{min})}\right)}{2\left(H_{\text{BDG}}^{(\text{max})} - H_{\text{BDG}}^{(\text{min})}\right)}, \tag{6.31}$$

with,

$$P_{k,1}^{(\text{2D})} = \exp\left(-\beta\left[\frac{x_k}{\pi\lambda_{\text{BS}}} + \left(H_{\text{BS}} - H_{\text{UE}}\right)^2\right]^{\frac{1}{2}} - \rho\right), \tag{6.32}$$

and, $\beta = 2\frac{\lambda_{\text{BL}}}{\pi}(E[W] + E[L])$, and $\rho = \lambda_{\text{BL}} E[W]\ E[L]$.

6.3.2.2 Min/Max based Scheme

Based on the above description of the proposed min/max based scheme, the expression of successful transmission probability of $Pc^{(\text{min/max})}$ is given by

$$Pc^{(\text{min/max})} = Pc_0 + (1 - Pc_0)P_{(\text{min/max})}. \tag{6.33}$$

where,

$$\begin{aligned}
P_{(\text{min/max})} &= Pr([SNR_{\text{DL}} \geq \gamma_{\text{th}}]\&[SNR_{\text{UL}} \geq \gamma_{\text{th}}]) \\
&= Pr(\min(SNR_{\text{DL}}, SNR_{\text{UL}}) \geq \gamma_{\text{th}}) \\
&= Pr(SNR(r) \geq \gamma_{\text{th}} | r = \arg\min(r_{\text{DL}}, r_{\text{UL}})) \\
&= \int_0^R \Pr\{SNR \geq \gamma_{\text{th}} \mid r\}\, f_{Min/Max}(r)\, dr \\
&= \int_0^R \Bigg[\ p_1 \Pr\left\{\frac{P_{\text{B}}\ A_{M2}\ s_1\ f_1\ r^{-\alpha_1}}{N_0} \geq \gamma_{\text{th}} \mid r\right\} \\
&+ p_2 \Pr\left\{\frac{P_{\text{B}}\ A_{M2}\ s_2\ f_2\ r^{-\alpha_2}}{N_0} \geq \gamma_{\text{th}} \mid r\right\}\Bigg]\ f_{Min/Max}(r)\, dr
\end{aligned} \tag{6.34}$$

By analogy, the expression of $\Pr\left\{\frac{P_{\text{B}}\ A_{M2}\ s_\xi\ f_\xi\ r^{-\alpha_\xi}}{N_0} \geq \gamma_{\text{th}} \mid r\right\}$ is given by

$$\Pr\left\{\frac{P_{\text{B}}\ A_{M2}\ s_\xi\ f_\xi\ r^{-\alpha_\xi}}{N_0} \geq \gamma_{\text{th}} \mid r\right\} = \frac{1}{2\sqrt{\pi}\ \Gamma(m_\xi)} \sum_{n=1}^{N} \frac{w_n}{\sqrt{x_n}}\ \Gamma\left(m_\xi, \frac{m_\xi}{\Omega_\xi}\ v_{\xi,n}\right) + R_N, \tag{6.35}$$

where,

$$v_{\xi,n} = \frac{\gamma_{\text{th}}\, N_0\, r^{\alpha_\xi}}{P_{\text{B}}\, A_{M2}}\; 10^{\frac{\sqrt{2\,\sigma_\xi^2\, x_n}}{10}}. \tag{6.36}$$

Now, using the change of variables: $x_{\text{DL}} = \pi\lambda_{\text{RL}}\Big[r^2 - (H_{\text{BS}} - H_{\text{RL}})^2\Big]$, the expression of p_ξ, and the Laguerre theorem, the final expression of $P_{\text{(min/max)}}$ is given by (6.37),

$$\begin{aligned} P_{\text{(min/max)}} = &\sum_{k=1}^{N} \frac{w_k}{\sqrt{\frac{x_k}{\pi\lambda_{\text{RL}}} + (H_{\text{BS}} - H_{\text{RL}})^2}} \sum_{\xi=1}^{2} \left\{ \frac{p_{k,\xi}}{2\sqrt{\pi}\,\Gamma(m_\xi)} \sum_{n=1}^{N} \left\{ \frac{w_n}{\sqrt{x_n}} \Gamma\Big(m_\xi, \frac{m_\xi}{\Omega_\xi}\, v_{\xi,n}\Big) + R_N \right\} \right\} \\ &\times \left\{ \Big[f_{\text{DL}}\text{CDF}_{\text{UL}} + f_{\text{UL}}\text{CDF}_{\text{DL}} \Big] \Big(1 - \text{CDF}_{\text{DL}}\, \text{CDF}_{\text{UL}}\Big)^{N_{\text{RL}}-1} \right\} + R_k, \end{aligned} \tag{6.37}$$

where

$$f_{\text{DL}} = \sum_{n_1=1}^{N_{\text{RL}}} \frac{x_k^{(n_1-\frac{1}{2})}\sqrt{\pi\,\lambda_{\text{RL}}}}{\Gamma(n_1)}, \tag{6.38}$$

$$\begin{aligned} f_{\text{UL}} = &\sum_{n_1=1}^{N_{\text{RL}}} \frac{\Big(\frac{x_k}{\pi\lambda_{\text{RL}}} + (H_{\text{BS}} - H_{\text{RL}})^2 - (H_{\text{UE}} - H_{\text{RL}})^2\Big)^{(n_1-\frac{1}{2})}}{\Gamma(n_1)} \\ &(\pi\,\lambda_{\text{RL}})^{n_1} \exp\Big(\pi\lambda_{\text{RL}}[(H_{\text{BS}} - H_{\text{RL}})^2 - (H_{\text{UE}} - H_{\text{RL}})^2]\Big), \end{aligned} \tag{6.39}$$

$$\text{CDF}_{\text{DL}} = 1 - \frac{1}{N_{\text{RL}}} \sum_{n_1=1}^{N_{\text{RL}}} \exp(-x_k) \sum_{u=0}^{n_1-1} \frac{(x_k)^u}{u!}, \tag{6.40}$$

$$\begin{aligned} \text{CDF}_{\text{UL}} = 1 - \frac{1}{N_{\text{RL}}} &\sum_{n_1=1}^{N_{\text{RL}}} \exp\Big(-\pi\lambda_{\text{RL}}[\frac{x_k}{\pi\lambda_{\text{RL}}} + (H_{\text{BS}} - H_{\text{RL}})^2 - (H_{\text{UE}} - H_{\text{RL}})^2]\Big) \\ &\times \sum_{u=0}^{n_1-1} \frac{\Big(\pi\lambda_{\text{RL}}[\frac{x_k}{\pi\lambda_{\text{RL}}} + (H_{\text{BS}} - H_{\text{RL}})^2 - (H_{\text{UE}} - H_{\text{RL}})^2]\Big)^u}{u!}, \end{aligned} \tag{6.41}$$

$$v_{k,\xi,n} = \frac{\gamma_{\text{th}}\, N_0 \left[\frac{x_k}{\pi\lambda_{\text{RL}}} + (H_{\text{BS}} - H_{\text{RL}})^2\right]^{\frac{\alpha_\xi}{2}}}{P_{\text{B}}\, A_{M2}}\; 10^{\frac{\sqrt{2\,\sigma_\xi^2\, x_k}}{10}}, \tag{6.42}$$

and,

$$p_{k,1} = 1 - p_{k,2} = P_{k,1}^{(\text{2D})} + \frac{\Big(1 - P_{k,1}^{(\text{2D})}\Big)\Big(H_{\text{BS}} - H_{\text{BDG}}^{(\text{min})}\Big)}{2\Big(H_{\text{BDG}}^{(\text{max})} - H_{\text{BDG}}^{(\text{min})}\Big)}, \tag{6.43}$$

with,

$$P_{k,1}^{(\text{2D})} = \exp\left(-\beta \left[\frac{x_k}{\pi\lambda_{\text{RL}}} + (H_{\text{BS}} - H_{\text{RL}})^2\right]^{\frac{1}{2}} - \rho \right). \tag{6.44}$$

6.3.2.3 Best Down-Link based Scheme (BDL)

By analogy to the min/max based scheme, the derivation of the best down-link based scheme expression is expressed as follows

$$Pc^{(\text{BDL})} = Pc_0 + (1 - Pc_0)P_{(\text{BDL})} \tag{6.45}$$

where,

$$\begin{aligned} P_{(\text{BDL})} &= \int_0^R \Pr\{SNR_{DL} \geq \gamma_{\text{th}} \mid r_{DL}\} f_{BDL}(r_{DL})\, dr_{DL} \\ &= \int_0^R \Bigg[p_1 \Pr\Bigg\{ \frac{P_{\text{B}}\, A_{M2}\, s_1\, f_1\, r_{DL}^{-\alpha_1}}{N_0} \geq \gamma_{\text{th}} \mid r_{DL} \Bigg\} \\ &+ p_2 \Pr\Bigg\{ \frac{P_{\text{B}}\, A_{M2}\, s_2\, f_2\, r_{DL}^{-\alpha_2}}{N_0} \geq \gamma_{\text{th}} \mid r_{DL} \Bigg\} \Bigg] f_{BDL}(r_{DL})\, dr_{DL} \end{aligned} \tag{6.46}$$

where f_{BDL} is the PDF of the corresponding distance within the best down-link based scheme (BDL)

$$f_{BDL} = N_{\text{RL}} f_{DL} \big(1 - \text{CDF}_{DL}\big)^{N_{\text{RL}}-1}, \tag{6.47}$$

The finale expression of $P_{(\text{BDL})}$ is presented by (6.48), where CDF_{DL} is given in (6.40).

$$\begin{aligned} P_{(\text{BDL})} = \sum_{k=1}^{N} \frac{w_k}{\sqrt{\frac{x_k}{\pi\lambda_{\text{RL}}} + \left(H_{\text{BS}} - H_{\text{RL}}\right)^2}} \sum_{\xi=1}^{2} \Bigg\{ \frac{p_{k,\xi}}{2\sqrt{\pi}\,\Gamma(m_\xi)} \sum_{n=1}^{N} \Big\{ \frac{w_n}{\sqrt{x_n}}\, \Gamma\Big(m_\xi, \frac{m_\xi}{\Omega_\xi}\, v_{\xi,n}\Big) + R_N \Big\} \Bigg\} \\ \times \Bigg\{ \Big(\sum_{n_1=1}^{N_{\text{RL}}} \frac{x_k^{(n_1-\frac{1}{2})}}{\Gamma(n_1)} \Big) \Big(1 - \text{CDF}_{DL}\Big)^{N_{\text{RL}}-1} \Bigg\} + R_k \end{aligned} \tag{6.48}$$

6.3.2.4 Best Up-Link based Scheme (BUL)

The successful transmission probability expression of up-link based scheme $Pc^{(\text{BUL})}$ is presented as

$$Pc^{(\text{BUL})} = Pc_0 + (1 - Pc_0)P_{(\text{BUL})} \tag{6.49}$$

where,

$$\begin{aligned} P_{(\text{BUL})} &= \int_0^R \Pr\{SNR_{UL} \geq \gamma_{\text{th}} \mid r_{UL}\} f_{BUL}(r_{UL})\, dr_{UL} \\ &= \int_0^R \Bigg[p_1 \Pr\Bigg\{ \frac{P_{\text{B}}\, A_{M2}\, s_1\, f_1\, r_{UL}^{-\alpha_1}}{N_0} \geq \gamma_{\text{th}} \mid r_{UL} \Bigg\} \\ &+ p_2 \Pr\Bigg\{ \frac{P_{\text{B}}\, A_{M2}\, s_2\, f_2\, r_{UL}^{-\alpha_2}}{N_0} \geq \gamma_{\text{th}} \mid r_{UL} \Bigg\} \Bigg] f_{BDL}(r_{UL})\, dr_{UL} \end{aligned} \tag{6.50}$$

The PDF of the corresponding distance within the best up-link based scheme is given by

$$f_{BUL} = N_{\text{RL}} f_{UL} \big(1 - \text{CDF}_{UL}\big)^{N_{\text{RL}}-1}, \tag{6.51}$$

The finale expression of $P_{\text{(BUL)}}$ is given by

$$P_{\text{(BUL)}} = \sum_{k=1}^{N} \frac{w_k}{\sqrt{\frac{x_k}{\pi\lambda_{\text{RL}}} + \left(H_{\text{RL}} - H_{\text{UE}}\right)^2}} \sum_{\xi=1}^{2} \left\{ \frac{p_{k,\xi}}{2\sqrt{\pi}\,\Gamma(m_\xi)} \sum_{n=1}^{N} \left\{ \frac{w_n}{\sqrt{x_n}} \Gamma\Big(m_\xi, \frac{m_\xi}{\Omega_\xi} v_{\xi,n}\Big) + R_N \right\} \right\}$$
$$\times \left\{ \Big(\sum_{n_1=1}^{N_{\text{RL}}} \frac{x_k^{(n_1-\frac{1}{2})}}{\Gamma(n_1)} \Big) \Big(1 - \text{CDF}_{UL}\Big)^{N_{\text{RL}}-1} \right\} + R_k \tag{6.52}$$

where,

$$\text{CDF}_{\text{UL}} = 1 - \frac{1}{N_{\text{RL}}} \sum_{n_1=1}^{N_{\text{RL}}} \exp(-x_k) \sum_{u=0}^{n_1-1} \frac{(x_k)^u}{u!}, \tag{6.53}$$

$$v_{k,\xi,n} = \frac{\gamma_{\text{th}}\, N_0 \left[\frac{x_k}{\pi\lambda_{\text{RL}}} + \left(H_{\text{RL}} - H_{\text{UE}}\right)^2\right]^{\frac{\alpha_\xi}{2}}}{P_{\text{B}}\, A_{M2}} \; 10^{\frac{\sqrt{2\,\sigma_\xi^2\, x_k}}{10}}, \tag{6.54}$$

and,

$$p_{k,1} = 1 - p_{k,2} = P_{k,1}^{\text{(2D)}} + \frac{\Big(1 - P_{k,1}^{\text{(2D)}}\Big)\Big(H_{\text{BS}} - H_{\text{BDG}}^{\text{(min)}}\Big)}{2\Big(H_{\text{BDG}}^{\text{(max)}} - H_{\text{BDG}}^{\text{(min)}}\Big)}, \tag{6.55}$$

with,

$$P_{k,1}^{\text{(2D)}} = \exp\left(-\beta \left[\frac{x_k}{\pi\lambda_{\text{RL}}} + \left(H_{\text{RL}} - H_{\text{UE}}\right)^2\right]^{\frac{1}{2}} - \rho \right). \tag{6.56}$$

Now, we present numerical results and evaluate the derived analytical expressions based on Monte Carlo simulations and using MatLab software. As previsouly described, we consider a 3-D space region ($R \times R \times R$, $R = 700$m) in a dense urban area. Let $N_0 = -100$ dBm, $\lambda_{\text{BL}} = 1e-5$, $H_{\text{BS}} = 15$m, $H_{\text{UE}} = 1.5$m, $H_{\text{RL}} = 4$ m ($\lambda_{\text{RL}} = \frac{N_{\text{RL}}}{2R\times 2R}$), $\tau = 0.88$dB/m, $\alpha_1 = 2$,$\alpha_2 = 4$, $\Omega_1 = \Omega_2 = 1$, $m_1 = 3$, $m_2 = 2$ [35, 76, 77].

Fig. 6.2 shows the successful transmission probability of the different schemes as a function of λ_{BS} when $N_{\text{RL}} = 15$. We can clearly see that, increasing the λ_{BS} offers a better performance in term of successful transmission probability. This is because increasing the number of BSs decreases the DL and UL distances, which results in SNR enhancement, so a better successful transmission probability can be observed. As proved analytically, the successful transmission

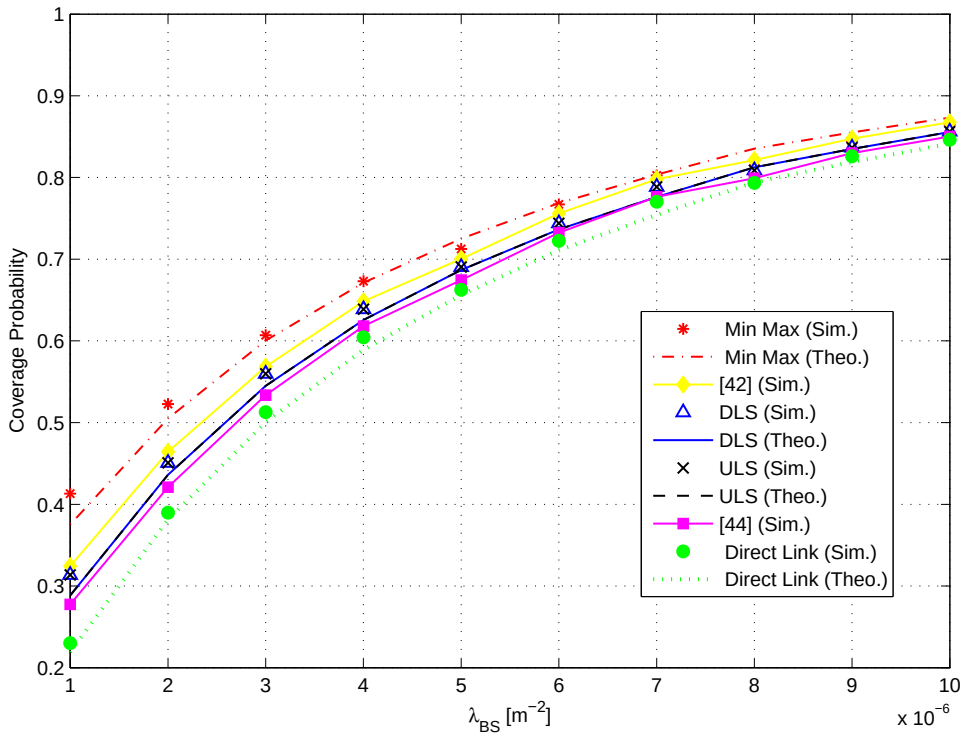

Figure 6.2: successful transmission probability of different schemes vs. λ_{BS} for $N_{\text{RL}} = 15$.

probability of min/max based scheme, [42] based scheme, [44] based scheme, BDL based scheme and BUL based scheme outperform that of the direct link one. The [42] based scheme is better compared to others because it selects the relay that have a LOS link with the receiver which can enhance the path loss and systematically the SNR. As for the BDL and BUL based scheme, they have approximately the same results. However, the min/max based scheme outperforms the other ones. This is due to the fact that the BDL and BUL, select the relay that has the minimum distance to BS, and to user, respectively, while the min/max selects the relay that provides the minimum distance among the maximum of the two distances between this relay and the BS, and this relay and the user. As for [44], the selection is based on the minimum sum of the distances from the D2D transmitter to the relay and the receiver to the relay respectively.

Fig. 6.3 illustrates the successful transmission probability of the min/max based scheme as a function of λ_{BS} for different values of N_{RL}. Obviously, increasing the number of available relays, does increase the successful transmission probability. This can be explained by the fact that when the number of relays is larger, then the distance between the selected one and the user is shorter, thus, a better SNR and necessarily a better coverage is obtained. However, as shown in figure, the enhancement from $N_{\text{RL}} = 15$ to $N_{\text{RL}} = 25$ is better than the second one, even if the number of

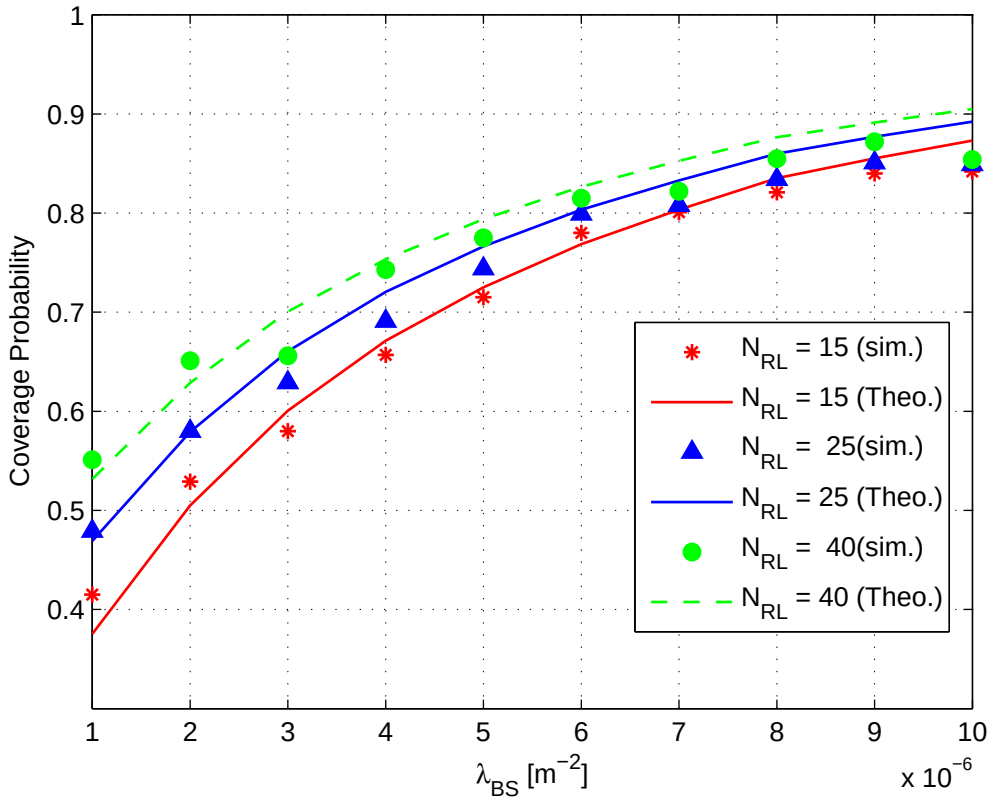

Figure 6.3: successful transmission probability of the min/max based scheme vs. λ_{BS} for different values of N_{RL}.

relay is increased by 15 relays. This is because, with a certain number of relays, the best relay is active at the best position and even if we add more available relays, the perfect one is reach.

Fig. 6.4 depicts the successful transmission probability of the different schemes as a function of λ_{BL}, with $N_{\text{RL}} = 15$. This figure shows that more the density of buildings increases, worse the successful transmission probability is. Since if the number of blockages increases, they further block the link between the transmitter and the receiver. This result confirms, as the above one, that the proposed min/max scheme is better in terms of successful transmission probability. Besides, we can clearly see that by increasing λ_{BL}, all the curves become nearer to the direct link. This can be explained by the fact that the links with relays are blocked which consequently impact the SNR.

6.4 Conclusion

In this chapter, considering blockages effects on 3-D mmWave based cellular networks, the fading channel is assumed to be Nakagami for both the NLOS and LOS environments. In order to enhance

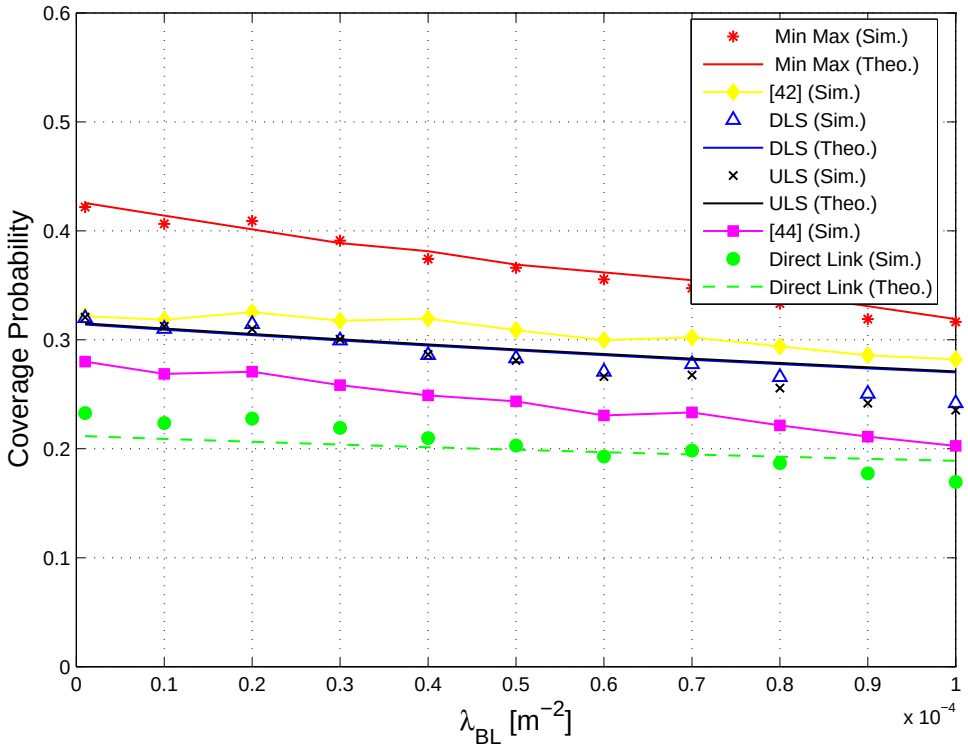

Figure 6.4: successful transmission probability of different schemes vs. λ_{BL} for $N_{\text{RL}} = 15$.

the coverage of the cellular network, we have proposed a new relay selection scheme that allows the BSs to search for available relays to complete the transmission from the BS to the destination UE, and consequently improving the SNR and the successful transmission probability. We have derived the expressions of the corresponding PDF and the successful transmission probability. The examined simulations results demonstrate that the proposed method outperforms the other ones and offers a better coverage.

Chapter 7

General Conclusions and Perspectives

7.1 General Conclusions

In this thesis, 3-D models have been proposed for cellular networks. The work has focused on 3-D modeling, evaluating and, enhancing the performances of the wireless communication systems. The contribution has aimed to provide new schemes that are applicable in new communications systems which operate in UHF and mmWave bands.

The Ph.D. thesis has been structured in 6 chapters:

The first chapter has presented the general introduction of the thesis. It has described the problem statement and the motivations. Then, the related works have been detailed and investigated. After that, the contributions of this thesis have been presented and detailed, and which have been mainly focusing on three axis; proposing a new 3-D space model for a cellular network, deriving closed form expressions of different evaluative performances metrics, and developing new efficient techniques that enhance the communication system performances. In addition the list of publications during the thesis period has been introduced. Finally, the thesis organization has been presented.

In chapter 2, we have detailed first the fading effects in wireless communications and have provided an overview of mathematics tools. Afterwards, we have presented the two 3-D models, of cellular networks operating in two frequency bands, namely UHF and mmWave bands. The first model considers a 3-D HetNet in the context of a high-rise building environment, where K-tiers of BSs are randomly located. Moreover, by considering the presence of blockages, we have presented another 3-D model using PPP and a Boolean scheme of rectangles in order to, respectively, describe the positions of different BSs and the geometry of blockages. Finally, we derive closed form expressions of the probability density function and the SNR of the two proposed

models, for both, UHF and mmWave bands.

In chapter 3, performance analysis of the 3-D wireless communication networks have been detailed. First, we have derived the average coverage probability expressions of a down-link Het-Net for a given set of parameters. Then, based on a 3-D model for K-tier heterogeneous cellular networks, a fair comparison between UHF and mmWave communication systems has been proposed. We have derived the expressions of the successful transmission probability, the average throughput, and the BER for the two transmission bands. The evaluation of the obtained results is exploited to highlight the advantage of the mmWaves communication systems when compared to the UHF systems. The results has confirmed that UHF systems provide more interesting performance in term of coverage probability and BER. However, mmWaves offer a better throughput. Analytical results have been validated by simulations, and comparative analysis of the different studies have been conducted.

The chapter 4, have presented performance analysis of blockage effects on urban cellular network. We have proposed an hybrid fading assumption; the LOS links are traditionally modeled by Rayleigh fading channels, while the Rice fading channels represent usually the NLOS links. The hybrid fading assumption tries to capture the two scenarios. In addition, we have derived the expressions of the probability of LOS for 2-D and 3-D cases, and, the coverage probability for different assumptions. The advantage of the hybrid fading assumption has been confirmed by simulation results.

In chapter 5, based on a 3-D cellular networks, we have proposed an algorithm for a performance enhancement. This algorithm has employed the energy harvesting for a better SNR, and consequently better delay and capacity. We have derived the expressions of the average delay of transmission, and the average ergodic capacity for the UHF transmission bands. The results have confirmed the advantage of the introduced schemes in enhancing wireless communication systems when compared to the standard schemes. This proposed EH based scheme has provided more interesting performance in term of the delay of transmission and the average ergodic capacity.

We have proposed in chapter 6 a new min/max based scheme that allows the BSs to search for available relays UE to complete the transmission from the BS to the destination UE, and consequently to improve the SNR and the probability of successful transmission. Based on a 3-D model for mmWave cellular networks with blockages effects, the fading has been assumed to be Nakagami for both the NLOS and LOS environments. We have derived the expressions of the corresponding PDF and the successful transmission probability. The examined simulations results demonstrate that the proposed method outperforms the other existing ones and offers a better

coverage.

7.2 Perspectives

In the following, we present five new axis as perspectives of this thesis.

7.2.1 Cloud Radio Access Networks (C-RANs)

Mobile operators have given significant attention to cloud radio access networks (C-RANs) due to their beneficial features of performance optimization and cost effectiveness. In C-RAN cooperated networks, the macro base stations can operate cooperatively with small base-stations as advanced wireless access network paradigm, where cloud computing is used to fulfill the centralized large-scale cooperative processing. In addition, the C-RAN mitigates the inter-Radio Remote Heads (RRH) interference by using efficient interference management techniques such as Coordinated multipoint (CoMP). The challenge to design full-duplex systems is to reduce self-interference, which is due to signal received from a local transmitting antenna is usually much stronger than signal received from other nodes. The main methods to reduce self-interference include analog cancelation techniques, digital cancelation, and antenna placement. The analog cancelation techniques treat self-interference as noise, and use noise canceling chips to reduce self-interference [17].

As perspective of this thesis, we can adopt the C-RAN for 3-D model based heterogeneous networks. Where, we can develop new techniques to manage the self-interference especially for mmWave frequencies.

7.2.2 Internet Of Thing (IOT)

As IOT is gaining popularity, this technology can support large amounts of data transmission efficiently and at very high bandwidth. In the near future, some of the prime objectives or demands that need to be addressed are increased capacity, improved data rate, decreased latency. The next generation wireless mobile communication technology 5G promises to fulfill the needs of complex IOT architectures.

We can extend the proposed models in this thesis work, by the use of the multi-BS spatial diversity in Ultra-Narrow-Band (UNB) networks. The advantage of this approach is the reduction of energy consumption, complexity and cost.

7.2.3 5G NR synchronization procedure

Similar to all mobile communication networks, synchronization in the time-frequency domain is a fundamental step that allows 5G NR user equipment to properly receive and transmit its data. Due to the wide range of frequencies that are defined for the 5G NR systems, the corresponding synchronization procedure becomes critical and presents many challenges, especially for the applications that would need accurate oscillators to reduce the large values of the frequency offset [108]. As perspective, we can extend the proposed schemes by employing 5G NR synchronization procedure, and propose new more robust schemes.

7.2.4 Non-orthogonal multiple access techniques

Non-orthogonal multiple access (NOMA) is one of the most promising radio access techniques in next-generation wireless communications. The baseline idea of NOMA is to serve multiple users using the same resource in terms of time, frequency, and space. Hence, we can extend the 3D cellular HetNets to evaluate the trade-off among the different parameters of the network and the employed NOMA technique.

7.2.5 Energy harvesting

Energy efficiency is a key indicator in the communication systems with limited lifetime of the batteries used to supply the wireless devices. Many efforts have been spent on the efficient use of battery energy. Therefore, seeking new source of energy to prolong the lifetime of the energy-constrained wireless network becomes a spotlight.

Recent progress in electronics have revealed that energy harvesting, a process that helps capturing and storing the energy derived from ambient or external sources, is an alternative for prolonging the lifetime of a wireless network and a key enabling technology in the development of wireless communication networks. Energy harvesting has received significant attention recently, where the surrounding energy can be harvested from a large variety of physical natures, such as solar, vibration, thermal or acoustic energy sources. Apart from the conventional energy harvesting methods, a new emerging solution is to avail ambient UHF signals, since UHF signals can carry energy and information at the same time. Thus, energy constrained nodes can scavenge energy and process the information simultaneously.

As perspective, we can evaluate the performance of the 3-D HetNets when energy harvesting is employed and the considered network comprises of a mixture of on-grid and off-grid small base

stations. The objective is to study the trade-off between energy efficiency and SINR outage of a typical user where energy efficiency is defined as the ratio of achievable data rate of a typical user and the corresponding grid power consumption.

Bibliography

[1] S. Niknam, "Interference Modeling and Performance Analysis of 5G Mmwave Networks," *PhD dissertation*, 2019.

[2] Ni. Bhandari, Sh. Devra, and K. Singh, "Evolution of Cellular Network: From 1G to 5G," *International Journal of Engineering and Techniques*, vol. 3, no. 5, pp. 98 – 105, 2017.

[3] M. Rumney, "LTE and the Evolution to 4G Wireless Design and Measurement Challenges," *Agilent Technologies Publication*, 2009.

[4] F. Khan, "LTE for 4G Mobile Broadband: Air Interface Technologies and Performance," *Cambridge University Press*, 2009.

[5] M. G. Kachhavay and A. P. Thakare, "5G Technology-Evolution and Revolution," *International Journal of Engineering and Techniques*, vol. 3, no. 3, pp. 1080 – 1087, 2014.

[6] M. Agiwal, A. Roy, and N. Saxena, "Next Generation 5G Wireless Networks: A Comprehensive Survey," *IEEE Communications Surveys Tutorials*, vol. 18, no. 8, pp. 1617 – 1655, 2016.

[7] W. Choi S. V. Hanly A. Lozano A. C. K. Soong J. G. Andrews, S. Buzzi and J. C. Zhang, "What Will 5G Be?," *IEEE Journal on Selected Areas in Communications*, vol. 32, no. 6, pp. 1065 – 1082, 2014.

[8] NR, "Physical Channels and Modulation Release 15," *document TS 38.211, V.15.4.0, 3GPP*, 2018.

[9] NR, "Multiplexing Channel Coding Release 15," *document TS 38.212, V.15.4.0, 3GPP*, 2018.

[10] NR, "Physical Layer Procedures for Control Release 15," *document TS 38.213, V.15.4.0, 3GPP*, 2018.

[11] M. Wang, J. Chen, E. Aryafar, and M. Chiang, "A Survey of Client-Controlled HetNets for 5G," *IEEE Access*, vol. 5, pp. 2842 – 2854, 2017.

[12] L. Chen, H. Jin, H. Li, J. B. Seo, Q. Guo, and V. Leung, "An Energy Efficient Implementation of C-Ran in Hetnet," *Vehicular Technology Conference (VTC2014-Fall)*, 2014.

[13] S. Parkvall, E. Dahlman, A. Furuskar, and M. Frenne, "NR: The New 5G Radio Access Technology," *IEEE Communications Standards Magazine*, vol. 1, no. 4, pp. 24 – 30, 2017.

[14] S. Borkar and H. Pande, "Application of 5G Next Generation Network to Internet of Things," *International Conference on Internet of Things and Applications (IOTA)*, pp. 443 – 447, 2016.

[15] L. Ignatova, A. Khakimov, Al. Mahmood, and A. Muthanna, "Analysis of the Internet of Things Devices Integration in 5G Networks," *Systems of Signal Synchronization, Generating and Processing in Telecommunications (SINKHROINFO)*, 2017.

[16] G. A. Akpakwu, B. J. Silva, G. P. Hancke, and A. M. Abu-Mahfouz, "A Survey on 5G Networks for the Internet of Things: Communication Technologies and Challenges," *IEEE Access*, vol. 6, pp. 3619 – 3647, 2018.

[17] Y. Niu, Y. Li, D. Jin, Li. Su, and A. V. Vasilakos, "A Survey of Millimeter Wave Communications (mmWave) for 5G: Opportunities and Challenges," *Wireless Networks*, vol. 21, no. 8, pp. 2657 2676, 2015.

[18] S. Bachtobji, A. Omri, k. Hassan, R. Bouallegue, and K. Raoof, "Performance Analysis of Energy Harvesting based Scheme for 3-D Cellular Networks," *International Wireless Communications and Mobile Computing Conference (IWCMC)*, pp. 1208 – 1212, 25-29 June 2018 Limassol, Cyprus.

[19] D. Kombate and Wanglina, "The Internet of Vehicles Based on 5G Communications," *IEEE International Conference on Internet of Things (iThings)*, 2016.

[20] S. Niknam, A. A. Nasir, H. Mehrpouyan, and B. Natarajan, "A Multiband OFDMA Heterogeneous Network for Millimeter Wave 5G Wireless Applications," *IEEE Access*, vol. 4, pp. 5640 – 5648, 2016.

[21] S. Niknam, B. Natarajan, and H. Mehrpouyan, "A Spatial-Spectral Interference Model for Millimeter Wave 5G Applications," *Proc. IEEE Veh. Tech. Conf.*, pp. 1 – 5, 2017.

[22] S. Niknam, B. Natarajan, and R. Barazideh, "Interference Analysis for Finite-area 5G mmWave Networks Considering Blockage Effect," *IEEE Access*, vol. 6, pp. 23 470 – 23 479, 2018.

[23] S. Niknam and B. Natarajan, "On the Regimes in Millimeter Wave Networks: Noise-limited or Interference-limited?," *IEEE Int. Conf. on Commun. Workshops*, 2018.

[24] S. Niknam, R. Barazideh, and B. Natarajan, "Cross-Layer Interference Modeling for 5G mmWave Networks in the Presence of Blockage," *IEEE Veh. Tech. Conf.*, pp. 1 – 5, 2018.

[25] Z. E. Ankarali, B. Pekoz, and H. Arslan, "Flexible Radio Access Beyond 5G: A Future Projection on Waveform, Numerology, and Frame Design Principles," *IEEE Access*, vol. 5, pp. 18295 – 18309, 2017.

[26] H. Dhillon, R. Ganti, F. Baccelli, and J. Andrews, "Modeling and Analysis of K-tier Downlink Heterogeneous Cellular Networks," *IEEE J. Sel. Areas Commun.*, vol. 30, no. 3, pp. 550 560, 2012.

[27] H. S. Dhillon, R. Ganti, and J. Andrews, "Load-Aware Modeling and Analysis of Heterogeneous Cellular Networks," *IEEE Trans. Wireless Commun.*, vol. 12, no. 4, pp. 1666 1677, 2013.

[28] S. Shamai and A. D. Wyner, "Information-Theoretic Considerations for Symmetric, Cellular, Multiple-Access Fading ChannelsPart I," *IEEE Transactions on Information Theory*, vol. 43, no. 6, pp. 1877 – 1894, 1997.

[29] S. Shamai and A. D. Wyner, "Information-Theoretic Considerations for Symmetric, Cellular, Multiple-Access Fading ChannelsPart II," *IEEE Transactions on Information Theory*, vol. 43, no. 6, pp. 1895 – 1911, 1997.

[30] J. G. Andrews, F. Baccelli, and R. K. Ganti, "A Tractable Approach to Coverage and Rate in Cellular Networks," *IEEE Transactions on Communications*, vol. 59, no. 11, pp. 3122 – 3134, 2011.

[31] H. Dhillon, T. Novlan, , and J. Andrews, "Coverage Probability of Uplink Cellular Networks," in *IEEE Global Commun. Conf. (GlobeCom), Anaheim, CA, USA*, 3-7 Dec 2012.

[32] D. Cao, S. Zhou, , and Z. Niu, "Optimal Combination of Base Station Densities for Energy-Efficient Two-Tier Heterogeneous Cellular Networks," *IEEE Transactions on Wireless Communications*, vol. 12, no. 9, pp. 4350 – 4362, 2013.

[33] Z. Pan and Q. Zhu, "Modeling and Analysis of Coverage in 3-D Cellular Networks," *IEEE Communications Letters*, vol. 19, no. 5, pp. 831 – 834, 2015.

[34] A. Omri and M. O. Hasna, "Modelling and Performance Analysis of 3-D Heterogeneous Cellular Networks," in *IEEE International Conf. on Commun. (ICC)*, Kuala Lumpur, Malaysia, 2016.

[35] T. Bai and Jr. R. W. Heath, "Coverage and Rate Analysis for Millimeter-Wave Cellular Networks," *IEEE Transactions on Wireless Communication*, vol. 14, no. 2, pp. 1100 – 1114, 2015.

[36] T. Bai, R. Vaze, and R. W. Heath Jr., "Analysis of Blockage Effects on Urban Cellular Network," *IEEE Transactions on Wireless Communication*, vol. 13, no. 9, pp. 5070 – 5083, Sept.2014.

[37] P. Liu, M. Di Renzo, and A. Springer, "Line-of-Sight Spatial Modulation for Indoor mmWave Communication at 60 GHz," *IEEE Transactions on Wireless Communications*, vol. 15, no. 11, pp. 7373 – 7389, 2016.

[38] D. Maamari, N. Devroye, and D. Tuninetti, "Coverage in mmWave Cellular Networks with Base Station Cooperation," *IEEE Transactions on Wireless Communications*, vol. 15, no. 4, pp. 2981 – 2994, 2016.

[39] S. Ki Yoo, S. L. Cotton, Y. J. Chun, W. G. Scanlon, and G. A. Conway, "Channel Characteristics of Dynamic Off-Body Communications at 60 GHz under Line-of-Sight (LOS) and Non-LOS Conditions," *IEEE Antennas and Wireless Propagation Letters*, vol. 16, pp. 1553 – 1556, 2017.

[40] N. Pandit, P. Panwar, D. Maharshi, and N. P. Pathak, "Indoor Radio Propagation Channel Modelling for Active Convertor Based Wireless System," *Applied Electromagnetics Conference (AEMC)*, 19 - 22 Dec. 2017.

[41] I. Atzeni, J. Arnau, and M. Kountouris, "Downlink Cellular Network Analysis with LOS/NLOS Propagation and Elevated Base Stations," *IEEE Transactions On Wireless Communications*, vol. 17, no. 1, pp. 142 – 156, Junary 2018.

[42] Sh. Wu, R. Atat, N. Mastronarde, and L. Liu, "Improving the Coverage and Spectral Efficiency of Millimeter-Wave Cellular Networks using Device-to-Device Relays," *IEEE Transactions On Communications*, vol. 66, no. 5, pp. 2251 – 2265, 2018.

[43] Mishra, P. Kumar, S. Pandey, and S. K. Biswash, "Efficient Resource Management by Exploiting D2D Communication for 5G Networks," *IEEE Access*, vol. 4, pp. 9910 – 9922, 2016.

[44] Yu Shanshan, Ju. Liu, Xi. Zhang, and Sh. Wu, "Social-Aware Based Secure Relay Selection in Relay-Assisted D2D Communications," *Computers, Materials Continua*, vol. 58, no. 2, pp. 505 – 516, 2019.

[45] Xi. Lin, J. G. Andrews, and A. Ghosh, "Spectrum Sharing for Device-to-Device Communication in Cellular Networks," *IEEE Transactions On Wireless Communications*, vol. 13, no. 12, pp. 6727 – 6740, December 2014.

[46] E. Hossain H. ElSawy and M. S. Alouini, "Analytical Modeling of Mode Selection and Power Control for Underlay D2D Communication in Cellular Networks," *IEEE Transactions on Communications*, vol. 66, no. 11, pp. 4147 – 4161, 2014.

[47] E. Hossain H. ElSawy and M. S. Alouini, "Analytical Modeling of Mode Selection for Moving D2D Enabled Cellular Networks," *IEEE Communications Letters*, vol. 20, no. 6, pp. 1203 – 1206, 2016.

[48] D. Benda, X. Chu, S. Sun, Tony Q. S. Quek, and A.Buckley, "PV Cell Angle Optimisation for Energy Arrival-Consumption Matching in a Solar Energy Harvesting Cellular Network," *IEEE International Conf. on Commun. (ICC)*, Paris, France, 21-25 May 2017.

[49] A. Ghazanfari, H. Tabassum, and E. Hossain, "Ambient RF Energy Harvesting in Ultra-dense Small Cell Networks: Performance and Trade-offs," *IEEE Wireless Communications*, vol. 23, no. 2, pp. 38 – 45, 2016.

[50] V. Kaur and S. Thangjam, "A Stochastic Geometry Analysis of RF Energy Harvesting based D2D Communication in Downlink Cellular Networks," *Information Processing (IICIP), 2016 1st India International Conference on*, 12-14 Aug. 2016.

[51] Y. L. Che, L. Duan, and R. Zhang, "Spatial Throughput Maximization of Wireless Powered Communication Networks," *IEEE Journal on Selected Areas in Communications*, vol. 33, no. 8, pp. 1534 – 1548, 2015.

[52] M. Seif, A. El-Keyi, K. G. Seddik, and M. Nafie, "Cooperative D2D Communication in Downlink Cellular Networks with Energy Harvesting Capability," *Wireless Communications and Mobile Computing Conference (IWCMC), 13th International*, 26-30 June 2017.

[53] S. Bachtobji, A. Omri, and R. Bouallegue, "Modelling and Performance Analysis of 3-D Mmwaves based Heterogeneous Networks," *International Wireless Communications and Mobile Computing Conference (IWCMC)*, pp. 72 – 76, 5-9 Sept 2016 Paphos, Cyprus.

[54] S. Bachtobji, A. Omri, R. Bouallegue, and K. Raoof, "Modelling and Performance Analysis of Mmwaves and Radio Frequency based 3-d Heterogeneous Networks," *IET Communications*, vol. 12, pp. 290 – 296, 22 March 2018.

[55] S. Bachtobji, K. Hassan, A. Omri, K. Raoof, and R. Bouallegue, "3-D Modeling and Analysis of Blockage Effects on the Performance of Urban Wireless Communication Systems," *International Conference On ICT Convergence (ICTC)*, 2018.

[56] S. Bachtobji, A. Omri, k. Hassan, R. Bouallegue, and K. Raoof, "Relay Selection Scheme for Device-to-Device based 3-D Millimeter-Wave Cellular Networks," *Submitted to IET Communications*.

[57] F. Baccelli and B. Blaszczyszyn, "Stochastic Geometry and Wireless Networks," *NOW publishers*, 2009.

[58] R. K. Ganti M. Haenggi, "Interference in Large Wireless Networks," *NOW publishers Inc*, 2009.

[59] A. Mouradian, "Modeling Dense Urban Wireless Networks with 3D Stochastic Geometry," *Performance Evaluation, Elsevier*, 2018.

[60] S. N. Chiu, D. Stoyan, W. S. Kendall, and J. Mecke, "Stochastic Geometry and its Applications," *John Wiley & Sons, Ltd*, 2013.

[61] J. F. C. Kingman, "Poisson Processes," *Oxford university press*, vol. 3, 1992.

[62] D. J. Daley and D. Vere-Jones, "An Introduction to the Theory of Point Processes," *Probability and its Applications (New York)*, vol. 3, 2003.

[63] M. Haenggi, "Stochastic Geometry for the Analysis and Design of 5G Cellular Networks," in *IEEE GLOBECOM, http://www.nd.edu/ mhaenggi/talks/globecom14.pdf*, Austin, TX, 2014.

[64] J. Teichmann, F. Ballani, and K. G. van den Boogaart, "Generalizations of Matern's Hard-Core Point Processes," *Spatial Statistics*, Sep 2012.

[65] M. Haenggi, "Mean Interference in Hard-Core Wireless Networks," *IEEE Communications Letters*, vol. 15, no. 8, pp. 792 – 794, 2011.

[66] M. Kiderlen and M. Hrig, "Matern's Hard Core Models of types I and II with Arbitrary Compact Grains," *17th SGSIA, Torun, Poland*, 13 June 2013.

[67] B. Cho, K. Koufos, and R. Jantti, "Bounding the Mean Interference in Matern Type II Hard-Core Wireless Networks," *IEEE Wireless Communications Letters*, vol. 2, no. 5, pp. 563 – 566, 2013.

[68] S. Y. Seidel and T. S. Rappap, "914 mhz path loss prediction models for indoor wireless communications in multifloored buildings," *IEEE Trans. Antennas Propag*, vol. 40, no. 2, pp. 207 217, Feb. 1992.

[69] C. Yitian and Y. Aimin, "Analysis of 2.4GHz WLAN Indoor and Outdoor Transmissions Path Loss," *Telecommun. Eng.*, vol. 7, no. 1, pp. 35 39, 2005.

[70] R. Jain, "Channel Models A Tutorial," *WiMAX Forum AATG*, February 2007.

[71] A. Goldsmith, "Wireless Communications," *Cambridge University Press*, 2005.

[72] I. A. Hemadeh, K. Satyanarayana, M. El-Hajjar, and L. Hanzo, "Millimeter-Wave Communications: Physical Channel Models, Design Considerations, Antenna Constructions and Link-Budget," *IEEE Communications Surveys Tutorials*, vol. 20, no. 2, pp. 870 – 913, 2017.

[73] D. M .J. Devasirvatham, C. Banerjee, R. R. Murray, and D. A. Rappaport, "Four-Frequency Radio Wave Propagation Measurements of the Indoor Environment in a Large Metropolitian Commercial Building," in *GlobeCom*, 1991.

[74] A. I. Sulyman, A. T. Nassar, M. K. Samimi, G. R. MacCartney, Jr. Theodore, S. Rappaport, and Abdulhameed Alsanie, "Radio Propagation Path Loss Models for 5g Cellular Networks in the 28 ghz and 38 ghz Millimeter-Wave Bands," *IEEE Communications Magazine*, vol. 19, no. 9, pp. 78–86, 2014.

[75] R. Cowan, "Objects Arranged Randomly in Space: An Accessible Theory," *Advances in Applied Probability*, vol. 21, no. 3, pp. 543 – 569, 1989.

[76] E. Turgut and M. C. Gursoy, "Coverage in Heterogeneous Downlink MillimeterWave Cellular Networks," *IEEE Transactions on Communications*, 2017.

[77] E. Turgut and M. C. Gursoy, "Uplink Performance Analysis in D2D-Enabled mmWave Cellular Networks," *Vehicular Technology Conference (VTC-Fall)*, 24-27 Sept.2017.

[78] A. AL-Hourani, S. Chandrasekharan, G. Kaandorp, W. Glenn, A. Jamalipour, and S. Kandeepan, "Coverage and Rate Analysis of Aerial Base Stations," *IEEE Transactions on Aerospace and Electronic Systems*, vol. 52, no. 6, pp. 30773081, 2016.

[79] A. Omri and M. Hasna, "Average Secrecy Outage Rate and Average Secrecy Outage Duration of Wireless Communication Systems With Diversity Over Nakagami-m Fading Channels," *IEEE Transactions on Wireless Communications*, vol. 17, no. 6, pp. 3822 – 3833, 2018.

[80] A. Prosperetti, "Advanced Mathematics for Applications," *Cambridge University Press, Cambridge*, 2011.

[81] L. Wang D. Liu, Y. Chen, M. Elkashlan, K. K. Wong, R. Schober, , and L. Hanzo, "User Association in 5G Networks: A Survey and an Outlook," *IEEE Communications Surveys Tutorials*, vol. 18, no. 2, pp. 1018 – 1044, 2016.

[82] T. S. Rappaport, Sh. Sun, R. Mayzus, H. Zhao, Y. Azar, K. Wang, G. N. Wong, J. K. Schulz, M. Samimi, and F. Gutierrez, "Millimeter Wave Mobile Communications for 5G Cellular: It Will Work!," *IEEE Access*, vol. 1, pp. 335 349, 2013.

[83] Z. Pi and F. Khan, "An Introduction to Millimeter Wave Mobile Broadband Systems," *IEEE Communications Magazine*, vol. 49, no. 6, pp. 101 107, 2011.

[84] S. Abu-Surra Z. Pi O. El Ayach, S. Rajagopal and R. Heath, "Spatially Sparse Precoding in Millimeter Wave MIMO Systems," *IEEE Transactions on Wireless Communications*, vol. 13, no. 3, pp. 1499 1513, 2014.

[85] M. Abramowitz and I. A. Stegun, "Handbook of Mathematical Functions with Formulas, Graphs, and Mathematical Tables," *U.S. Dept. Commerce*, vol. 10, 1972.

[86] K. A. Hamdi, "Capacity of MRC on Correlated Rician Fading Channels," *IEEE Transactions on Communications*, vol. 56, no. 5, pp. 708 – 711, 2008.

[87] T. Bai, R. Vaze, and R. Heath, "Using Random Shape Theory to Model Blockage in Mandom Cellular Networks," *Proc. of Int. Conf. on Signal Processing and Communications (SPCOM)*, pp. 1 – 5, Jul. 2012.

[88] A. Ghosh and et al, "Heterogeneous Cellular Networks: From Theory to Practice," *IEEE Communications Magazine*, vol. 50, no. 6, pp. 54 64, Jul. 2012.

[89] D. Taylor, H. Dhillon, T. Novlan, and J. Andrews, "Pairwise Interaction Processes For Modeling Cellular Network Topology," *Proc. of Global Commun. Conf. (GLOBECOM)*, p. 4524 4529, Dec. 2012.

[90] L. Yang and M. S. Alouini, "On the Average Outage Rate and Average Outage Duration of Wireless Communication Systems With Multiple Cochannel Interferers," *IEEE Transactions on Wireless Communications*, vol. 3, no. 4, pp. 1142 – 1153, 2004.

[91] I. S. Gradshteyn and I. M. Ryzhik, *Table of Integrals, Series, and Products*, Elsevier Inc., 2007.

[92] D. Zhao, C. Huang, Y. Chen, F. Alsaadi, and S. Cui, "Resource Allocation for Multiple Access Channel With Conferencing Links and Shared Renewable Energy Sources," *IEEE J. Sel. Areas Commun.*, vol. 33, no. 3, pp. 423 437, Mar. 2015.

[93] E. Hossain and M. Hasan, "5G Cellular: Key Enabling Technologies and Research Challenges," *IEEE Instrumentation Measurement Magazine*, vol. 18, no. 3, pp. 11 – 21, Jun. 2015.

[94] L. Huang and M. Neely, "Utility Optimal Scheduling in Energy Harvesting Networks," *IEEE/ACM Transactions Networks*, vol. 21, no. 4, pp. 1117 1130, Aug. 2013.

[95] M. Alibakhshi-Kenari, M. Naser-Moghadasi, R. Ali Sadeghzadeh, B. S. Virdee, and E. Limiti, "Periodic Array of Complementary Artificial Magnetic Conductor Metamaterials-Based Multiband Antennas for Broadband Wireless Transceivers," *IET Microwaves, Antennas Propagation*, vol. 10, no. 15, pp. 1682 1691, December 2016.

[96] Kh. M. Morshed, K. P. Esselle, and M. Heimlich, "Dielectric Loaded Planar Inverted-f Antenna for Millimeter-Wave 5G Hand Held Devices," *2016 10th European Conference on Antennas and Propagation (EuCAP)*, pp. 1 – 3, December 2016.

[97] Z. Pi and F. Khan, "An Introduction to Millimeter-Wave Mobile Broadband Systems," *IEEE Communications Magazine*, vol. 49, no. 6, pp. 101 – 107, 2011.

[98] C. R. Anderson and T. S. Rappaport, "In-Building Wideband Partition Loss Measurements at 2.5 and 60 Ghz," *IEEE Transactions on Wireless Communication*, vol. 3, no. 3, pp. 101 – 107, 2011.

[99] K. Tekkouk, J. Hirokawa, R. Sauleau, M. Ettorre, M. Sano, and M. Ando, "Dual-layer Ridged Waveguide Slot Array Fed by a Butler Matrix with Sidelobe Control in the 60-GHz Band," *IEEE Trans. Antennas Propagat.*, vol. 63, no. 9, pp. 3857 – 3867, 2015.

[100] M. El Shorbagy, R. M. Shubair, M. I. AlHajri, and N. Kh. Mallat, "On the Design of Millimetre-Wave Antennas for 5G," *16th Mediterranean Microwave Symposium (MMS), Abu Dhabi, United Arab Emirates*, 14-16 Nov. 2016.

[101] M. Alibakhshikenari, B. S. Virdee, Chan H. See, R. A. Abd-Alhameed, F. Falcone, and E. Limiti, "Super-Wide Impedance Bandwidth Planar Antenna for Microwave and Millimeter-Wave Applications," *Sensors*, 2019.

[102] J. Hirokawa, "Millimeter-Wave Antenna Technologies for 5G Mobile Communication Systems," *IEEE International Workshop on Electromagnetics: Applications and Student Innovation Competition (iWEM), Nanjing, China*, 16-18 May 2016.

[103] M. Alibakhshikenari, B. S. Virdee, Chan H. See, R. A. Abd-Alhameed, F. Falcone, and E. Limiti, "Beam-Scanning Leaky-Wave Antenna Based on CRLH-Metamaterial for Millimeter-Wave Applications," *IET Microwaves, Antennas Propagation*, vol. 6, March 2019.

[104] M. Ando J. Hirokawa, K. Morimoto, "Beam-Switching Single-Layer Post-Wall Waveguide Slot Array Controlling Crossover Sidelobes," *Euro. Conf. Antennas Propagat.*, vol. 3, Nov.2007.

[105] A. V. Alejos, M. G. Sanchez, and I. Cuinas., "Measurement and Analysis of Propagation Mechanisms at 40 GHz: Viability of Site Shielding Forced by Obstacles," *IEEE Transactions on Vehicular Technology*, vol. 57, no. 6, pp. 3369 – 3380, 2008.

[106] Y.W. P.Hong, W.J. Huang, and C.C. Jay Kuo, "Cooperative Communications and Networking: Technologies and System Design," *Springer*, JULY 2010.

[107] I.F. Akyildiz, W.Y. Lee, M. C. Vuran, and S. Mohanty, "A Survey on Spectrum Management in Cognitive Radio Networks," *IEEE Communications Magazine*, pp. 40–48, APRIL 2008.

[108] A. Omri, M. Shaqfeh, A. Ali, and H. Alnuweiri, "Synchronization Procedure in 5G NR Systems," *IEEE Access*, vol. 7, pp. 41286 – 41295, 2019.

Titre : **Analyse de performance des techniques de transmission numériques en 3D**

Mots clés : Analyse des performances, Cinquième génération (5G), Géométrie stochastique, Modélisation 3-D, Onde millimétrique (mmWave), Réseaux cellulaires hétérogènes

Résumé : Les réseaux 5G présentent de nombreux défis et opportunités pour la conception des réseaux sans fil denses. Par conséquent, des efforts de recherche substantiels sont consacrés aux problèmes de la modélisation 3-D dans les réseaux HetNets basés sur les mmWave et la récupération d'énergie respectivement. Ainsi, la modélisation et l'amélioration des performances des réseaux cellulaires hétérogènes 3-D pour la prochaine génération méritent une étude approfondie, qui est l'objectif principal de cette thèse. Le travail de recherche présenté dans cette thèse a deux axes principaux. Premièrement, nous nous concentrons sur la modélisation en 3D des réseaux de communication sans fil.
Ces modèles décrivent non seulement le système lorsque les blocages sont négligés, mais permettent également de modéliser les obstacles (tels que les bâtiments) afin d'étudier leur effet et de proposer une solution pour les surmonter. Deuxièmement, de nouvelles techniques de transmission sont proposées pour améliorer les performances des systèmes de communication sans fil urbains. Ainsi, nous introduisons une technique basée sur la récupération d'énergie (EH) tel que l'objectif est de réduire le délai de transmission et améliorer la capacité ergodique. Sur cette base, le délai de transmission moyen et les expressions de capacité ergodique sont détaillés et dérivés. Enfin, en considérant une hypothèse de canal nakagami-m pour les communications à ondes millimétriques, nous proposons un nouveau schéma min / max pour améliorer le taux de réussite de la transmission. Ce schéma est basé sur la sélection d'un relais disponible pouvant assister à la transmission.
.

Title : **Performance Analysis of Enhancement Techniques for 3-D Cellular Networks**

Keywords : Performance Analysis, Fifth Generation (5G), Stochastic Geometry, 3-D Modeling, MillimeterWave (mmWave), Heterogeneous Cellular Networks

Abstract : With the explosive growth of mobile data demand, cellular networks have experienced several major evolutions, from the first generation to the present the fifth generation new radio cellular networks. These networks can cover a larger geographical area, with high network capacity, and low power consumption. For the next generation, the cellular networks consist in deploying a big number of small cells, such as femto-cells and picocells, which offers a lager zone of radio coverage. In fact, cell densification presents a simple and efficient solution to increase the network capacity, which relies on densely reusing the spectrum across a geographical area and hence brings base stations closer to users. Thus, the 3-D modeling and the performance enhancement of the increasingly heterogeneous cellular networks become important issues. The current thesis focuses on the study and the enhancement of 3-D cellular networks. The research work introduced in this thesis has two main axes. First, we focus on three-dimensional modeling of wireless communication networks. These models, not only describe the system when the blockages effect are neglected, but also capable of modeling the obstacles (such as buildings) in order to study their effect and propose solution to overcome. Second, new transmission schemes are proposed to enhance the performances of the urban wireless communication systems.